UNIVERSIDAD AUTONOMA DE MADRID

Facultad de Ciencias

Departamento de Biología Molecular

Role of CPEB4 in Huntington's Disease and in Autism Spectrum Disorder

Tesis Doctoral

Alberto Parras Rodríguez

Madrid

2017

Facultad de Ciencias

Departamento de Biología Molecular

Memoria de Investigación presentada por

Alberto Parras Rodríguez

Licenciado en Biotecnología

Para optar al grado de ***Doctor***

por la ***Universidad Autónoma de Madrid***

Role of CPEBs in Huntington's Disease and in Autism Spectrum Disorder

Trabajo dirigido por el ***Dr. José Javier Lucas Lozano***

Profesor de Investigación del Consejo Superior de Investigaciones Científicas (CSIC)

La presente tesis ha sido realizada en el Centro de Biología Molecular "Severo Ochoa", centro mixto CSIC y UAM.

El laboratorio del Dr. Lucas también forma parte del Centro de Investigación Biomédica en Red para Enfermedades Neurodegenerativas (CIBERNED)

“Un hombre cobarde no conquista una mujer bonita”
Antonio Martínez Ares

“Un invencible no es aquel que siempre gana sino el que nunca se rinde”
Antonio Martín

“A ritornello, a ritornello, hay una estella que brilla en el cielo...”
Juan Carlos Aragón

Disponibles sólo en el formato impreso

Disponibles sólo en el formato impreso

INDEX

ABBREVIATIONS

ACSF: Artificial cerebrospinal fluid

AD: Alzheimer's disease

ANOVA: Analysis of variance

AON: Antisense oligonucleotides

APA: Alternative polyadenylation

ARE: AU-rich elements

AS: Alternative splicing

ASD: Autism spectrum disorder

ATP: Adenosine triphosphate

ATXN3: Ataxin 3

AUTS2: Autism susceptibility candidate 2

BDNF: Brain-derived neurotrophic factor

BSA: Bovine serum albumin

BW: Body Weight

CaMKII: Ca^{2+}/calmodulin-dependent protein kinase II

Cat.: Category

CMV: Cytomegalovirus

CNS: Central nervous system

CNV: Copy number variations

CPE: Cytoplasmic polyadenylation elements

CPEB: Cytoplasmic polyadenylation binding protein

CTRL: Control

Cx: Cerebral cortex

dT: Deoxy-thymidine

DJC: Downstream junction count

DMEM: Dulbeco's modified eagle's medium

DN: Dominant negative

DNA: Deoxyribonucleic acid

DRPLA: Dentatorubral-pallidoluysian atrophy

EDTA: Ethylenediaminetetraacetic acid

EGTA: Aminopolycarboxylic acid

EPM: Elevated plus maze

ER: Endoplasmic reticulum

ESPC: Excitatory postsynaptic currents

f.c.: Fold change

FDR: False discovery rate

FL: Full-length

FMRP: Fragile X mental retardation protein

FOXP1: Forkhead box protein 1

FPKM: Fragments per kilo bases of exons for per million mapped reads

FXS: Fragile X syndrome

GAM: Generalized additive model

GO: Gene ontology

GT: Gene trap

HD: Huntington's disease

HEPES: 4-(2-hydroxyethyl)-1-piperazineethanesulfonic acid

Hex: Hexanucleotide

Hire-PAT: High resolution poly(A) tail

HTT: Huntingtin

Hz: Hertz

IBs: Inclusion bodies

ID: Identification

IHC: Immunohistochemistry

IT15: Interesting transcripts 15

KDa: Kilodalton

KEGG: Kyoto encyclopedia of genes and genomes

KO: Knockout

KTN1: Kinectin 1

LCD: Low complexity domain

LME: Linear mixed effects

LSD: Least significant difference

LV: lateral ventricle

MATS: Multivariate analysis of transcript splicing

mESPC: Miniature excitatory postsynaptic currents

MIA: Maternal immune activation

mRNPS: messenger ribonucleoproteins

MTT: Mutant huntingtin

MXE: Mutually exclusive exons

NLGN: Neuroligin

NLS: Nuclear location signal

NMDG: N-methyl-D-glucamine

OCT: Optimum cutting temperature

OF: Open field

OR: Odds ratio

ORF: Open reading frame

PAS: Polyadenylation site

PAT: Polyadenylation test

PBE: Pumilio binding element

PBS: Phosphate buffered saline

PCR: Polymerase chain reaction

PD: Parkinson's disease

PFA: Paraformaldehyde

PolyQ: Polyglutamine

Poly(A): Polyadenine

Poly(U): Polyuracil

PSI: Percent spliced in

PTC: Premature termination codon

PUF: Pumilio and FBF

qRT-PCR: Quantitative reverse transcription polymerase chain reaction

R.f.: Representation factor

RAN: Repeat associated non-ATG

RIN: RNA integrity number

RIP: RNA immunoprecipitation

RMA: Robust multiarray average

RNA: Ribonucleic acid

RNABP: RNA binding proteins

RRM: RNA recognition motif

SA: Splice acceptor

SAp: Social approach

SCA: Spinocerebellar ataxia

SDS: Sodium dodecyl sulfate

SE: Skipped exon

SEM: Standard error of the mean

SFARI: Simons foundation autism reaseach iniciative

SJC: Splice junction count

SNV: Single nucleotide variants

SSC: Saline sodium citrate

St: Striatum

STX6: Syntaxin 6

RAN: Repeat associated non-ATG

Tg: Transgenic

tTA: Tetracycline transactivator

UJC: Upstream Junction Count

UTR: Untranslated region

UsV: Ultrasonic vocalization

WGCNA: Weighted gene go-expression network analysis

WT: Wild type

ZnF: Zinc-finger

ABSTRACT

Huntington's disease (HD) is a neurodegenerative disorder characterized by motor disturbance, cognitive decline and psychological dysfunction. Cytoplasmic polyadenylation element binding proteins 1-4 (CPEB1-4) are a family of proteins that regulate translation of specific mRNAs by modulating their poly(A) tail length. CPEBs participate in synaptic plasticity however their role in etiology of neurodegenerative diseases has not been studied. Based on different lines of evidence, we reasoned that altered CPEB function might contribute to HD.

The first aim of this thesis was to explore the status of CPEBs in HD. We found CPEB1/CPEB4 imbalance in HD brain and an aberrant poly(A) tail length with concomitant alteration of their encoded protein levels. This alteration prominently affects HD-, Alzheimer's- and Parkinson's disease-related genes. Therefore, CPEB-dependent altered polyadenylation becomes a new molecular signature in neurodegeneration useful to identify novel effectors like the striatal atrophy-associated gene *KTN1* whose decreased mRNA-adenylation and protein levels provide a possible explanation for HD preponderant striatal affectation.

Strikingly, we noticed that high confidence autism spectrum disorder (ASD) risk genes were overrepresented among CPEB4 targets. This finding led us to hypothesize CPEB4 as a new hub in ASD gene expression. ASD is a neurodevelopmental disorder that manifests in childhood by impaired social communication and restrictive and repetitive behaviors. Genetic contribution to ASD resides on risk gene variants that are individually minimally penetrant. Since environmental factors also underlie idiopathic ASD, it is crucial to identify altered regulators able to orchestrate multiple ASD genes along neurodevelopment.

Thereby, the second aim of this thesis was to study the status of CPEB4 in idiopathic ASD patients and to determinate its potential role in ASD risk gene regulation. We found that CPEB4 transcripts are mis-spliced in favor of the isoform lacking a neuronal-specific microexon in ASD brains. Then, genome-wide polyadenylation analysis revealed a new molecular signature of global poly(A) tail shortening with concomitant reduction of their protein levels that prominently affects high-confidence ASD genes. Equivalent CPEB4-selective splicing isoform-imbalance in mice is sufficient to mimic the mRNA polyadenylation and induces ASD-like neuroanatomical, electrophysiological and behavioral phenotypes.

Collectively, these data support a key role of CPEB-mediated altered poly(A) in HD and across neurodegenerative diseases and unravel CPEB4 as a new node in ASD gene expression.

INTRODUCTION

1. HUNTINGTON'S DISEASE

1.1. First evidence

Huntington's disease (HD), also known as Huntington's chorea is a progressive neurodegenerative disorder characterized by motor disturbance, cognitive decline and behavioral and psychological dysfunction (Vonsattel and DiFiglia, 1998). It is inherited in an autosomal dominant manner and affects about 1 in 15,000 individuals in North America and Europe (Pringsheim et al., 2012).

The original descriptions of chorea date from the Middle Ages and it was initially named ''Saint Vitus's dance'' because affected individuals would dance in circles for hours until they dropped from exhaustion (Vale and Cardoso, 2015). But, in 1872 this chorea was named Huntington's disease after George Huntington provided the classical description (Rub et al., 2015).

The highest prevalence of HD is found in the people who lives in the Lake Maracaibo in Venezuela, and studies in this population led to the identification of the genetic change causing HD (Gusella et al., 1983; HDCRG, 1993).

1.2. Mutation

The genetic defect for HD was mapped to the short arm of chromosome 4 (Gusella et al., 1983). After an arduous search, the mutation was identified as an abnormal expansion of the CAG (Cytosine, Adenine, Guanine) triplet repeats within the coding region of the gene "IT15" (Interesting Transcripts 15) also called huntingtin (*HTT*) gene. This mutation produces an expanded stretch of polyglutamine (polyQ) near the amino-terminal end (exon 1) (Andrew et al., 1993). In the non-HD population, *HTT* ranges from 9 to 35 CAG copies, with an average median of between 17 and 20 repeats. However, CAG expansions exceeding 35-40 repeats result in the disease (Kremer et al., 1994) (Figure 1A).

The length of the CAG expansion correlates with severity and it shows strong inverse correlation with the age of disease onset (Figure 1B). Juvenile onset is associated with HTT carrying about 75 or more repeats (Saudou and Humbert, 2016). HD exhibits paternal anticipation, a greater expansion of the trinucleotide repeat with paternal transmission (Ranen et al., 1995).

As mentioned, HD is autosomal dominant, but there are rare cases with both alleles expanded (homozygous patients). This homozygous mutation does not influence age at onset, but disease progression can be more severe (Lee et al., 2012).

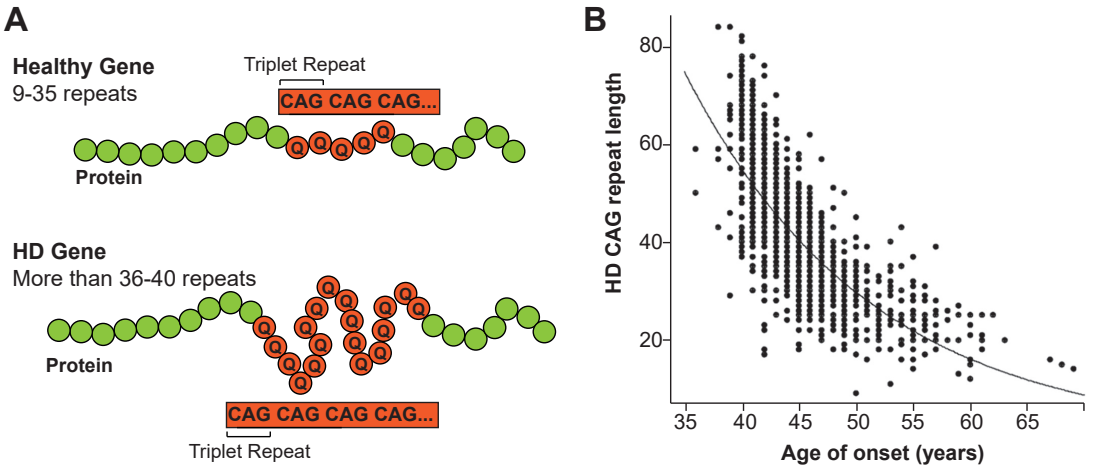

Figure 1: HD mutation in Huntingtin gene. (A) CAG repeat in a healthy and HD gene. (B) Plot from HD subjects of known age at neurologic onset. It is plotted the CAG repeat length (x-axis) against age of onset (y-axis). The line represents the best-fit simple logarithmic regression to the data (Gusella and MacDonald, 2009).

1.3. Neuropathology

HTT either wild type or mutant (mHTT) is ubiquitously expressed in all cells, but main of the changes of HD identified so far occurs in the brain, where intensity of the degenerative process differs among specific brain compartments (e.g., striatum, cerebral cortex, white matter, hippocampus, thalamus or cerebellum) or systems (e.g., basal ganglia or limbic system) (Vonsattel, 2008).

Degeneration primarily affects the striatum (neuronal loss and gliosis), but other regions may also be damaged at early stages, such as the cerebral cortex (Cx). HD postmortem brains show degeneration of selective neuronal population, the majority of striatal GABAergic medium spiny neurons and, to a lesser extent, cortical pyramidal neurons of layers V and VI (Vonsattel and DiFiglia, 1998; Wang et al., 2014). The vulnerability of the striatum (St) is associated with the size of the CAG expansion (Furtado et al., 1996), and a system for grading severity and evolution of the striatal pathology was established (Vonsattel et al., 1985). This classification system for HD has five grades (0-4) designated in ascending order of severity.

HD is characterized by the presence of abnormal depositions of huntingtin fragments, inclusion bodies (IBs), in the nuclei (Davies et al., 1997) and in the neuropil (Gutekunst et al., 1999), that show a fibrillar ultrastructure. The IBs were located in the striatum, cerebral cortex, cerebellum, and the spinal cord and they are pathological hallmark of HD (Arrasate and Finkbeiner, 2012). Recently rod-like Tau-immunopositive deposits also have been discovered along neuronal nuclei (Fernandez-Nogales et al., 2014).

1.4. Symptoms

In HD, although the number of CAG repeats is negatively correlated with the age of symptom onset (Wexler et al., 2004), there is not a clear correlation with symptom profile. Indeed, it has been demonstrated in monozygotic twins that environmental factors are important in the phenotypic expression (Gomez-Esteban et al., 2007). Now, it is well established that symptoms result from major neurodegeneration in both the Cx and basal ganglia (Mehrabi et al., 2016; Thu et al., 2010).

The most characteristic symptoms in HD patients include defects in voluntary motor performance, cognitive decline and physiological alterations (Waldvogel et al., 2012). The most distinctive, well recognized and primary symptom is the development of involuntary choreic movements (Huntington, 1872) immediate consequence of corticostriatal dysfunction (Estrada-Sanchez and Rebec, 2013). Further, patients initially display hyperkinetic movements but they are progressively replaced by bradykinesia, rigidity and dystonia (Thompson et al., 1988).

Patients show selective and progressive dysfunction of cognitive capacities, impairment in attention, executive function and finally culminate in dementia (Ho et al., 2003). The three main neuropsychiatric syndromes include apathy, irritability and depression (Thompson et al., 2012). Another hallmark in HD is the weight loss despite efforts to maintain a higher caloric intake (Marder et al., 2009).

The most common cause of death of HD patients is primary infectious and dysphagia leading to aspiration pneumonia (Heemskerk and Roos, 2012) followed by cardiovascular diseases and suicide (Sorensen and Fenger, 1992).

1.5. Huntingtin

The human *HTT* gene encodes a 348-kDa multidomain protein with 3142 aminoacids (UniProt, 2015). The N-terminal region (exon 1) contains the expandable polyQ stretch (HDCRG, 1993). In contrast to other exons, exon 1 shows poor conservation during evolution (Harjes and Wanker, 2003).

HTT transcripts and protein are ubiquitously expressed but at different levels throughout most tissues and, as expected, abundant in the central nervous system (CNS) (Marques Sousa and Humbert, 2013). HTT shows a wide distribution at the subcellular level being found in nucleus, cytoplasm and dendrites (Trottier et al., 1995), and it is associated with endoplasmic compartments, mitochondria, microtubules or plasma membrane (Harjes and Wanker, 2003).

The principal function of HTT is not completely understood, but HTT could be considered a multifunctional protein involved in several pathways through its scaffold characteristics. This idea is supported by the huge list of HTT-interacting proteins that have been identified. These proteins play a role in several processes as endocytosis, autophagy, apoptosis, ciliogenesis, cell signaling or transcriptional regulation, suggesting that HTT is involved in all of them (Harjes and Wanker, 2003; Saudou and Humbert, 2016). Certainly, HTT is essential for embryonic development, as evidenced by the facts that knockout (KO) mice die at an early developmental stage (Nasir et al., 1995), and HTT is important in neurogenesis (Godin et al., 2010).

1.6. Pathogenesis

HTT mutation could induce both loss of function and a gain of toxic function (Liot et al., 2016). But, at least 11 inherited neurological disorders are known to be caused by CAG expanded repeats encoding a polyQ stretch (SCA1-3, SCA17 or DRPLA). This suggests that a toxic gain of function is principally responsible for the disease (La Spada and Taylor, 2010). However, the molecular and cellular pathways underlying neurodegeneration are still unknown.

The toxic functions acquired by mutant HTT may involve the full length HTT, polyQ short N-terminal fragments (Bates et al., 2015) and also non-polyQ C-terminal fragments (El-Daher et al., 2015). In addition, others toxic mechanisms might include the accumulation of sense and antisense repeat associated non-ATG (RAN) translation proteins (Banez-Coronel et al., 2015), and there is evidence supporting that CAG repeat-containing RNA might be directly involved in neurotoxicity (Nalavade et al., 2013).

Some of the multiple cellular pathways that have been implicated in HD pathogenesis include: transcriptional dysregulation (Kumar et al., 2014), excitoxicity, vesicular transport (Zuccato et al., 2010), autophagy (Kiriyama and Nochi, 2015) or mitochondrial dysfunctions (Liot et al., 2016), ubiquitin–proteasome system impairment (Ortega and Lucas, 2014) or splicing alteration (Cabrera and Lucas, 2016; Fernandez-Nogales et al., 2014) among others.

1.7. Mouse models

Mouse models of HD mimic many aspects of the human disease. These transgenic (Tg) mice are powerful tools that let us advance in our understanding of disease, and also evaluate efficacy of potential new treatments. It is important to question what

mouse model should to be used (Ehrnhoefer et al., 2009; Menalled and Brunner, 2014). Tg mouse models can be divided into three categories depending on how they were engineered:

- Exon 1 Tg models express N-terminal fragment of human *HTT* gene with expanded CAG repeat. For example, R6/1-2 mice (Mangiarini et al., 1996) are the most widely used because they have a robust phenotype and early onset, or HD94 conditional Tg mice which display conditional expression of a similar transgene (Yamamoto et al., 2000).
- Full-length Tg models express the polyQ mutation in the full-length human *HTT* gene. Some examples are YAC128 and BACHD mice that carry yeast or bacterial artificial chromosome (Gray et al., 2008; Slow et al., 2003).
- Knock-in models have the CAG sequence inserted into the endogenous mouse *Htt* gene, as for example zQ175 (Menalled et al., 2012) that present a relatively slow progression of phenotype.

2. AUTISM SPECTRUM DISORDER

2.1. Definition

Autism spectrum disorder (ASD) is the most common neurodevelopmental disorder that manifests during early childhood (DSM-V, 2013). Symptoms are most marked during infancy and many individuals improve with age (Delorme et al., 2013; Jones et al., 2014). ASD comprises different phenotype outcomes and ages of onset, but the actual ASD diagnostic criteria is defined (DSM-V, 2013) as follows:

- Persistent deficits in social communication and interaction; deficits in social-emotional reciprocity, nonverbal communicative and developing relationships.
- Restricted, repetitive patterns of behavior, interests, or activities.

Other comorbidities such as intellectual disability, language impairment, microcephaly or craniofacial dysmorphology (Stessman et al., 2016), epilepsy (Tuchman and Rapin, 2002), motor deficiencies (Setoh et al., 2016) or anxiety (White et al., 2009) are frequent in ASD subjects.

ASD has a prevalence of about 1 in 160 people worldwide (Elsabbagh et al., 2012) and it is interesting to note that it is more common in males than in females, with a ratio of 4:1 (Van Wijngaarden-Cremers et al., 2014).

The causes and pathogenic mechanisms of ASD remain unknown. Although it is highly heritable, strong evidence indicates that the causes include both genes and environmental factors (Geschwind and State, 2015).

2.2. Syndromic vs. non-syndromic

ASD can be classified in syndromic and non-syndromic, a distinction that is exclusively based on clinical criteria (Sztainberg and Zoghbi, 2016).

Syndromic is used to describe cases where ASD diagnosis is secondary to an existing condition with additional phenotypes and/or dysmorphic features. The etiology is usually known and can involve chromosomal abnormalities, copy number variations (CNV) or mutations in a single gene with high penetrance for ASD, such as in Fragile X syndrome (FXS) (Verkerk et al., 1991), Angelman syndrome (Donlon, 1988) or Rett syndrome (Amir et al., 1999).

The term ***non-syndromic*** is used in cases where ASD is the primary diagnosis and no additional symptoms are present, typically referred to as “idiopathic autism”. Although in most of the cases, the etiology is unknown, cumulative evidence has

proven that there is a genetic factor involved (Baudouin et al., 2012; Sztainberg and Zoghbi, 2016).

2.3. Genetics

ASD is a multigenic disorder, which is highly heritable as evidenced by studies on the recurrence risk in families and twins (Sandin et al., 2014). Using traditional genetic approaches, over 100 genes have been identified that contribute to idiopathic ASD risk. These monogenic disorders are rare, and together they are estimated to represent ~5% of ASD cases, for example, NLGN3-4 (Jamain et al., 2003) or FOXP1 (Hamdan et al., 2010).

Whole-genome microarray studies allowed the identification of copy number variants, such as duplications and deletions (Sebat et al., 2007). They affect many loci and contribute to other ~5% of ASD cases (Abrahams and Geschwind, 2008; Betancur, 2011). More recently, the whole-exome sequencing on large ASD cohorts has revolutionized gene discovery. These studies have pinpointed about 120 new ASD risk genes with *de novo* coding single nucleotide variants (SNVs) and *de novo* insertion deletions (indels) (De Rubeis et al., 2014; Iossifov et al., 2014).

Overall, according to current estimates, perhaps more than 1000 risk genes are likely to be involved in ASD (De Rubeis and Buxbaum, 2015; Geschwind and State, 2015; Willsey and State, 2015). The entire database of known genes with a risk factor linked to ASD can be found in Simons Foundation Autism Research Initiative (SFARI) website (http://sfari.org/).

2.4. Environment

Although genetic mutations contribute to a sizeable amount of occurrences of ASD, recent estimates suggest that 50–60% of the risk of ASD is unaccounted for, which implies that environmental factors contribute substantially to the risk of this disorder (Estes and McAllister, 2015) (Figure 2). Consistent with this idea is the fact that almost all genetic risk factors for ASDs can be found in unaffected individuals (Robinson et al., 2016) and twin studies equally provided evidence for genetics and environmental factors in ASD risk (Sandin et al., 2014).

A wide range of environmental factors have been proposed to contribute to ASD causality (Grabrucker, 2012; Homberg et al., 2016). The list, which is expanding given our greater understanding of the disorder, according to most up-to-date research includes the following factors:

- ***Pre-natal:*** Failures in early fetal brain development have been linked to a higher risk of ASD, for instance, maternal nutrient deprivation, toxins (Negi et al., 2010), stress (Kinney et al., 2008), maternal immune activation (MIA) by infection or autoimmune disease (Estes and McAllister, 2016; Ornoy et al., 2015).
- ***Post-natal:*** Brain development lasts throughout adolescence and many factors can hinder this process, for instance, gut microbiome (Sharon et al., 2016) immune system abnormalities, allergies, infection (Estes and McAllister, 2015) and exposure of children to drugs or toxins (Yasuda et al., 2011).

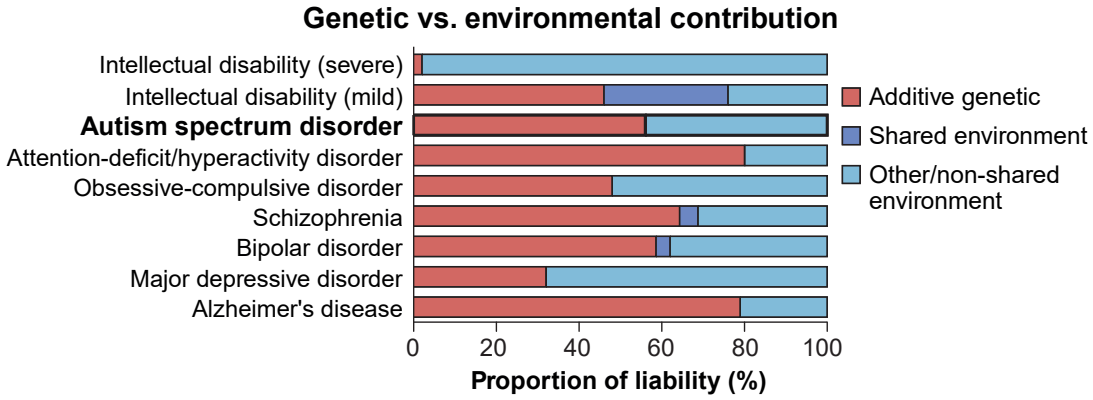

Figure 2: Genetic and environmental contribution to liability for neuropsychiatric disease. Liability estimates are compiled for various neuropsychiatric disorders (ASD in bold) derived from large-scale twin and/or population-based studies (Gandal et al., 2016).

Overall, it appears likely that in the majority of cases, genetic risk entails a predisposition to ASD, while its actual onset requires a further environmental reason (Nardone and Elliott, 2016). Therefore, it is essential to identify in idiopathic ASD altered regulators, able to orchestrate the expression of multiple ASD susceptibility genes along normal and altered neurodevelopment.

3. CPEB-MEDIATED TRANSLATIONAL CONTROL

3.1. mRNA processing and translational control

mRNA translational control in eukaryotic cells allows rapid alteration of protein concentrations for maintaining homeostasis or modulating changes (Buffington et al., 2014). Gene expression begins with the synthesis of mRNA (pre-mRNA) from the DNA template by RNA polymerase II. The path from transcription to translation includes many steps of regulation that make crucial contributions to accurate gene control (Huang et al., 2015; Jarvelin et al., 2016). They can be summarized:

mRNA processing: maturation often occurs during mRNA synthesis in the nucleus (Bentley, 2014; Darnell, 2013). This process include: *capping*; a 7-methylguanosine cap to the 5‘ (Ramanathan et al., 2016), *splicing*; the removal of introns and ligation of exons (Alpert et al., 2016) and formation of a 3‘ end by cleavage and addition of a poly(A) tail; *polyadenylation* (Di Giammartino et al., 2011).

Transport: mature mRNA associate with a wide variety of proteins to make a particle called, messenger ribonucleoproteins (mRNPs) (Bentley, 2014). This particles are competent for export to the cytoplasm by nuclear pore complexes (Katahira, 2015).

Translation: once in the cytoplasm, mRNAs are circularized, and they are the common target of translational control (Weill et al., 2012). mRNA translation can be divided in three regulated phases:

- In the ***initiation***, the ribosomes bind to the mRNA and scan the 5’ untranslated region (UTR) until they find the initiation AUG start codon. Most regulation is exerted at this first stage (Sonenberg and Hinnebusch, 2009).
- Then, polypeptide chain is elongated. Despite the simplicity of ***elongation***, regulation can and does occur (Richter and Coller, 2015).
- Finally, ***termination*** occurs in response to a stop codon and the polypeptide chain is released from the mRNA and ribosome, whose recycling is controlled. (Jackson et al., 2012).

3.2. Translation control by changes in poly(A) tail length

In the nucleus, most of mRNAs acquire a non-templated poly(A) tail of 250–300 adenine residues, fundamental for mRNA stability and nuclear export. The pre-mRNA includes cis-acting regulatory sequences and auxiliary trans-acting factors that indicates specific poly(A) site (PAS) (Curinha et al., 2014). The most important

cis-element is the conserved hexanucleotide (Hex), mainly consisting of AAUAAA or AUUAAA located 10–30 nucleotides upstream of the PAS (Shi and Manley, 2015).

In the cytoplasm, poly(A) tail acts synergistically with the 5′ cap to facilitate translation initiation. Nuclear polyadenylation occur by default, but subsequent control of its length is highly regulated both in the nucleus and in the cytoplasm, thereby contributing to the regulation of the stability, transport and translation (Weill et al., 2012). Thus, many mechanisms and factors involved in regulating nuclear and cytoplasmic polyadenylation have been identified:

Alternative polyadenylation (APA) is a widespread mechanism that allows a single gene to encode multiple mRNA transcripts. Pre-mRNAs, are cleaved and polyadenylated in more than one site, thus generating 3′ UTRs of different lengths (Di Giammartino et al., 2011).

Deadenylation can be followed by decapping and mRNA degradation (Parker and Song, 2004). However transcripts with short poly(A) can also be stable but in a translationally silent state that can be reactivated by cytoplasmic ***polyadenylation*** (Weill et al., 2012; Zhang et al., 2010).

3.3. Cis-tras -acting element in polyadenylation

Regardless of the final outcome, whether mRNA degradation or translational silencing o reactivation, de- or poly-adenylation is carried out through a complex combinatorial arrangement of *cis-acting* regulatory sequences. These sequences are specifically recognized and regulated by a large number of *trans-acting* factors, which can be RNA-binding proteins (RNABP) or noncoding RNAs. Most of these regulatory sequences reside in the 3′ untranslated region (UTR) but they are also present in the 5′ UTR or even in the open reading frame (ORF) (Charlesworth et al., 2013; Weill et al., 2012). For example:

AU-rich elements (ARE) consisting mainly of AUUUA pentamer repeats, which are recognized by different ARE-binding proteins such as TTP or ELAV1 (Khabar, 2016).

Pumilio-binding sites are sequences in the 3′ UTR containing a conserved UGUR (R is a purine) sequence which are recognized by Pumilio and FBF (PUF) family members (Wang et al., 2013).

Cytoplasmic polyadenylation elements (CPE) consisting of the $UUUUA_{1-3}U$ sequence and they are recognized by the CPE binding (CPEB) proteins (Villalba et al., 2011).

3.4. CPEB-family of proteins

The cytoplasmic polyadenylation element binding (CPEB) proteins are RNABPs which regulate the length of the poly(A) tail and the pseudocircularization of the mRNA (Fernandez-Miranda and Mendez, 2012).

The CPEB-family of proteins is composed of four paralogs in vertebrates (CPEB1-4), where CPEB1 constitutes a distant branch of the family and CPEB2-4 are closely related each other (Wang and Cooper, 2010). CPEB orthologs are present in other species but in different numbers, such as Orb 1-2 in *Drosophila* (Stepien et al., 2016), cpb1-3 and fog-1 in *C. elegans* (Lamont and Kimble, 2007) or CPEB in *Aplysia* (Si et al., 2003b). Exon structures of CPEB orthologs among vertebrates are almost identical, and the phylogenetic tree clearly demonstrated that they are better conserved across species than across paralogs (Wang and Cooper, 2010) (Figure 3). This high conservation between species indicates that natural selection operates against the deleterious effects of allelic variants (Omer et al., 2016).

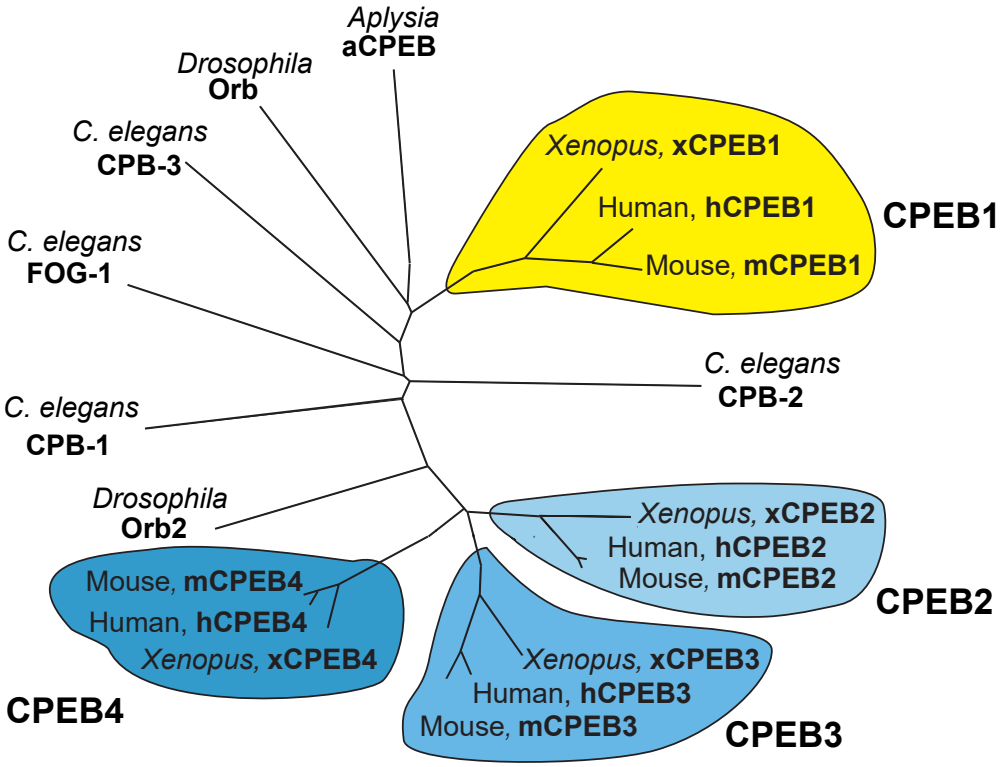

Figure 3: CPEB family of RNA-binding proteins. Phylogenetic tree of the most representative CPEB proteins based on a multiple sequence alignment using complete protein sequences. CPEB1 in vertebrate (yellow) is the most distant member of the family. However, CPEB2-4 (blue) are closely related and placed in the same branch. Modified from Fernandez-Miranda and Mendez, 2012.

All CPEB proteins have a similar structure. The carboxyl-terminus domain is conserved in all CPEB proteins, it is composed by two RNA recognition motifs (RRMs) and two zinc-finger (ZnF) like motifs (Tsuda et al., 2014). The N-terminal is a regulatory domain which is highly variable among CPEBs (Fernandez-Miranda and Mendez, 2012) (Figure 4). A number of reports have shown that CPEBs may bind the same mRNAs, both in vertebrates (Novoa et al., 2010) and in *Drosophila* (Stepien et al., 2016). mRNAs require two *cis-acting* sequences in the 3'UTR to recruit CPEBs, the conserved Hex and the nearby consensus or non-consesus CPE sequences (Pique et al., 2008). This suggests that different CPEBs may act differently at the regulation of the same transcripts.

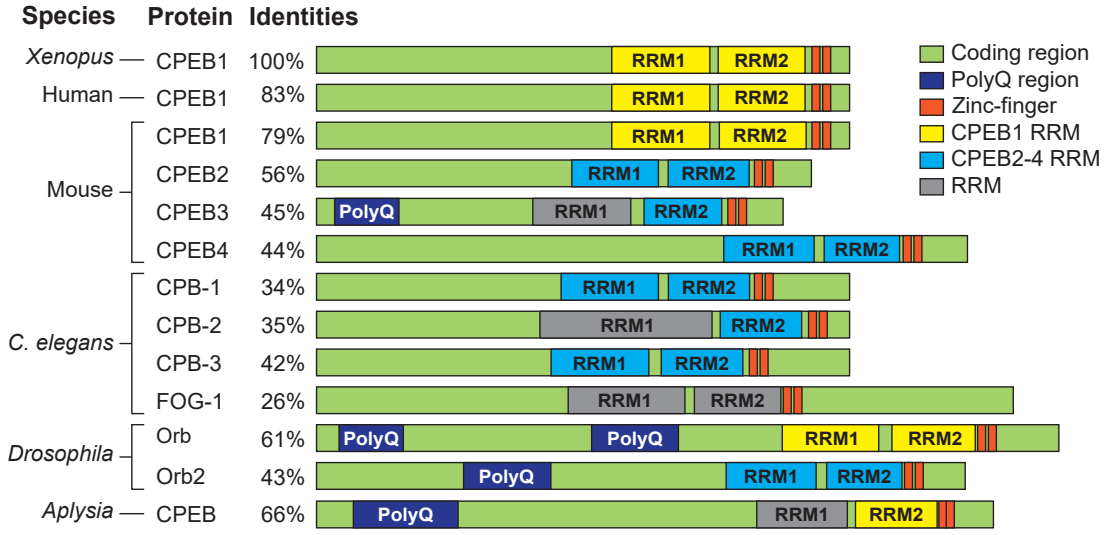

Figure 4: Structural comparisons among CPEBs from several species. CPEBs share a conserved RRMs (RNA recognition motifs) and zinc-fingers (ZnFs) at the C-terminal. PolyQ refers to polyglutamine rich stretches. The percent identities refer to comparisons relative to Xenopus CPEB1. Modified from Ivshina et al., 2014.

3.5. Regulation of CPEB levels and activities

Up to 30%-40% of genes have functional CPEs and be CPEB-regulated although in different spatiotemporal patterns. CPEBs have dual functions as translational activators (poly(A) elongation) or repressors (stored mRNA in a silent state) (Figure 5). Furthermore, the CPEs define a combinatorial code, based on their number and distance to the PAS, as well as the presence of additional *cis-acting* elements, to determine the spatiotemporal translation pattern (Pique et al., 2008).

Moreover, CPEBs are subjected to different regulatory signals. CPEB1 is phosphorylated by Aurora kinase A, CDC2 (Mendez et al., 2002; Mendez et al., 2000) and Ca^{2+}/calmodulin-dependent protein kinase II (CaMKII) (Atkins et al., 2005; Atkins et al., 2004), while CPEB4 activity is regulated by ERK2 and CDK1-mediated

phosphorylation. Unphosphorylated CPEB4 sequesters CPE-containing mRNAs into inactive liquid-like droplets but when it is hyperphosphoryated CPEB4 is kept in a monomeric and active state (Guillen-Boixet et al., 2016).

On the other hand, CPEB3 is regulated by SUMOylation (Drisaldi et al., 2015), phosphorylation (Kaczmarczyk et al., 2016), and by Neuralized1-mediated monoubiquitination (Pavlopoulos et al., 2011) apart from being degraded by Calpain2 (Wang and Huang, 2012).

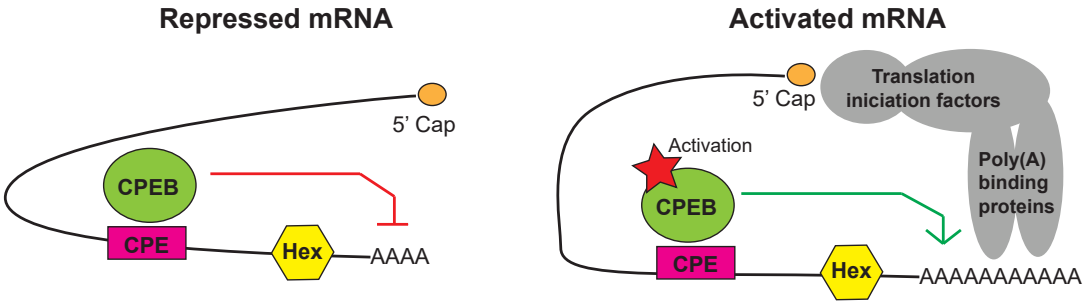

Figure 5: CPEB-mediated translational repression and activation. CPEB proteins are shown as a circle and CPE and the Hex sequences are indicated as a square and hexagon, respectively. Binding of CPEBs to CPEs induce the formation of a repressed closed-loop of mRNA. When CPEBs are activated (red star) promote cytoplasmic polyadenylation resulting in efficient translation.

Also, CPEBs autoregulate themselves or by other CPEB, for example CPEB4 is translationally activated by CPEB1 (Igea and Mendez, 2010) and by a feed-back loop (Calderone et al., 2016). In addition, all CPEBs express more than one isoform generated by alternative splicing. These different variants affect both the ORFs and the UTRs and are evolutionarily conserved (Theis et al., 2003; Wang and Cooper, 2010). Different isoforms vary their regulation, functions, and even their tissue specificity (Johnson et al., 2015; Kaczmarczyk et al., 2016; Skubal et al., 2016). Thus, increasing the level of complexity in translational control exerted by the CPEB-family.

Apart from their well described role in cytoplasmic poly(A) tail length regulation, CPEBs have been also implicated in nuclear functions. All CPEB proteins shuttle to the nucleus (Kan et al., 2010). There, CPEB1 mediates pre-mRNA alternative polyadenylation site and alternative splicing (AS) (Bava et al., 2013; Lin et al., 2010), and CPEB4 nuclear accumulation is correlated with reduced programmed cell death in response to endoplasmic reticulum stress (Kan et al., 2010).

3.6. CPEB-mediated processes and pathways

In addition to the well established role of CPEBs in oogenesis, they regulate many biologicals processes (Ivshina et al., 2014).

Cell proliferation, senescence and cancer. CPEBs are very important for meiotic and mitotic temporal translational control (Kim et al., 2011; Novoa et al., 2010). Surprisingly, despite their proliferative function, they also can induce senescence (Burns et al., 2011; Xiaoping et al., 2013). Finally, CPEBs has been linked to tumor growth, invasiveness or angiogenesis, however, different CPEBs appear to play diverse roles in cancer, as tumor suppressors or oncogenic effects (Chen et al., 2016; Nagaoka et al., 2016; Ortiz-Zapater et al., 2011).

Metabolism. Evidence linking CPEB1 and CPEB4 to metabolism has been reported. CPEB1-deficient human fibroblasts show enhance rates of glycolysis (Burns and Richter, 2008) and CPEB1 KO display aberrant glucose metabolism (Alexandrov et al., 2012) and deficient brain mitochondrial ATP production (Oruganty-Das et al., 2012). Recently, it was found that CPEB4 is required for adaptation to high-fat-diet- and ageing induced endoplasmic reticulum stress (Maillo et al., 2017).

Development. CPEBs have been studied in depth in oocyte maturation (Reyes and Ross, 2016), and have been demonstrated that they play important role in *Drosophila* (Hafer et al., 2011), *C.elegans* (Kimble and Crittenden, 2007) and also mouse development (Sousa Martins et al., 2016) with CPEB4 being expressed at high levels in the developing brain and spinal cord (Shin et al., 2016; Theis et al., 2003).

3.7. CPEB functions in the nervous system

The four CPEB paralogs are widely expressed in brain (Lein et al., 2007; Theis et al., 2003) where they play important roles. Proof of this is that all KO mice of each CPEB show neurological alterations. ***CPEB1 KO*** mice show perseverative hippocampal-dependent memory and defects in long-term potentiation (Alarcon et al., 2004; Berger-Sweeney et al., 2006). ***CPEB2 KO*** mice show alteration of cholinergic neurons (Lai et al., 2016). ***CPEB3 KO*** mice exhibit enhanced hippocampal-dependent short-term memory (Chao et al., 2013). Finally, ***CPEB4 KO*** pyramidal neurons possess slightly elongated dendritic spines (Tsai et al., 2013).

3.7.1. CPEBs in synaptic plasticity

The implication of CPEBs in synaptic plasticity is well known. Synaptic plasticity is the term applied to the ability of synapses to undergo morphological and biochemical changes in response to stimulation. Neurons have the capacity to distinguish between synapses that have been stimulated (experienced) versus those that have not (naïve) (Ivshina et al., 2014; Richter, 2007).

Many forms of long-term synaptic plasticity require local protein synthesis in the post-synaptic compartment (Sutton and Schuman, 2006). CPEB1 associates with kinesin and dynein that transport mRNAs to dendrites (Huang et al., 2003). Also, CPEBs and other components of cytoplasmic polyadenylation machinery are present in dendrites (Udagawa et al., 2012; Wu et al., 1998) where they trigger mRNA-specific polyadenylation and local translation (Huang et al., 2006; Pavlopoulos et al., 2011).

The half-life of newly synthesized proteins is short and it cannot explain the persistence of synaptic plasticity. Some groups suggested that CPEB, at least in *Aplysia* (Si et al., 2010) and *Drosophila* (Khan et al., 2015) might form a prion in neurons and be self-propagated and extremely long-lived, thus constituting a tag at activated synapses. This is possible because *Aplysia* CPEB (Si et al., 2003a; Si et al., 2003b), *Drosophila Orb2* (Majumdar et al., 2012) and mammaliam CPEB3 (Stephan et al., 2015) contain a prion-like poly Q/N-rich regions and form amyloid-like aggregates that would act as prions.

3.7.2. CPEBs and neurological disease

There is no evidence of CPEBs being directly implicated with in neurological disease. However, a mouse model that expresses an artifactual (or aberrant) low complexity domain of CPEB4 protein shows impaired motor axon branching and abnormal neuro-muscular formation suggesting a potential implication of CPEB4 in neurodevelopmental disease (Shin et al., 2016).

Also, *FMRP* (fragile-X mental retardation protein) KO mice show fragile X syndrome (FXS) features that are rescued in FMRP/CPEB1 double KO mice (Udagawa et al., 2013). FXS is a monogenic form of autism that it is caused by inactivation of the *FMR1* gene (Verkerk et al., 1991). In the absence of FMRP, protein synthesis is elevated by 15–20%, which is likely causative for the syndrome (Darnell and Klann, 2013). The protein synthesis in double FMRP/CPEB1 KO mice is normal suggesting that translational homeostasis was restored (Udagawa et al., 2013).

4. EVIDENCE LINKING CPEBS TO NEUROLOGICAL DISEASE

4.1. CPEBs and HD

We reasoned that altered CPEB function might contribute to HD based on the following evidence:

First. Spinocerebellar ataxia type 3 (SCA3) is the most common dominantly inherited ataxia and it is caused by CAG repeat expansion (encoding polyQ) in *ATXN3* gene (Ikeda et al., 1996). Genome-wide screen for suppressors or enhancers of pathogenic polyQ Ataxin-3 in a *Drosophila* SCA3 model showed that overexpression of orb2 (CPEB2-4 ortholog) is a suppressors of retinal degeneration (Bilen and Bonini, 2007). A later study showed that upregulation of orb2 rescued abnormal wing posture and locomotor defects and ameliorates the retina degenerative effect of SCA3 fly models (Shieh and Bonini, 2011).

Second. Interestingly, CPEB3, *Drosophila* orb2 and *Aplysia* CPEB, contain a polyQ domain that confer them prion-like properties (Majumdar et al., 2012; Raveendra et al., 2013; Stephan et al., 2015) important for the maintenance of long-term memory (Khan et al., 2015; Si et al., 2010).

Third. Several studies have linked brain-derived neurotrophic factor (BDNF) and HD with major loss of BDNF protein in HD brain probably contributing to the clinical manifestations of the disease (Zuccato and Cattaneo, 2014). In cultured neurons it was found that *BDNF* mRNA is associated with HTT and CPEB1 (Ma et al., 2010). *BDNF* mRNA has two cis-acting CPE motifs in its 3'UTR (Oe and Yoneda, 2010) and they are required for dendritic targeting by binding to CPEB1 (Baj et al., 2016; Vicario et al., 2015).

Forth. Microarray and gene ontology (GO) differential analysis of mRNAs associated with polysomes in wild type (WT) and CPEB1 KO mouse embryonic fibroblasts revealed that HD related genes are prevalent among those mistranslated in the absence of CPEB1 (Alexandrov et al., 2012).

Fifth. mRNAs associated with CPEB4 were previously identified by RNA immunoprecipitation (RIP) from human pancreatic cancer cells (RWP-1) (Ortiz-Zapater et al., 2011) and by GO analysis we found that HD related genes as the second category both in number and significance (Figure 6).

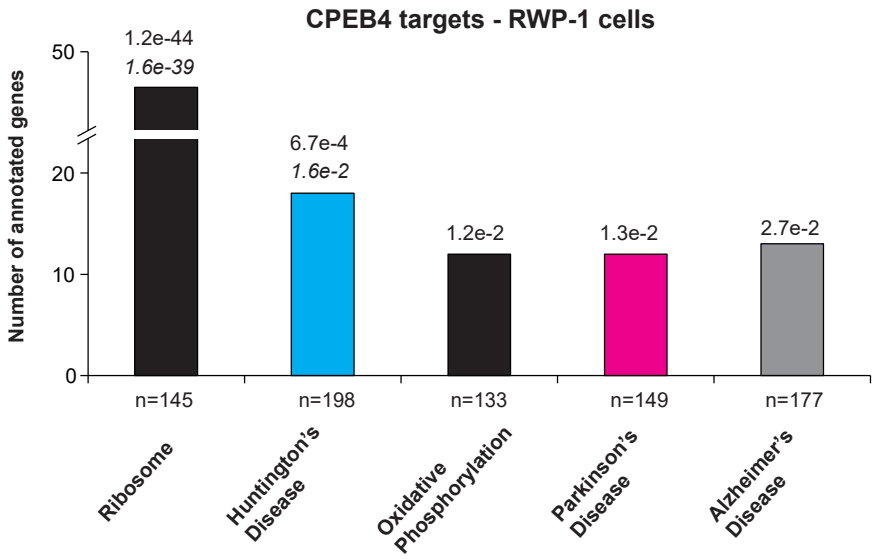

Figure 6: GO analysis of CPEB4 targets from RWP-1 cells. Gene count histogram from gene ontology using DAVID functional analysis of CPEB4 coimmunoprecipitated mRNAs from RWP-1 cells (Ortiz-Zapater et al., 2011). Total number of annotated genes per category represented under bars. Significative p-values and Benjamini-Hichberg in italic, above the bars.

4.2. CPEBs and ASD

In view of these lines of evidence linking CPEB and HD, the first aim of this thesis was to explore the status of CPEBs in HD and the potential genome-wide poly(A) tail changes of target mRNAs. Strikingly, this serendipitously led us to discover that most autism risk genes are targets of CPEB4, which originated the corresponding hypothesis that CPEB4 could be implicated in ASD etiology. Indeed, this fits with the fact that CPEB4 is expressed at high levels in developing brain (Shin et al., 2016; Theis et al., 2003).

OBJETIVES

1. Analysis of CPEBs in human and mouse HD brain.

2. Analysis of global poly(A) tail changes in R6/1 mouse model of HD.

3. Determine the relative contribution of CPEB1 and CPEB4 to poly(A) changes in HD and find CPEB dependent pathways and gene modules.

   Then, unbiased observation of enrichment of ASD risk genes within CPEB4-regulated transcripts, originated the following:

4. Study the possible alteration of CPEB4 in idiopathic ASD brain and its potential pathological implication.

5. Generation of different mouse models that mimic the CPEB4 alterations found in idiopathic ASD for subsequent poly(A) analysis.

6. Characterize ASD-like phenotype in CPEB4-modified mouse models.

RESULTS

1. ANALYSIS OF CPEBS IN HUMAN AND MOUSE HD BRAIN

1.1. Analysis of protein and mRNA levels of CPEBs in HD brain

To determine whether misregulation of CPEBs could contribute to HD, we first analyzed their levels by western blot in postmortem brain samples from human control and HD subjects. In St, the most affected region in HD, we observed a dramatic increase (453%, p=0.037) of CPEB1 and an almost total disappearance of CPEB4 (83% decrease, p=0.001), but no significant changes in the levels of CPEB2 or CPEB3 proteins (Figure 7).

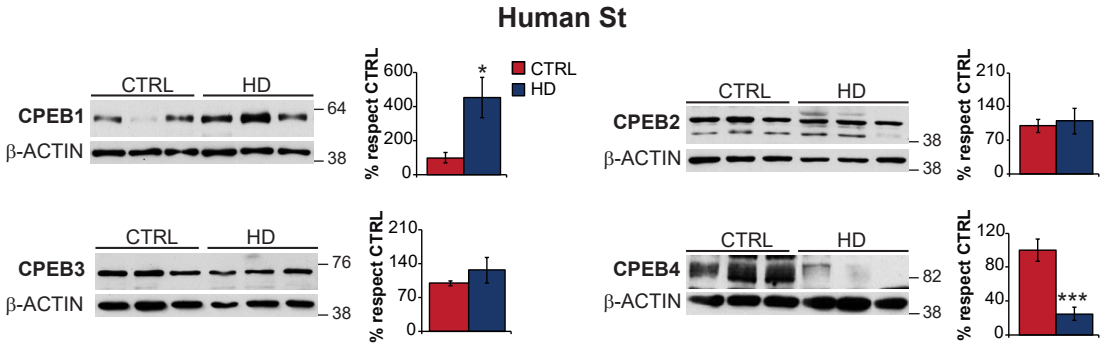

Figure 7: Western blot analysis of CPEBs in human St. Levels of CPEB1, CPEB2, CPEB3 and CPEB4 protein in controls (n=4-5) and HD patients (n=5-6) striatum. Data are shown as mean ± SEM. * p < 0.05, *** p < 0.001.

We then analyzed the R6/1 transgenic mouse model of expanded CAG/polyQ disease that ubiquitously expresses N-terminal Htt with 115 CAG repeats and develops a rapidly progressing disease phenotype (Mangiarini et al., 1996). As for human HD brain, we observed increased CPEB1 (159%, p=0.018) and decreased CPEB4 (35% decrease, p=0.04) levels in St of R6/1 mice with no significant changes in the levels of CPEB2 or CPEB3 (Figure 8).

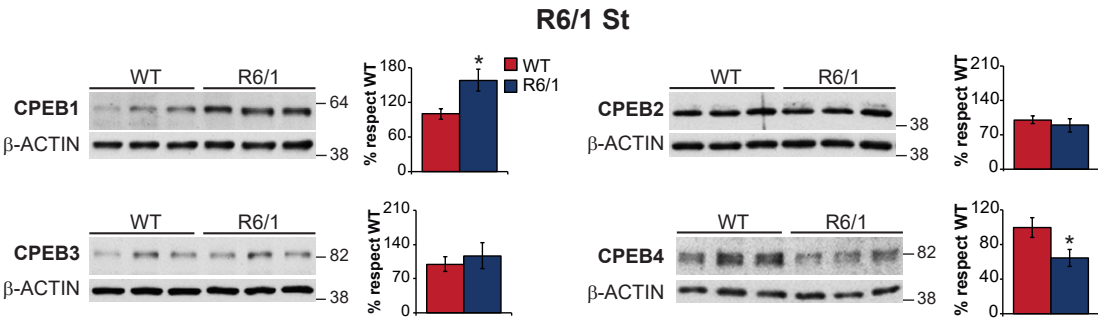

Figure 8: Western blot analysis of CPEBs in R6/1 mice St. Levels of CPEB1, CPEB2, CPEB3 and CPEB4 protein in WT (n=7) and R6/1 mice (n=7) striatum. Data are shown as mean ± SEM. * p < 0.05.

Similar results were observed in St of the slow disease progression HD94 mice (Figure 9A) that express N-terminal Htt with 94 CAG repeats in forebrain neurons (Diaz-Hernandez et al., 2005; Yamamoto et al., 2000). However, in HD94 mice and in the also slow disease progression zQ175 knock-in mouse model of HD (Menalled et al., 2012), only the decreased CPEB4 levels reached statistical significance (Figures 9A-B), thus suggesting that changes in CPEB4 might precede changes in CPEB1.

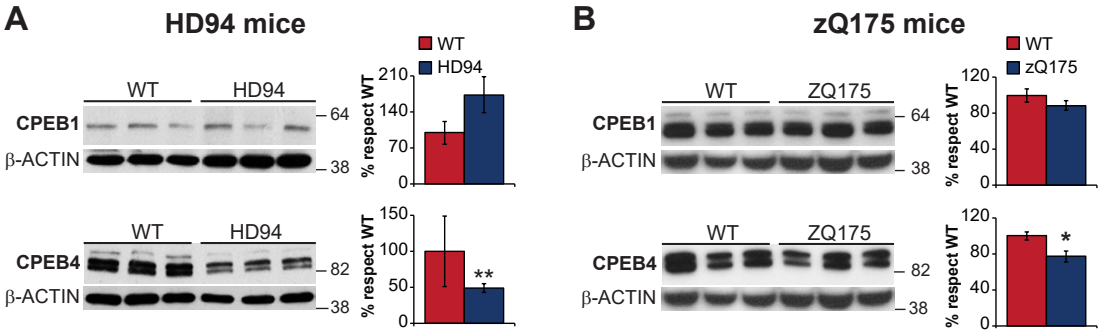

Figure 9: Western blot analysis of CPEBs in St of HD mouse models. Levels of CPEB1 and CPEB4 protein, (A) in WT (n=8) and HD94 mice (n=6), (B) in WT (n=6) and zQ175 mice (n=6) striatum. Data are shown as mean ± SEM. * $p < 0.05$. ** $p<0.01$.

In general, the described imbalance in CPEB1/CPEB4 protein levels in St of HD patients and R6/1 mice did not correlate with matching alterations of their transcript levels (Figures 10A-B).

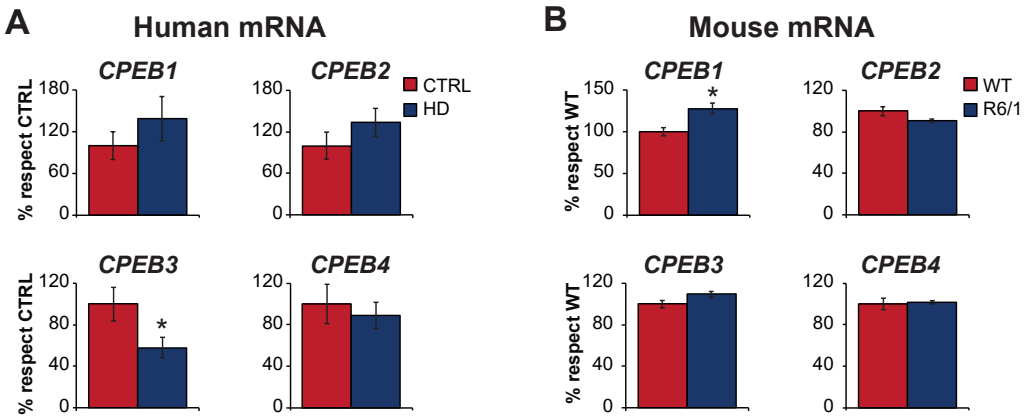

Figure 10: qRT-PCR analysis of CPEBs in St of HD patients and R6/1 mice. mRNA levels of CPEB1, CPEB2, CPEB3 and CPEB4 (A) in human (n=5 for control and n=9 for HD patients) and (B) mouse (n=7 for WT and R6/1 mice). Data are shown as mean ± SEM. * $p < 0.05$.

Conclusion: St from HD patients and mouse models showed a CPEB1/CPEB4 imbalance, being CPEB1 levels increased and CPEB4 decreased. These protein levels do not correlate with transcripts levels, suggesting a posttranscriptional regulation.

1.2. Analysis of pattern of CPEBs in HD brain

In good agreement with its RNP activity, CPEB4 is found in a cytoplasmic punctate pattern in mouse brain tissue. When we compared WT and R6/1 mice, the St decrease in CPEB4 levels was also evident in R6/1 mice (Figure 11).

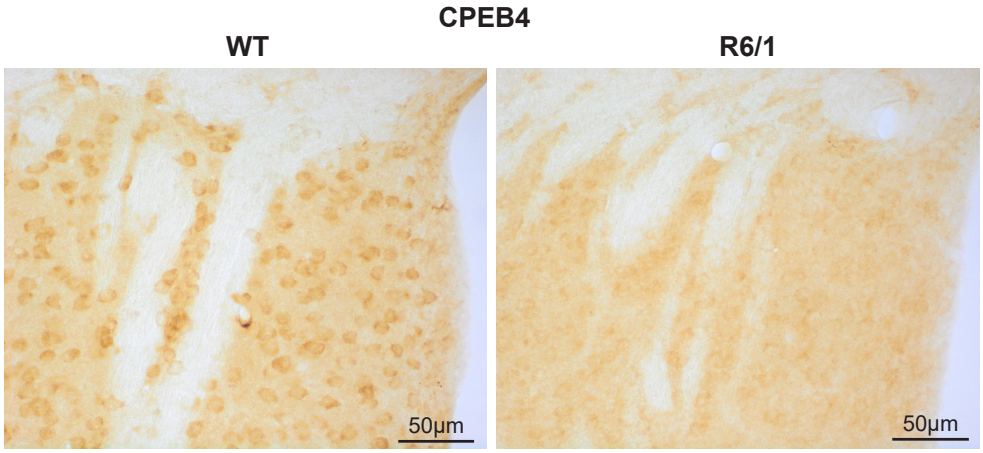

Figure 11: CPEB4 pattern in mouse St. CPEB4 expression determined by immunohistochemistry in sagittal sections of WT and R6/1 mice St. The scale bar indicates 50 µm.

However, we did not found evidence of CPEB4 was sequestered into the characteristic polyQ-containing IBs of HD tissue (Figure 12).

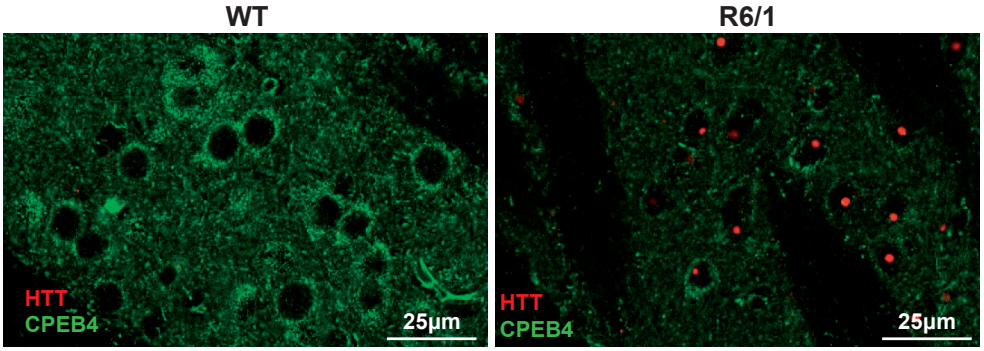

Figure 12: CPEB4 is not sequestered in HD inclusion bodies. Double Immunofluorescence with antibodies to CPEB4 (green), and HTT IBs (red) in sagittal sections of WT and R6/1 mice St.

Since CPEB3 is specifically known to aggregate through its Q-rich N-terminal domain, we also performed immunostaining for CPEB3 both in human HD and R6/1 tissue and controls. This revealed similar CPEB3 level and distribution between HD and control samples and no accumulation into IBs (data not shown).

Conclusion: CPEB4 level by IHC shows a dramatic decrease in R6/1 St and no evidence of any of the CPEBs being sequestered in characteristic IBs of HD mice.

2. ANALYSIS OF GLOBAL POLY(A) CHANGES IN R6/1 MOUSE MODEL OF HD

2.1. Genome-wide poly(A) alteration by poly(U) chromatography and microarray analysis

The main function of CPEBs is to regulate the cytoplasmic polyadenylation. To explore whether altered CPEBs levels in HD resulted in polyadenylation alteration of target mRNAs, we analyzed genome-wide the poly(A) tail length changes associated with HD in the R6/1 mouse model. For this, we performed poly(U) chromatography on RNA purified from St of WT and R6/1 mice. Differential elution with 25 and 90% formamide yields two fractions of RNAs with, respectively, short and long poly(A) tails which were analyzed by microarray hybridization (Figure 13).

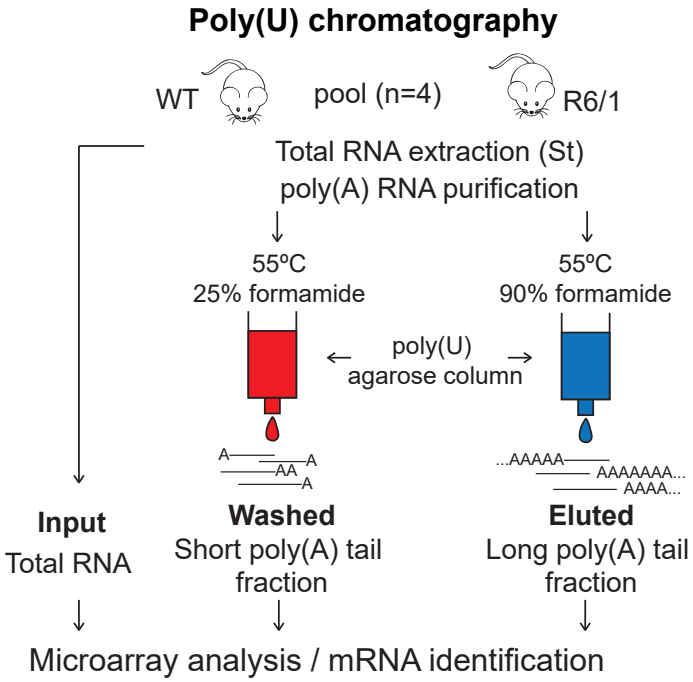

Figure 13: Chromatography and microarray analysis. Schematic view of the procedures for the poly(U) chromatography experiment from St of WT and R6/1 mice 7 month-old.

Altogether, transcripts of 3,968 genes are differentially polyadenylated in R6/1 vs. WT mice: 1,980 transcripts whose poly(A) tails get shortened and 1,988 transcripts whose poly(A) tails get lengthened in R6/1 mice (Figures 14A-B).

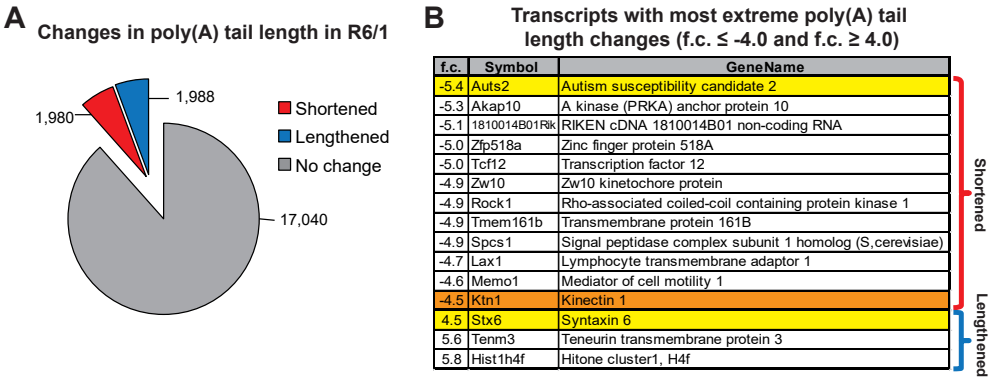

Figure 14: mRNA with most extreme poly(A) tail changes in R6/1 mice. (A) Pie chart of differentially polyadenylated transcripts, shortened (red) or lengthened (blue), in R6/1 mice. (B) Transcripts whose poly(A) tail is shortened (f.c. ≤ -4.5) or lengthened (f.c. ≥ 4.5) in St of R6/1 vs. WT mice. In yellow, genes for which poly(A) tail alteration correlates with altered protein levels as verified by western blot. In orange, gene identified by data mining as linked to striatal atrophy.

The gene with the most extreme poly(A) tail shortening in HD mice is autism susceptibility candidate 2 (AUTS2) (Figure 14B). We then tested whether this correlates with altered protein levels in St of R6/1 mice. As expected, AUTS2 protein levels show a strong decrease in St of R6/1 mice without changes at the mRNA level (Figures 15A-B) and similar results were obtained with human striatal tissue samples from control and HD cases (data not shown). Among the genes with most prominent poly(A) tail elongation in R6/1 St, we analyzed syntaxin 6 (STX6) (Figure 14B) and we found a significant increase in its protein levels in the St of R6/1 mice that does not correlate with increased transcript levels (Figures 15A-B).

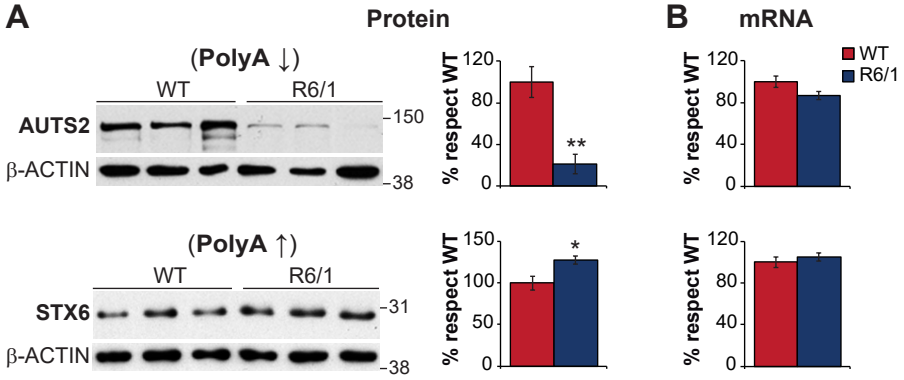

Figure 15: Western blot and qRT-PCR analysis of genes with the most extreme poly(A) tail changes in R6/1 mice. (A) Levels of AUTS2 and STX6 protein (n=7 for WT and R6/1 mice). (B) mRNA levels of for Auts2 and Stx6 (n=7 for WT and R6/1 mice). Data are shown as mean ±SEM. * $p < 0.05$, **$p<0.01$.

Conclusion: St of R6/1 mice shows a global transcriptomic poly(A) tail length alteration with 9.42% genes showing deadenylation and 9.46% elongation. The most affected transcripts show a concomitant change in the corresponding protein levels without changes in mRNA level. This suggests that CPEB1/CPEB4 imbalance impacts global poly(A) status which is associated to protein changes in St of R6/1 mice.

2.2. GO analysis of transcripts with poly(A) tail altered in R6/1

To explore whether the observed changes in poly(A) length in affected genes might be contributing to HD pathogenesis, we performed GO analysis on the 1,844 genes with poly(A) fold change (f.c.) above 2. This confirmed the expected enrichment in HD related genes anticipated by the enrichment observed for CPEB4 binding transcripts in pancreatic cancer cells, (Figures 6 and 16A). Strikingly, we also observed an even more significant enrichment for Alzheimer's disease (AD) related genes and also significant enrichment for Parkinson's disease (PD), as well as ubiquitin mediated proteolysis genes (Figures 16A-B).

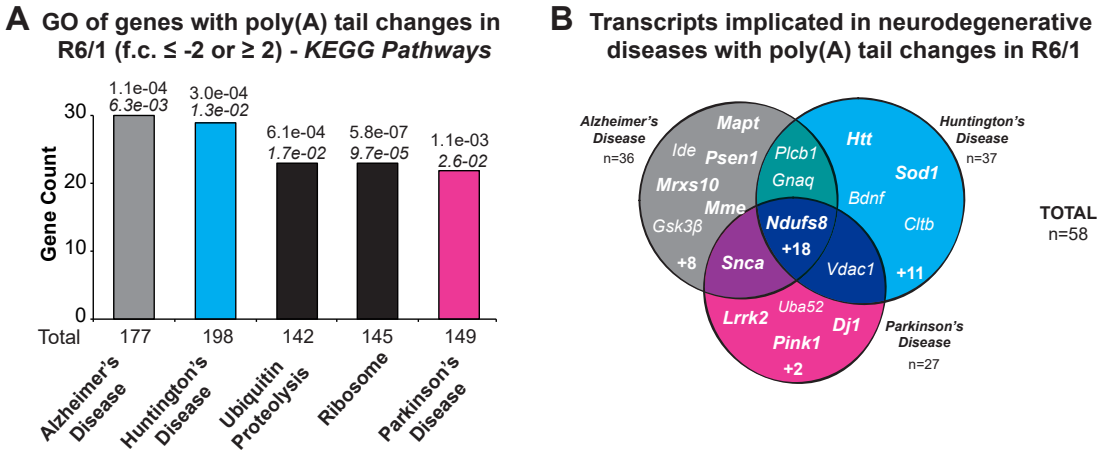

Figure 16: GO analysis of transcripts with poly(A) tail altered in R6/1 reveals neurodegeneration affected genes. (A) Gene count histogram from GO analysis using DAVID resources of mRNAs with changes in poly(A) tail length in R6/1 mice (f.c. ≤ -2 or ≥ 2). Total number of annotated genes per category represented under bars. Significative p-values and Benjamini-Hichberg in italic, above the bars. (B) Venn diagram of transcripts implicated in neurodegenerative diseases whose poly(A) tails are significantly shortened or lengthened in R6/1 (f.c. ≤ -1.5 or ≥ 1.5). Grey circle represents AD, blue HD and pink PD related genes.

Interestingly, among the 240 AD, HD and/or PD related genes that generate transcripts with altered poly(A) tail in R6/1 mice, many correspond to genes responsible for monogenic forms of familial neurodegenerative diseases such as *Psen1*, *Mapt*, *Scna*, *Lrrk2*, *Pink1*, *Park7*, *Sod1* and *Htt* itself (Hardy and Gwinn-Hardy, 1998; Klein and Westenberger, 2012). As well as to other genes highly implicated in HD pathogenesis such as *Bdnf* (Zuccato and Cattaneo, 2009) and in AD pathogenesis such as *Ide* (Nalivaeva et al., 2014) and *Gsk3*β which is involved in both diseases (Fernandez-Nogales et al., 2015; Hernandez et al., 2013) (Figure 16B).

Most importantly, lengthened poly(A) tail in transcripts of the AD related gene *Mapt* in R6/1 mice correlates with increased protein levels as previously described (Fernandez-Nogales et al., 2014). Similarly, shortened poly(A) tail in *Gsk3*β transcript corresponds to decreased protein levels as also showed (Fernandez-Nogales et al., 2015). Regarding PD related genes, shortened poly(A) tail in *Snca* transcript

corresponds to decreased protein levels (Figure 17). Also, bioinformatics analysis of the 3'UTR (Pique et al., 2008) show the presence of CPE sequences in all of these genes (Figure 17).

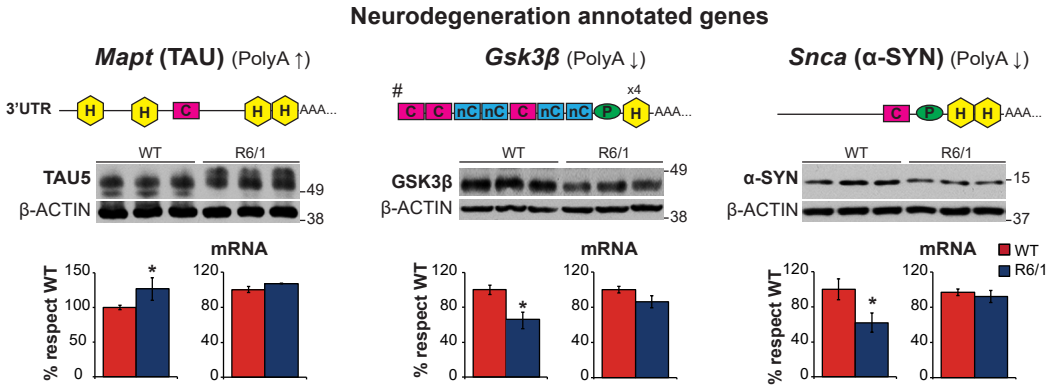

Figure 17: 3' UTR, western blot and qRT-PCR analysis of neurodegeneration annotated genes with poly(A) tail altered in R6/1. 3'UTR of *Mapt, Gsk3β* and *Snca* mouse genes (upper panels). # *Gsk3β* 3'UTR is only showed the 5' extreme. [C] = Canonical CPE, [nC] = Non-Canonical CPE, (P) = Pumilio binding element, {H} = Hexanucleotide. In lower panels, levels Mapt (TAU), GSK3β and Snca (α-SYN) protein and its mRNA levels in St of R6/1 mice (n=7 for WT and R6/1 mice).

Conclusion: St of R6/1 mice shows alteration of polyadenylation and protein levels of multiple neurodegeneration causing genes. These results therefore strongly support a causative role of CPEB dysfunction and global poly(A) tail length-alteration in HD and possibly also other neurodegenerative diseases and provide an explanation for the altered protein levels of multiple AD- and PD-related genes previously reported in HD in the absence of matching changes in their transcript levels.

2.3. Study of the striatal atrophy associated gene Kinectin 1 in HD brain

After seeing that altered polyadenylation in R6/1 prominently affects genes previously known to participate in the etiology of neurodegenerative diseases, we performed data mining in search of genes not previously annotated as neurodegeneration-causing and that might contribute to basal ganglia dysfunction or atrophy. Kinectin 1 (*Ktn1*) is one of the genes showing remarkable poly(A) tail shortening in R6/1 mice (Figure 14B). Interestingly, in a recent genome-wide association study of common variants that affect volume of subcortical regions, the strongest effect was found for the putamen in a locus that affects expression of *KTN1* and a direct correlation is found between *KTN1* expression in frontal cortex and striatal volume (Hibar et al., 2015b). As expected, bioinformatics analysis of the 3'UTR of both mouse and human *KTN1* genes revealed the presence of CPE sequences in both species and h*KTN1* is detected by the algorithm that predicts functional CPEs (Pique et al., 2008). We then found by western blot decreased KTN1 protein levels both in Cx and St of R6/1 mice and HD patients (Figure 18).

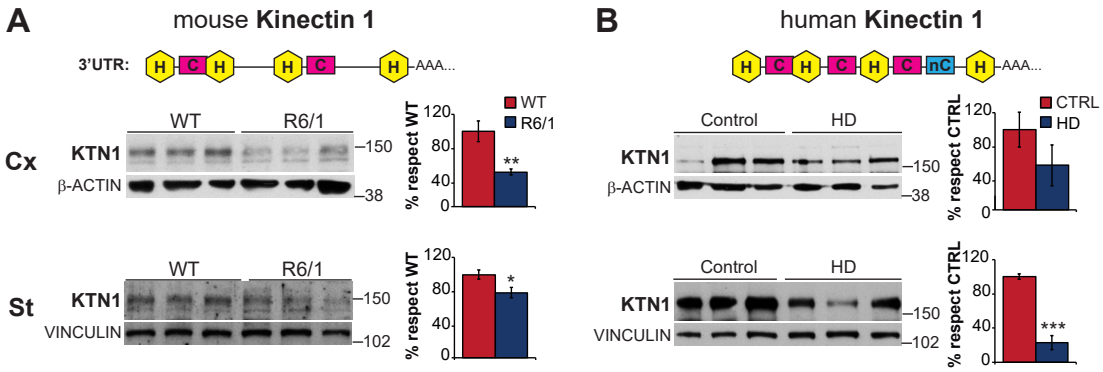

Figure 18: 3' UTR and western blot analysis of KTN1 in HD patients and R6/1 mice. *KTN1* 3'UTR of (A) mouse and (B) human genes. In lower panels, western blot analysis of mouse and human KTN1 protein levels in Cx (upper panels, n=7 for WT and n=6 for R6/1 mice and n=4 for controls and HD patients) and in St (lower panels, n=7 for WT and R6/1 mice and n=8 for controls and n=5 for HD patients). [C] = Canonical CPE, [nC] = Non-Canonical CPE, {H} = Hexanucleotide. Data are as mean ±SEM. * $p < 0.05$, ** $p < 0.01$, *** $p < 0.001$.

This HD-associated decrease is also evident by immunohistochemistry in both species and in both structures (Figure 19).

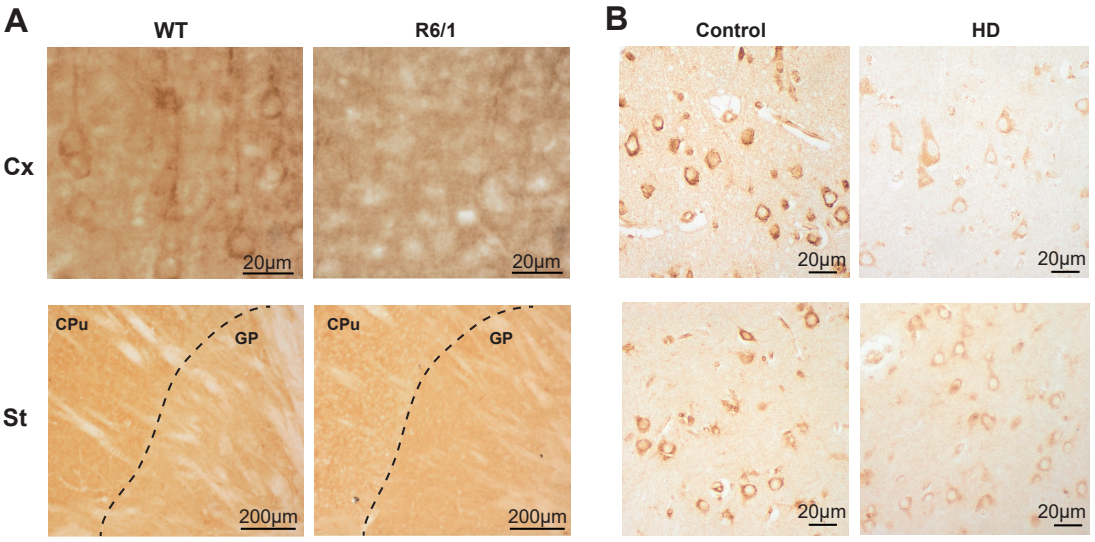

Figure 19: KTN1 pattern in HD patients and mice Cx and St. (A) KTN1 expression determined by immunohistochemistry in sagittal sections of WT and R6/1 mice Cx (upper panels) and St (lower panels). CPu = Caudate Putamen, GP = Globus Pallidus. (B) Immunohistochemistry of KTN1 expression in sections of formalin-fixed paraffin-embedded of human controls and HD patients Cx (upper panels) and St (lower panels).

Conclusion: *KTN1* is striatal atrophy associated gene that shows poly(A) shorting in R6/1 mice and presents functional CPEs. Protein levels of KTN1 are decreased in Cx and St of both, R6/1 mice and HD patients. These findings suggest that CPEB dependent alteration of polyadenylation may contribute to the prominent striatal atrophy of HD brains through inducing decreased protein levels of KTN1.

3. DETERMINE THE RELATIVE CONTRIBUTION OF CPEB1 AND CPEB4 TO POLY(A) CHANGES IN HD AND FIND CPEB DEPENDENT PATHWAYS AND GENE MODULES

3.1. CPEB1 and CPEB4 RNA immunoprecipitation and microarray analysis in St of WT and R6/1 mice

To determine the relative contribution of CPEB1 and CPEB4 to the mentioned poly(A) tail length changes or to find new pathways or modules CPEBs dependent, we performed RNA immunoprecipitation (RIP) followed by microarray analysis with striatal RNA from WT and R6/1 mice (Figure 20).

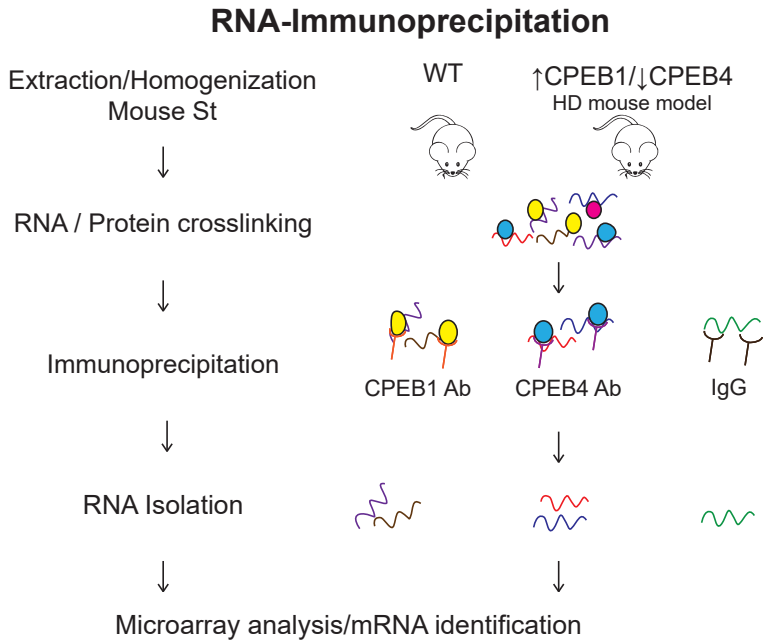

Figure 20: RNA-immunoprecipitation and microarray analysis. Schematic view of the RIP procedures on St RNA from WT and HD mice.

This genome wide identification revealed that, regardless of genotype, 7.9% of transcripts were bound only by CPEB4, 5.8% only by CPEB1 and 7.0% by both (Figure 21A). When we compared the CPEB-specific targets with the changes in polyadenylation linked to HD, the only observed biased distribution was for CPEB4-specific mRNAs, as these were enriched within the transcripts with shortened poly(A) tail (Figure 21B).

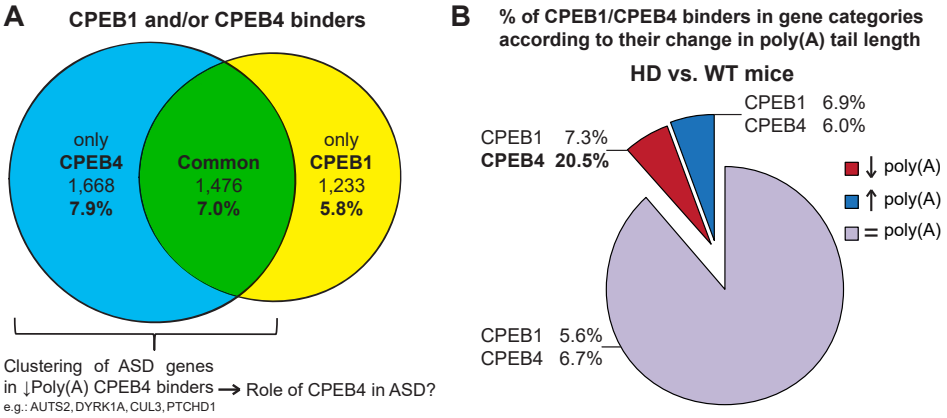

Figure 21: Comparison of CPEB1 and/or CPEB4 binders with transcripts with poly(A) tail changes in HD mice. (A) Number and percentage of CPEB1 and/or CPEB4 binders in St of WT and HD mice according to RIP experiment. (B) Percentage of CPEB1 only or CPEB4 only binders with shortened (red), lengthened (blue) and unaltered (purple) poly(A) tail in HD mice.

Interestingly, the largest fold change (f.c.) corresponded to the mRNA of *Auts2* (Figure 22A), a gene linked to ASD (Liu et al., 2015; Sultana et al., 2002). We then realized that transcripts from other high confidence ASD genes, like *Dyrk1a*, *Cul3*, and *Ptchd1* (Cat.1-2 in SFARI https://gene.sfari.org/autdb/GS_Home.do) were among the top forty CPEB4-targets with most prominent poly(A) shortening (f.c. ≤ -3.0). This enrichment of ASD risk genes is highly significant (29.7 fold enrichment, p= 2e-04; (Figure 22B).

A **CPEB4 binders with shortened poly(A) tail length (f.c. ≤ -3.0)**

Nº	Score	Symbol	Gene Name
1	-5.4	Auts2	Autism susceptibility candidate 2
2	-5.3	Akap10	A kinase (PRKA) anchor protein 10
3	-4.9	Rock1	Rho-associated coiled-coil containing protein kinase 1
4	-4.5	Ktn1	Kinectin 1
5	-3.9	Slk	STE20-like kinase
6	-3.9	Kpnb1	Karyopherin (importin) beta 1
7	-3.9	Ssr3	Signal sequence receptor, gamma
8	-3.8	Rp2h	Retinitis pigmentosa 2 homolog (human)
9	-3.8	Bach2	BTB and CNC homology 2
10	-3.7	Cpsf6	Cleavage and polyadenylation specific factor 6
11	-3.7	Pan3	PAN3 polyA specific ribonuclease subunit homolog
12	-3.6	Tmx3	Thioredoxin-related transmembrane protein 3
13	-3.6	Ube2d3	Ubiquitin-conjugating enzyme E2D 3
14	-3.6	Epha3	Eph receptor A3
15	-3.6	Zfx	Zinc finger protein X-linked
16	-3.5	Crbn	Cereblon
17	-3.4	Rnd3	Rho family GTPase 3
18	-3.4	Dyrk1a	Dual-specificity tyrosine-(Y)-phosphorylation regulated kinase 1a
19	-3.4	Hey2	Hairy/enhancer-of-split related with YRPW motif 2
20	-3.4	Mynn	Myoneurin
21	-3.3	Cers6	Ceramide synthase 6
22	-3.2	Klhl28	Kelch-like 28
23	-3.2	Plagl1	Pleiomorphic adenoma gene-like 1
24	-3.2	Dtwd2	DTW domain containing 2
25	-3.2	9630041G16Rik	RIKEN cDNA 9630041G16 gene
26	-3.2	Arl6ip6	ADP-ribosylation factor-like 6 interacting protein 6
27	-3.2	Ccdc88a	Coiled coil domain containing 88A
28	-3.2	Sp3	Trans-acting transcription factor 3
29	-3.2	Ctso	Cathepsin O
30	-3.2	Cul3	Cullin 3
31	-3.2	2810474O19Rik	RIKEN cDNA 2810474O19 gene
32	-3.1	Tmco5	Transmembrane and coiled-coil domains 5
33	-3.1	Camk4	Calcium/calmodulin-dependent protein kinase IV
34	-3.1	Zhx1	Zinc fingers and homeoboxes 1
35	-3.1	Cep290	Centrosomal protein 290
36	-3.0	Eif4a2	Eukaryotic translation initiation factor 4A2
37	-3.0	Wnt5a	Wingless-related MMTV integration site 5A
38	-3.0	Metap2	Methionine aminopeptidase 2
39	-3.0	Ptchd1	Patched domain containing 1
40	-3.0	Birc6	Baculoviral IAP repeat-containing 6

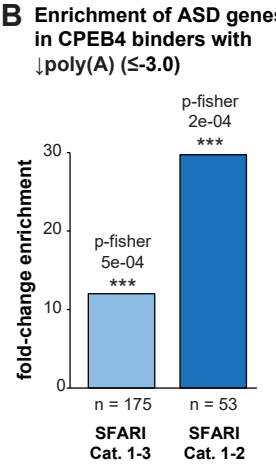

Figure 22: CPEB4 binders with the most shortened poly(A) tail. (A) Fold change (f.c), symbol and gene name and (B) Fold enrichment of high confidence ASD genes (SFARI Cat. 1-3 and Cat. 1-2) in CPEB4 binders in WT St whose poly(A) tail is shortened in an HD mouse model (f.c. ≤ -3.0). P-fisher value above bars. *** p<0.001.

Conclusion: Genes with shortened poly(A) tail in R6/1 mice show enrichment of CPEB4 binders. These CPEB4 targets with poly(A) shortening show a high enrichment of ASD risk genes. This serendipitous finding led us to hypothesize a role of CPEB4 in ASD gene expression.

3.2. Enrichment analysis of CPEB binders in functional co-expression modules and ASD risk genes

To further explore the potential of CPEB4 as a key mediator of gene expression reprogramming associated with ASD pathogenesis, we analyzed the incidence of CPEB4 binders in a compiled set of 155 ASD genetic risk candidates from the SFARI database (ASD SFARI). CPEB4 binders are highly enriched (odds ratio [OR]=2.7, p=2e-06) and also in a smaller curated list of ASD only genes (OR=2.6, p=6e-05) which cause ASD, but not intellectual disability (Figure 23A). CPEB1 target mRNAs were enriched to a lesser and less significant extent than CPEB4 binders, probably reflecting the common CPEB1/CPEB4 target mRNAs.

We then performed enrichment analysis of the CPEB4 targets within the functional co-expression modules that represent shared pathology in ASD brain as identified in previous gene array (Voineagu et al., 2011) and RNA-seq studies (Parikshak et al., 2016). CPEB4 binders are overrepresented in the array-identified ASD-associated modules, ASD.M16-array (OR=1.9, p=1e-05) and ASD.M12-array (OR=1.4, p=2e-02) that correspond to genes involved in neuroinflammation and synaptic processes respectively. Further in the RNA-seq identified modules, CPEB4 binders are enriched the most in the ASD.M12-RNAseq (OR=2.7, p=8e-08) and also in ASD.M16-RNAseq (OR=1.5, p=7e-03) and ASD.M4-RNAseq (OR=1.7, p=8e-04) which are involved in synapse and synaptic processes and downregulated in ASD samples (Figure 23B).

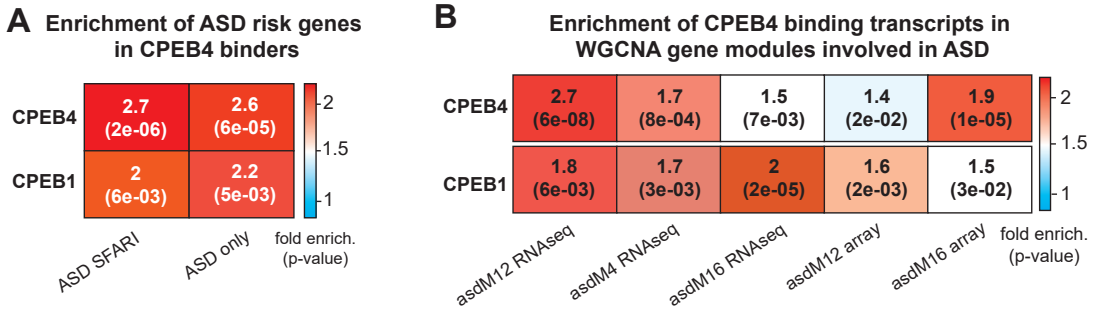

Figure 23: Enrichment of CPEB4 and CPEB1 binders (A) in ASD risk genes (ASD SFARI) and hand curated, excluding intellectual disability genes (ASD only), (B) in co-expression network modules involved in ASD (ASDM12, M4 & M16 RNAseq and asdM12 & M16 array).

Next, we analyzed the incidence of functional CPE elements (http://genome.crg.es/CPE/; 93% experimental validation accuracy) in the 3' UTRs of mRNAs of ASD genes, specifically the genes in the highest confidence categories (Cat. 1-3) of the SFARI database and the 39 genes harboring rare *de novo* protein disrupting mutations (ASD39 list) identified in the two most largest whole exome sequencing studies in simplex ASD (De Rubeis et al., 2014; Iossifov et al., 2014). 68.8% of the genes in the two most confident categories SFARI Cat.1-2 and 79.5% of the ASD39 genes contained functional CPEs versus only 35.8% in the whole genome and 39.2% in the genes with elevated expression in brain (Figure 24A). These percentages were even higher if non-consensus (TTTTACT, TTTTAAAT or TTTTCAT), but experimentally validated, CPEs were included in the algorithm with up to 100 % potential targets in the ASD39 list.

Most of these CPE-containing ASD mRNAs correspond to CPEB4 targets, as we found a highly significant enrichment in CPEB4-bound mRNAs among the high confidence ASD gene. Thus, CPEB4 binders represented 50.9% of the genes SFARI (Cat.1-2), 53.3% in the most validated SFARI category (Cat.1) and 65.8% in the ASD39 list, versus 15.1% in the brain transcriptome and 24.2% in the genes overexpressed in brain (Figure 24B).

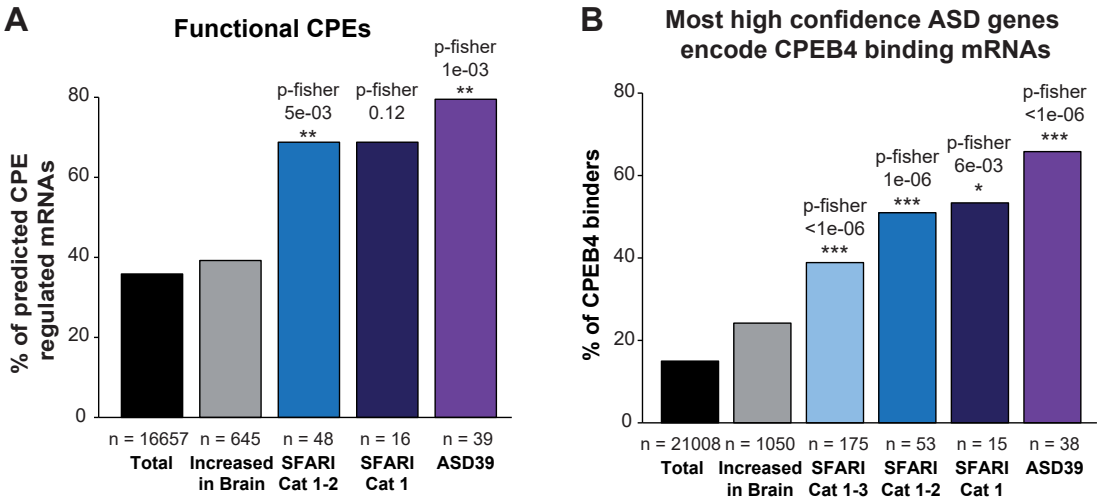

Figure 24: Incidence of functional CPEs and CPEB4 binders in ASD risk genes. (A) Percentage of human transcripts with functional CPEs in their 3'UTR and (B) percentage of CPEB4-binding transcripts according to RIP experiment in: whole transcriptome (total), genes with increased protein levels in brain and high confidence ASD genes (SFARI Cat. 1-3 and ASD39 list). Number of genes in each category under bars, and p-fisher value above bars. * p<0.05, **p<0.01, *** p<0.001.

Conclusion: CPEB4 binding transcripts are enriched within both risk-genes and gene-modules involved in ASD. Indeed, the majority of high confidence ASD genes harbor functional CPEs in their 3' UTR. Altogether, these data suggest that a large number of mRNAs encoding factors associated with ASD are regulated by CPEB4-mediated polyadenylation.

4. STUDY THE POSSIBLE ALTERATION OF CPEB4 IN IDIOPATHIC ASD BRAIN AND ITS POTENTIAL PATHOLOGICAL IMPLICATION

4.1. Analysis of CPEB4 protein, mRNA levels and splicing alterations in human idiopathic ASD brain

We then decided to explore whether CPEB4 is altered in brains of idiopathic ASD patients and, given the general cross-regulation of CPEBs, we analyze also the rest of CPEBs both at the transcript and protein levels. When we analyzed the RNA-seq data from samples of BA9 postmortem prefrontal cortex (Cx) of 43 idiopathic ASD patients and 63 neurotypical control subjects (Parikshak et al., 2016), we found unaltered transcript levels for CPEB1 and CPEB2, a slight decrease in CPEB3 transcript levels (p=0.02) and a slight increase in CPEB4 transcript levels in ASD (p=0.035, Figure 25).

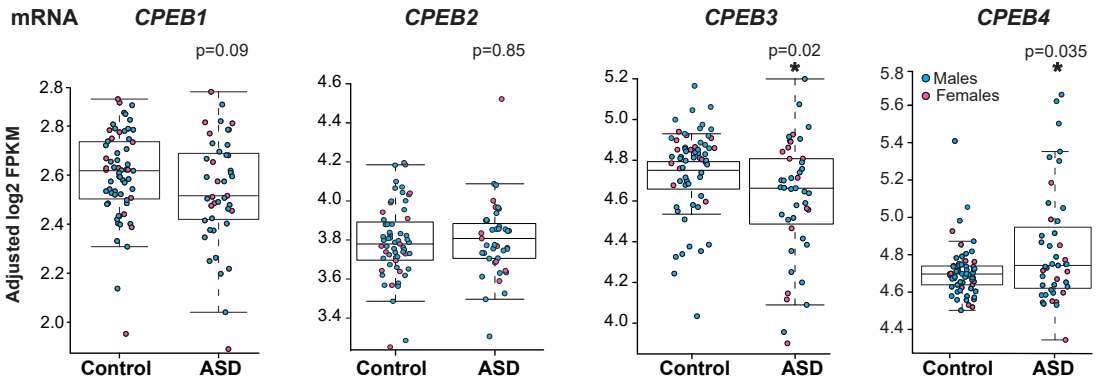

Figure 25: qRT-PCR analysis of CPEBs in patients with ASD. CPEBs mRNA levels in idiopathic human ASD Cx samples according to RNA-seq data (Parikshak et al., 2016). n=43 for control, n=63 for ASD. * p<0.05

Interestingly, western blot analysis revealed that only CPEB4 protein levels are altered in BA8/9 Cx of idiopathic ASD cases (Figures 26). More precisely, CPEB4 protein levels are decreased despite increased transcript levels thus indicating prominent posttranscriptional regulation in line with the multiple CPE sequences in its mRNA 3'UTR and the reported CPEB1- and CPEB4-mediated forward amplification loop (Calderone et al., 2016; Igea and Mendez, 2010). Interestingly, since CPEB4 levels in control subjects are high in early life and then decline, the decreased levels in ASD cases under 40 years (83.5% reduction, p=0.016) get even more significant if only the youngest cases are considered (Figure 26).

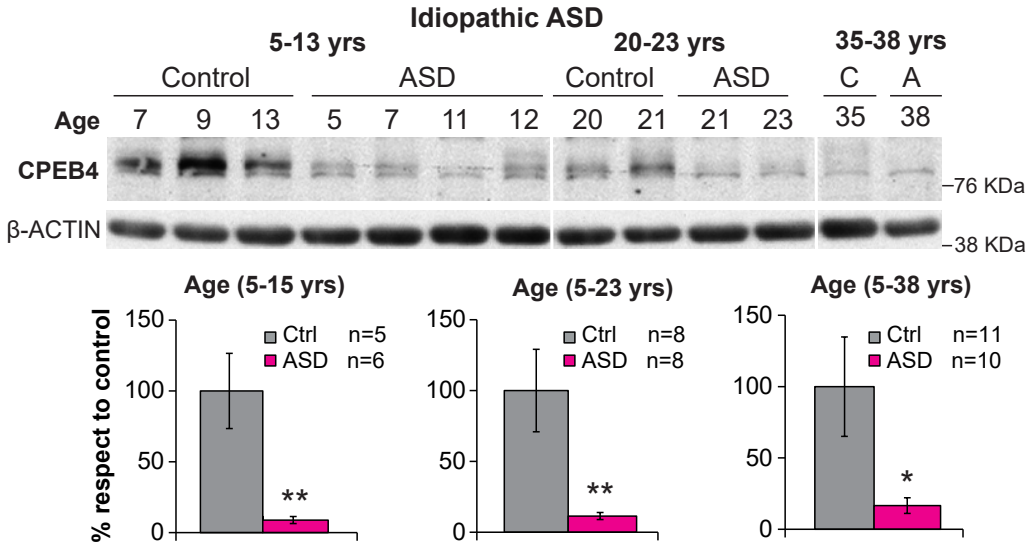

Figure 26: Western blot analysis of CPEB4 in Cx (BA9) of idiopathic ASD patients; stratified by age and n indicated in histogram. Data are shown as mean ± SEM. * $p < 0.05$, ** $p < 0.01$.

Splicing alterations (Voineagu et al., 2011; Xiong et al., 2015) particularly of microexons (Irimia et al., 2014) have been reported in ASD. We thus analyzed RNA-seq data from control (n=81) and ASD (n=82) subjects (Parikshak et al., 2016) for potential splicing alterations in mRNAs of the different CPEBs.

Only CPEB4 showed splicing alteration in ASD samples. Interestingly, we found highly significant skipping of the 24-nt neuronal-specific microexon (exon 4) in the mutually exclusive event with exon 3 (8.2%, p=0.004) thus favoring the formation of the CPEB4Δ4 mRNA isoform (Figure 27A-B). We also found highly significant inclusion of exon 3 in the CPEB4Δ3 vs. full length (FL-CPEB4) skipped exon event (8.5%, p=0.003) which, together with an almost significant exclusion of exon 4 in the FL-CPEB4 vs. CPEB4Δ4 skipped exon event (6.3%, p=0.077), further contribute to increase the proportion of CPEB4Δ4 isoform (Figure 27B).

Since the microexon encodes the 8-aminoacid B variable region (Theis et al., 2003), the favored CPEB4Δ4 isoform lacks multiple motifs for posttranslational modifications such as phosphorylation by AKT, S6K, PKA or PKC (NETPHOS 2.0 and Theis et al., 2003) (Figure 27A). This is suggestive of a dominant negative (DN) effect of CPEB4Δ4 -not only over CPEB4 but possibly over other CPEBs- by sequestering CPE-regulated mRNAs in line with what has been observed for non-phosphorylatable CPEB4 mutants regarding other residues (Guillen-Boixet et al., 2016). This DN effect would explain the observed disruption of the CPEB4 translational autoamplification loop.

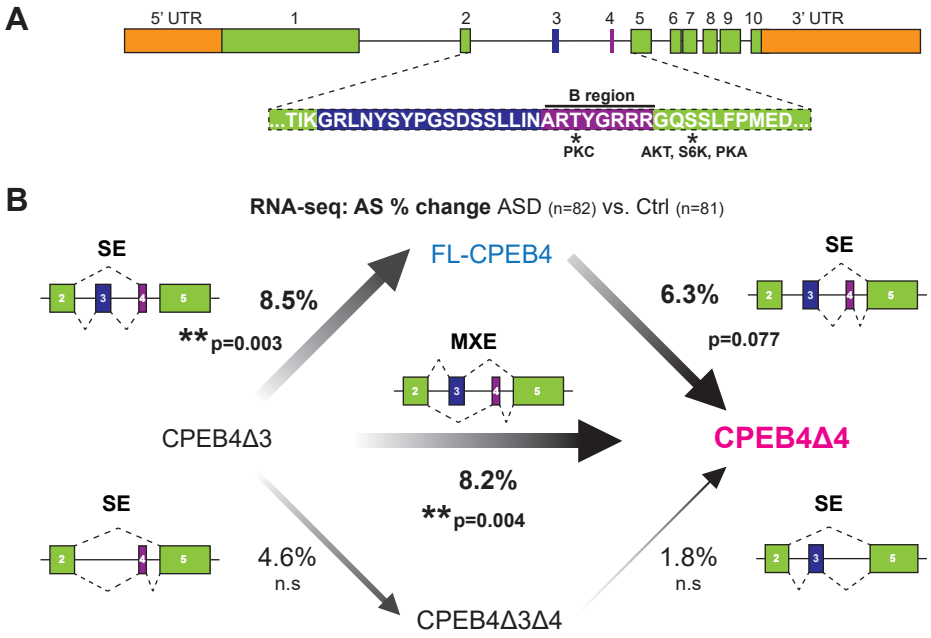

Figure 27: Analysis of CPEB4 splicing isoforms in ASD brains by RNA-seq data. (A) Schematic view of alternatively spliced exons (3-blue and 4-purple) of human CPEB4 mRNA. Inclusion of neural specific microexon 4 (B region) originates putative phosphorylation sites by PKC, AKT, S6K and PKA (residues marked with *). (B) Diagram representing the transitions (in percentage) between CPEB4 isoforms favored in ASD cases vs. control subjects according to the RNA-seq data (SE = skipped exon, MXE = mutually exclusive exons).

We then performed absolute qRT-PCR analysis to check whether the observed altered splicing events do in fact result in a net increase in the CPEB4Δ4 isoform and to interrogate the relative proportion of each of the four possible isoforms due to alternative splicing of exon 3 and exon 4 (full-length, CPEB4Δ3, CPEB4Δ4 and CPEB4Δ3Δ4) (Figure 28A). The most abundant mRNA isoform in control subjects is FL-CPEB4 (56%) followed by CPEB4Δ4 (21%). As anticipated by the splicing analysis by RNAseq, ASD subjects showed a significant increase of the CPEB4Δ4 isoform at the expense of the FL-CPEB4 isoform (Figure 28B). This way, the 56:21 FL-CPEB4:CPEB4Δ4 ratio in controls becomes 46:31 in ASD subjects (Figure 28C).

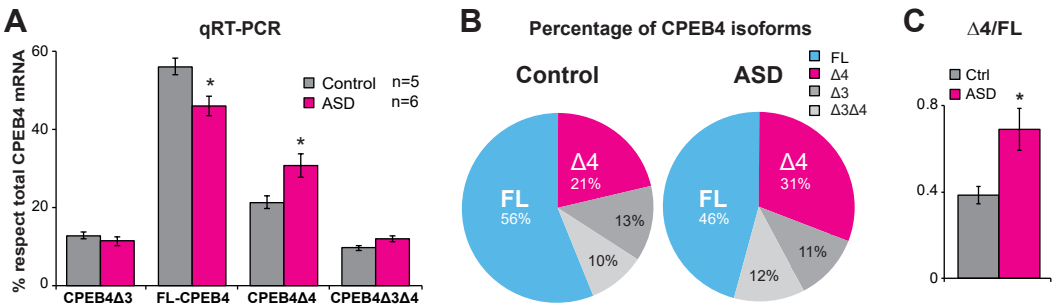

Figure 28: Analysis of CPEB4 splicing isoforms in ASD brains by qRT-PCR. (A-B) Percentage of each CPEB4 splicing isoform with respect to total CPEB4 mRNA, control (n=5) and ASD (n=6) subjects, age: 5-23 years old. Data are shown as mean ± SEM. n.s. non-significant, *p<0.05, **p<0.01. (C) CPEB4Δ4/FL-CPEB4 ratio.

Conclusion: Idiopathic ASD brains show: reduced CPEB4 protein levels and CPEB4 mis-splicing, in particular an aberrant skipping of a neuronal-specific microexon that generates a CPEB4 variant potentially refractive to regulation. All of these results confirm the alteration of CPEB4 in ASD patients.

4.2. Genome-wide poly(A) tail changes and concomitant protein alteration in idiopathic ASD brains

To test if the observed alteration of CPEB4 has an impact on mRNA polyadenylation in brains of idiopathic ASD cases, we explored potential genome-wide changes in mRNA poly(A) tail length and in particular of the ASD genes. For this, we performed poly(U)-chromatography on RNA purified from postmortem BA8/9 Cx tissue of control subjects (n=5; 5-21 years-old) and idiopathic ASD patients (n=6, 7-23 years old). Differential elution with 25% and 90% formamide yields two fractions of mRNAs with, respectively, short and long poly(A) tails, which were then analyzed by microarray hybridization (Figure 29).

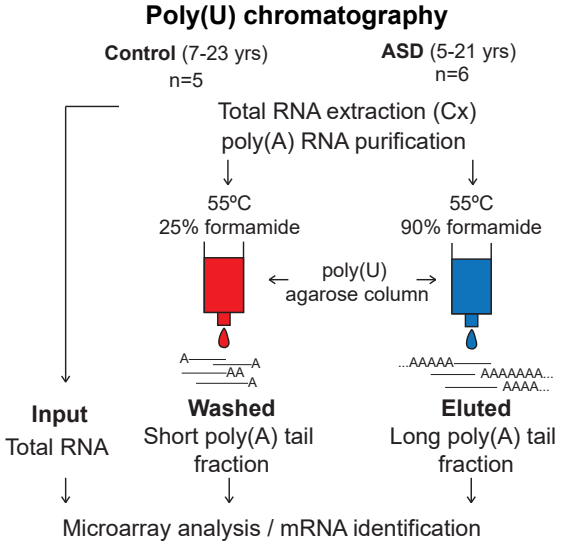

Figure 29: Poly(U) chromatography and microarray analysis. (A) Schematic view of the poly(U) chromatography/microarray analysis experiment on RNA samples of Cx (BA8/9) from control (n=5) and ASD cases (n=6).

We observed that 10.2% of transcripts show poly(A) tail lengthening in ASD while 9.1% transcripts show poly(A) tail shortening (Figure 30). However, when ASD causing genes were specifically analyzed, we observed that deadenylation was the most salient feature. Remarkably, the highly significant poly(A) tail-shortening of ASD genes was progressively exacerbated with increased causality-confidence in the SFARI category gene modules (Figure 30). Thus, genes with shortened poly(A) reached 19.1% in SFARI Cat.3, 26.3% in SFARI Cat.2, and 50% in SFARI Cat.1 (p= 1e-03, 6e-03

and 7e-04 respectively). Likewise, the incidence of transcripts with increased poly(A) tail length decreases along increasing causality confidence (6.2% in SFARI Cat.3, 2.6% in SFARI Cat.2, and 0% in SFARI Cat.1) (Figure 30).

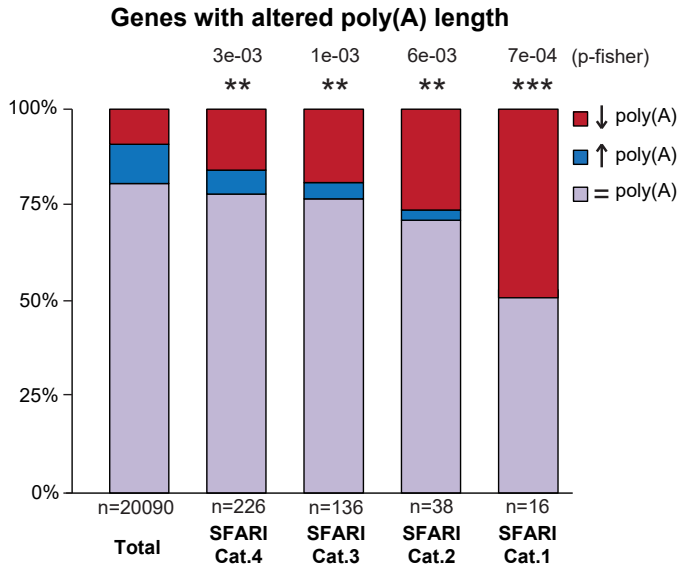

Figure 30: Analysis of genes with poly(A) changes in ASD brains. Percentage of genes with shortened (red), lengthened (blue) or unaltered (purple) poly(A) tail length in ASD, in the whole transcriptome and in high confidence ASD genes (SFARI Cat.4 to Cat.1). P-fisher enrichment value of percentage of transcripts with poly(A) shortened in each SFARI Cat. above bars. ** p<0.01. *** p<0.001.

As expected, the CPEB4 binders are highly affected by this poly(A) tail shortening. In SFARI Cat.1-3 genes, CPEB4 binders represent 59% of the genes with shortened poly(A) ($p = 0.026$) versus 28.5% of the lengthened ones and 29.3% of the unchanged (Figure 31), thus supporting that deadenylation in ASD genes is due to CPEB4.

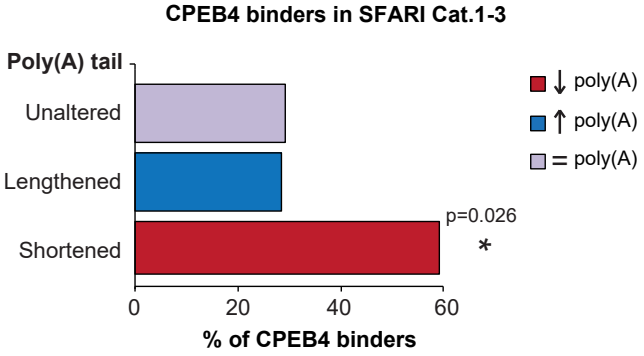

Figure 31: CPEB4 binders in ASD causing genes. Percentage of CPEB4 binders in ASD causing genes (SFARI Cat.1-3) for each poly(A) subgroup (shortened, lengthened and unaltered) in idiopathic ASD brains.

Finally, to determine the consequences of the ASD-associated poly(A) tail shortening on protein expression, we performed western blot analysis in BA8/9 Cx tissue of controls and idiopathic ASD cases. The two CPEB4 target mRNAs with

most significant poly(A) shortening in SFARI Cat.1, namely *PTEN* and *DYRK1A*, show significantly decreased protein levels in ASD cases (Figure 32A), despite showing similar or even higher transcript levels (Figure 32B). Similarly, proteins encoded by SFARI Cat.2-3 genes with CPEB4-binding mRNAs that got deadenylated in ASD, show a similar significant decrease (RBFOX1) or a trend towards decreased levels (FOXP1, WAC, AUTS2) without any parallel alterations in transcript levels (Figures 32A-B). *PCHD9*, an SFARI Cat.4 gene whose transcript is bound by CPEB4 and shows one of the most prominent shortenings in poly(A) tail-length, also shows decreased protein levels despite significant increase in its transcript levels (Figures 32A-B).

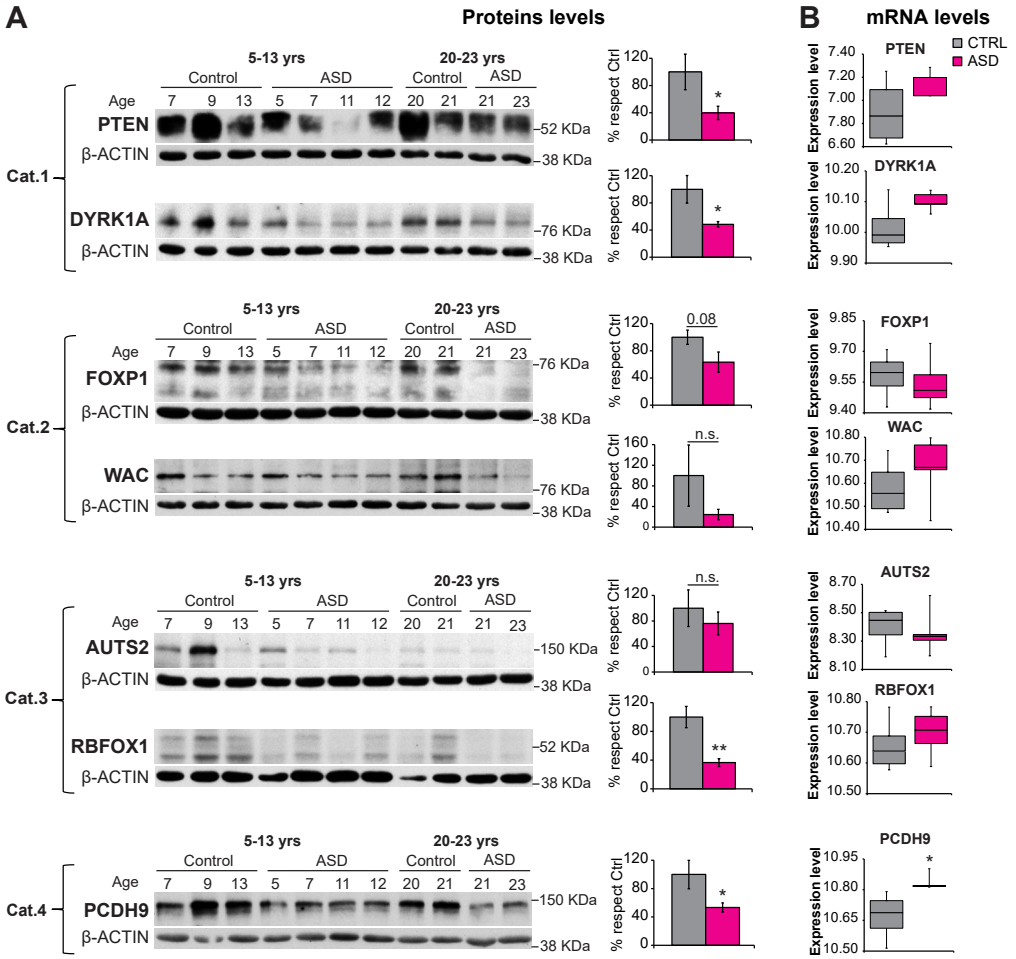

Figure 32: Protein and mRNA levels of ASD causing genes in ASD brains. (A) Protein and (B) mRNA expression levels of selected ASD genes whose poly(A) tail is shortened in idiopathic ASD samples (n=6) vs. control (n=5). Data are shown as mean ± SEM. n.s. non-significant, * p<0.05, ** p<0.01.

Conclusion: Idiopathic ASD brains show transcript-deadenylation of highly confidence ASD causing genes due to CPEB4 with concomitant decreased protein levels without changes in mRNA levels.

This led us to propose the decreased of levels of proteins encoded by deadenylated CPEB4 target mRNA as a new molecular signature in idiopathic ASD brains.

5. GENERATION OF DIFFERENT MOUSE MODELS THAT MIMIC THE CPEB4 ALTERATIONS FOUND IN IDIOPATHIC ASD FOR SUBSEQUENT POLY(A) ANALYSIS

5.1. Mouse models with modified CPEB4 expression

To further determine if CPEB4 alterations play a causal role in polyadenylation and translation of mRNAs of ASD genes, we generated different mouse models to mimic the specific changes observed in brains of idiopathic ASD patients.

To mimic the decrease in CPEB4 protein level we used two models of CPEB4-deficiency (Figures 33A-B). First, one with heterozygous gene trap (GT) between exons 1 and 2 (CPEB4 GT/+ mice), showing partial reduction of CPEB4 protein (Figure 33A) without alteration in the ratio of the four alternative splicing-generated transcript isoforms (data not shown). This model expresses truncated CPEB4 (Figure 33A), more precisely the exon 1-encoded low complexity domain (LCD) (Hu et al., 2014; Shin et al., 2016). Second, a homozygous gene targeted deletion of constitutive exon 2 (Calderone et al., 2016; Shin et al., 2016; Tsai et al., 2013) that results in a premature stop codon (CPEB4 KO mice) and shows full suppression of CPEB4 protein (Figure 33B).

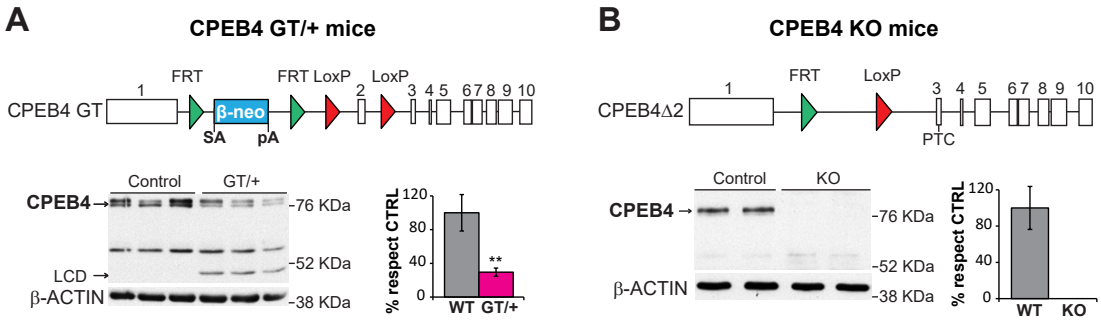

Figure 33: CPEB4 in GT and KO mice. (A) Schematic view of CPEB4 GT mice construct and Western blot analysis of CPEB4 protein levels (n=7). The gene trap (GT) cassette contains splice acceptor (SA), LacZ-neo (β-neo) and polyadenylation sequence (pA); low complexity domain (LCD) isoform. (B) Schematic view of CPEB4Δ2 mice (CPEB4 KO) construct and Western blot analysis of CPEB4 protein levels (n=2). Gene targeted deletion of the constitutive 82-nt exon 2 that results in a premature termination codon (PTC). Data are shown as mean ± SEM. ** p<0.01.

We next sought to explore the effect of a change in the CPEB4Δ4/FL-CPEB4 ratio, as observed in idiopathic ASD brains but without decreased CPEB4 global levels. For this aim, we generated mice with conditional neuronal-specific overexpression of CPEB4Δ4 isoform (TgCPEB4Δ4 mice, Figure 34A). No perinatal lethality was observed as the percentage of born TgCPEB4Δ4 mice matched the one expected with mendelian distribution (Figure 34B).

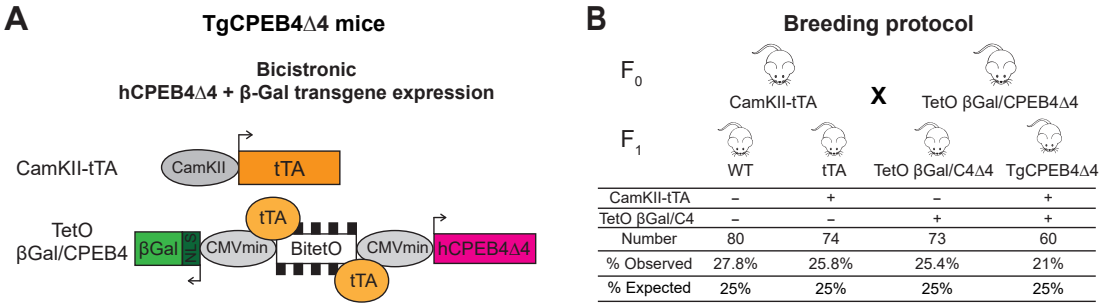

CamKII-tTA	–	+	–	+
TetO βGal/C4	–	–	+	+
Number	80	74	73	60
% Observed	27.8%	25.8%	25.4%	21%
% Expected	25%	25%	25%	25%

Figure 34: Generation of TgCPEB4Δ4 mice. (A) Schematic view of TgCPEB4Δ4 mice construct: tTA (a.k.a. Tet-Off) is under control of the CamKII promoter and activates the BiTetO construct with NLS-β-Gal sequence in one direction and human CPEB4Δ4 in the other. (B) Breeding protocol to obtain TgCPEB4Δ4 mice. Number of mice, percentage of births observed and expected for the four experimental genotypes are shown in the table.

TgCPEB4Δ4 mice were indistinguishable from their WT and single transgenic littermates from birth to weaning. However, at this age (3 weeks), up to 40% of TgCPEB4Δ4 mice start showing cranial dysmorphology and hydrocephalus. TgCPEB4Δ4 mice with cranial dysmorphology die prematurely with a mortality peak at the age of 7 weeks (Figure 35A). The 60% of TgCPEB4Δ4 mice with normal cranial morphology do not develop hydrocephalus, do not present any obvious abnormality and do not show premature death (at least up to the oldest tested age of 20 months), but they are significantly smaller that their control littermates from the age of 3 weeks on (Figure 35B). For further characterization of TgCPEB4Δ4 mice in the rest of this study, we decided to restrict the analysis to the mice with normal cranial morphology.

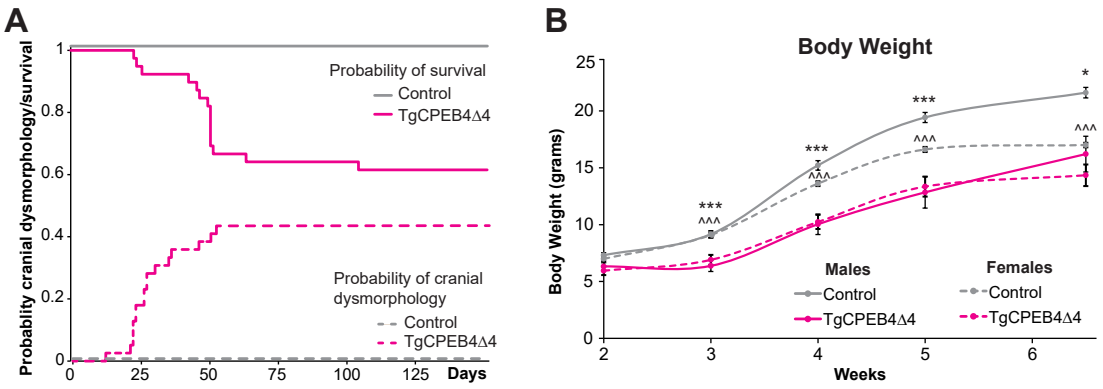

Figure 35: Life Span, cranial dysmorphology and body weight in TgCPEB4Δ4. (A) Kaplan-Meier curve for cumulative survival (continuous line) and probability of developing cranial dysmorphology (dashed line). n=44 for control, n=39 for TgCPEB4Δ4 mice. (B) Control and TgCPEB4Δ4 mice body weight (grams) evolution. Males (continuous line): n=25 control, n=9 TgCPEB4Δ4 mice. Females (dashed line): n=26 control, n=7 TgCPEB4Δ4 mice. Data are shown as mean ± SEM. * p<0.05. ***p<0.001.

Transgene expression in TgCPEB4Δ4 mice takes place in neurons of forebrain structures such as Cx, St and Hipp. We can observe both overexpression of β-Gal reported (Figure 36A) and CPEB4Δ4 protein in mouse forebrain (Figures 36B).

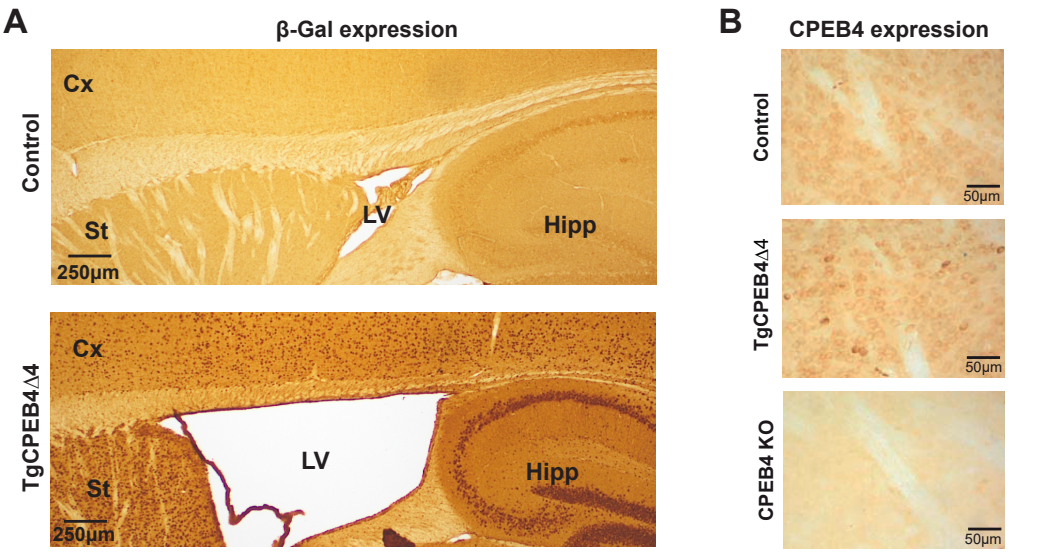

Figure 36: β-Gal and CPEB4 expression in TgCPEB4Δ4 forebrain. (A) Immunohistochemistry showing β-Gal staining in neuronal nuclei in forebrain of a 1.5-month-old control and TgCPEB4Δ4 mice. Cx: cortex. St: striatum. Hipp: hippocampus. LV: lateral ventricle. Scale bars represent 250 µm. (B) St CPEB4 immunohistochemistry shows cytoplasm pattern in control, overexpressing neurons in TgCPEB4Δ4 mice and no staining in CPEB4 KO. Scale bars represent 50 µm.

Absolute qRT-PCR analysis revealed an imbalance of the alternative splicing-generated isoforms (Figure 37A) similar to that observed in brain of idiopathic ASD patients (Figure 28A). Interestingly, total CPEB4 protein level in TgCPEB4Δ4 mice are highly increased at late embryonic age but only moderately increased in young adult (1.5 months) and no longer increased after 12-months despite significantly increased transcript levels at all age (Figure 37B).

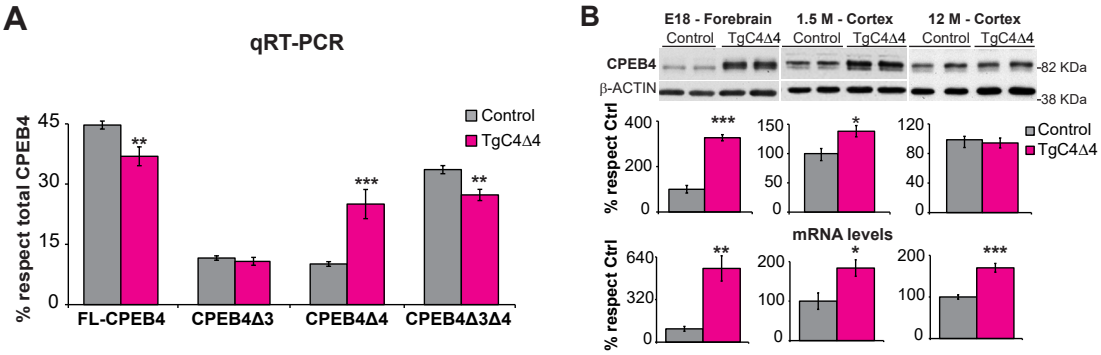

Figure 37: CPEB4 splicing isoforms, mRNA and protein levels in TgCPEB4Δ4. (A) Percentage of each *Cpeb4* splicing isoform with respect to total *Cpeb4* mRNA, obtained by absolute qRT-PCR in St of controls (n=9) and TgCPEB4Δ4 mice (n=7), 1.5-month-old. (B) Western blot (upper panels) and qRT-PCR (lower panels) analysis of CPEB4 in control and TgCPEB4Δ4 mice at embryonic day 18 (n=3), 1.5-month-old (n=7) and 12-month-old (n=4).

Interestingly, the level of CPEB4 protein does not seem to be different in TgCPEB4Δ4 mice with or without hydrocephalus (Figure 38A) and no changes in transcript or protein levels of the other CPEBs were observed in TgCPEB4Δ4 mice (Figure 38B-C).

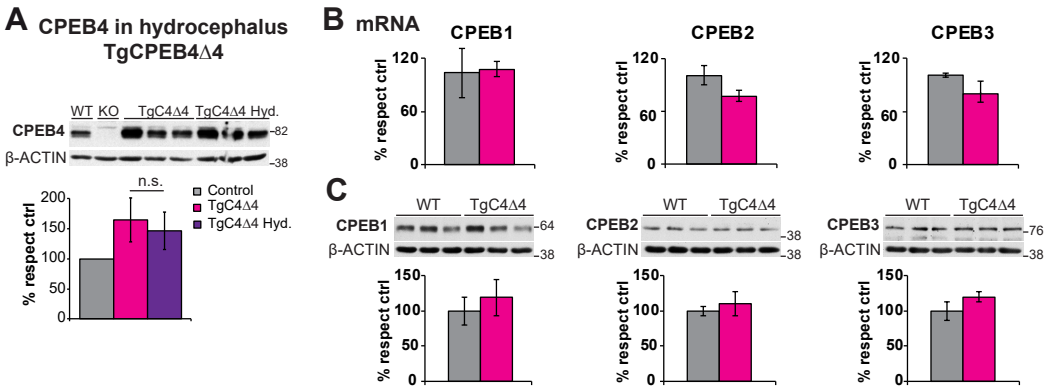

Figure 38: CPEBs mRNA and levels in TgCPEB4Δ4. (A) Western blot analysis of CPEB4 protein levels in TgCPEB4Δ4 mice (5-week-old) with or without hydrocephalus (n=6). (B) mRNA expression by qRT-PCR analysis and (C) protein levels by Western blot of the all CPEBs in control (n=3) and TgCPEB4Δ4 (n=3) mice forebrain (embryonic day 18). Data are shown as mean ± SEM. n.s = non-significant.

Conclusion: We generated mouse models that mimic either CPEB4 deficiency (CPEB4 GT and KO mice) and CPEB4 mis-splicing in favor of the isoform lacking a neuronal-specific microexon (TgCPEB4Δ4 mice), that we observe in idiopathic ASD patients.

5.2. Genome wide poly(A) tail analysis in brains of mouse models with modified CPEB4 expression

RNAs from mice with partial or complete ablation of CPEB4, were subjected to poly(U)-chromatography followed by microarray analysis (Figures 39A-B). Both models showed similar changes in ASD genes polyadenylation but these were opposite to what we observed in ASD patients (Figure 30), i.e. CPEB4 deficient mice show prominent poly(A) lengthening in genes of SFARI Cat.3, .2, or .1 (Figures 39A-B).

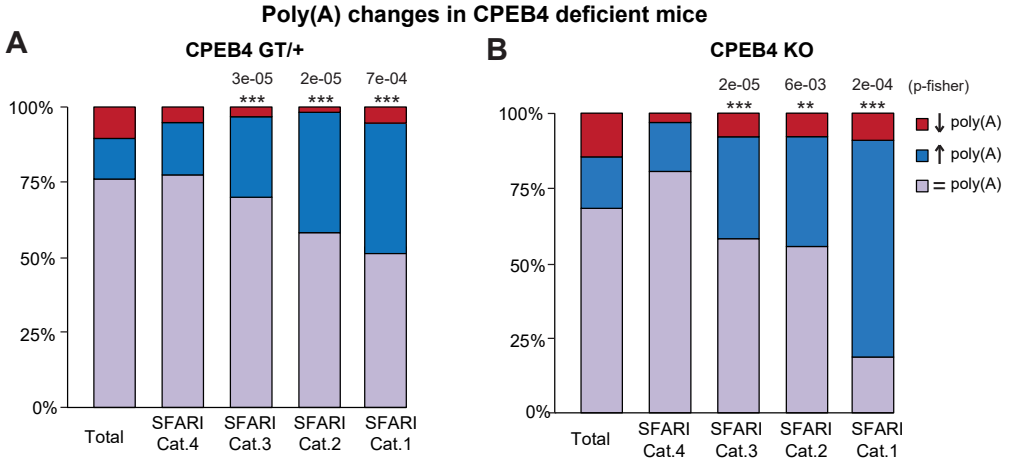

Figure 39: Poly(A) changes in CPEB4 deficient mice. Percentage of poly(A) tail changes in (A) CPEB4 GT/+ and (B) CPEB4 KO mice in Cx-St samples, in the total transcriptome and in high confidence ASD genes (SFARI Cat.4 to 1). Poly(A) shortening (red), lengthening (blue) and no change (purple). P-fisher enrichment value of percentage of transcripts with lengthened poly(A) in each SFARI category with respect to the total transcriptome above bars. ** p<0.01, *** p<0.001.

Therefore, we concluded that the decreased polyadenylation of ASD related mRNAs in ASD brains is not a direct consequence of their reduced CPEB4 levels. However, poly(U)-chromatography of TgCPEB4Δ4 mice revealed a pattern of poly(A) tail length changes in ASD genes (Figure 40) very similar to the one observed in idiopathic ASD patients (Figure 30) with predominant deadenylation that gets progressively exacerbated with the increasing causality confidence of the ASD gene category. Thus, 12.5% of the whole transcriptome shows poly(A) tail shortening in TgCPEB4Δ4 mice and this increases to 26% in SFARI Cat.3, 32% in SFARI Cat.2, and 47% in SFARI Cat.1 genes (p=7e-04, 1e-02 and 7e-03 respectively) (Figure 40).

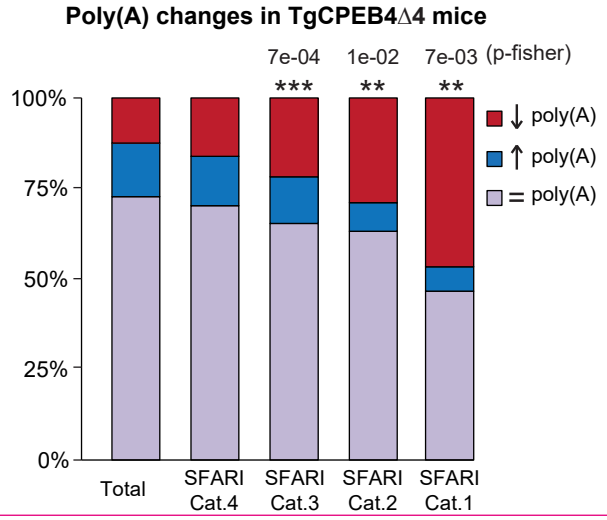

Figure 40: Poly(A) changes in TgCPEB4Δ4. Percentage of poly(A) tail changes in Cx-St samples in the total transcriptome and in high confidence ASD genes. P-fisher enrichment value of percentage of transcripts with shortened poly(A) in each SFARI category above bars. ** p<0.01, *** p<0.001.

To further confirm the poly(A) tail alteration detected by poly(U) chromatography, deadenylation of *Auts2* mRNA was also verified by poly(A) tail (PAT) and Hire (high resolution) -PAT analyses (Figures 41A-B).

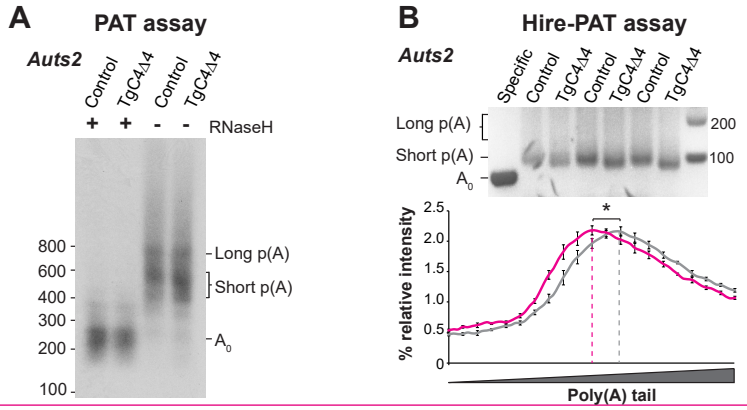

Figure 41: PAT and Hire-PAT assays of *Auts2* in Control and TgCPEB4Δ4 mice. (A) PAT assay of *Auts2* in control and TgCPEB4Δ4 mice (n=2). RNaseH (+) lines show transcripts devoid of poly(A) tail (A_0); RNaseH (-) lines show a smear that correlates with the different poly(A) tail length. (B) Hire-PAT assay and quantification of *Auts2* poly(A) tail i (n=3). Data are shown as mean ± SEM. *p<0.05.

Interestingly, poly(A) tail changes in ASD and TgCPEB4Δ4 mice are equivalent not only because both show poly(A) shortening for ASD genes. More important, global transcriptome poly(A) alteration is coincident in ASD patients and TgCPEB4Δ4 mice. This is evidenced by the highly significant overlap (p<7e-43) between the total of genes with shortened poly(A) tail, as well as between the total of genes with lengthened poly(A) tail in ASD patients and TgCPEB4Δ4 mice (p<6e-111) (Figure 42).

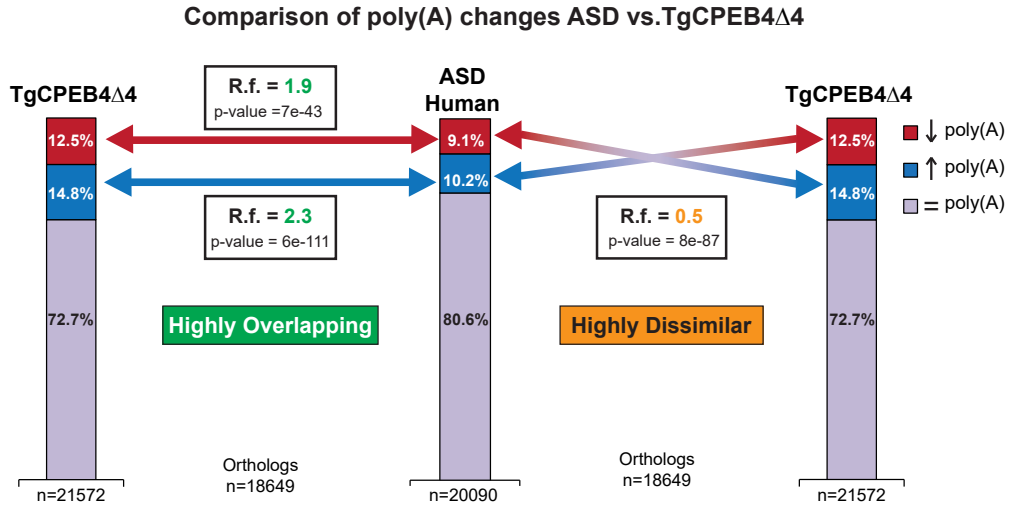

Figure 42: Comparison of genes with poly(A) changes ASD vs. TgCPEB4Δ4 mice. Percentage of genes with shortened (red), lengthened (blue) or unaltered (purple) poly(A) tail length in ASD Cx (BA8/9) samples and Cx-St in mice in the whole transcriptome is shown inside the columns. Representation factor (R.f.) and p-values of transcripts with poly(A) changes in same direction (left panel) and in opposite direction (right panel).

Conclusion: CPEB4 deficiency mouse models show prominent poly(A) lengthening in ASD risk genes, opposite to ASD patients. However, TgCPEB4Δ4 mice show a poly(A) alteration coincident to that in human ASD cases, not only in ASD risk genes (predominant deadenylation), but also in global transcriptome. These data therefore demonstrate that imbalance in CPEB4 splicing isoforms in transgenic mice results in poly(A) tail length-changes equivalent to those in idiopathic ASD human cases.

5.3. Western blot analysis of deadenylated ASD risk genes in TgCPEB4Δ4 mice

To confirm that poly(A) tail changes in TgCPEB4Δ4 mice impact in alteration of protein levels, we performed Western blot analysis. As was the case for the ASD patients, poly(A) tail shortened in the TgCPEB4Δ4 mice correlated with reduced protein levels of ASD genes. Analysis of the SFARI Cat. 1-3 genes which generate CPEB4-binding transcripts revealed that the two genes with most shortened poly(A) tail, namely *Zbtb20* and *Tnrc6b*, showed significant St and Cx reduction in protein levels, without concomitant transcript level changes (Figures 43A-B). Similarly, the third most deadenylated transcript (*Pten*) showed a tendency to decrease in Cx. We

also found significant St and Cx -decreases in protein levels for *Chd2*, *Foxp1*, *Wac*, *Auts2*, and *Rbfox1* in TgCPEB4Δ4 mice. Interestingly, SFARI Cat.4 genes with robust poly(A) tail shortening such as *Gpc6* also show decreased protein levels in the absence of transcript level changes (Figures 43A-B).

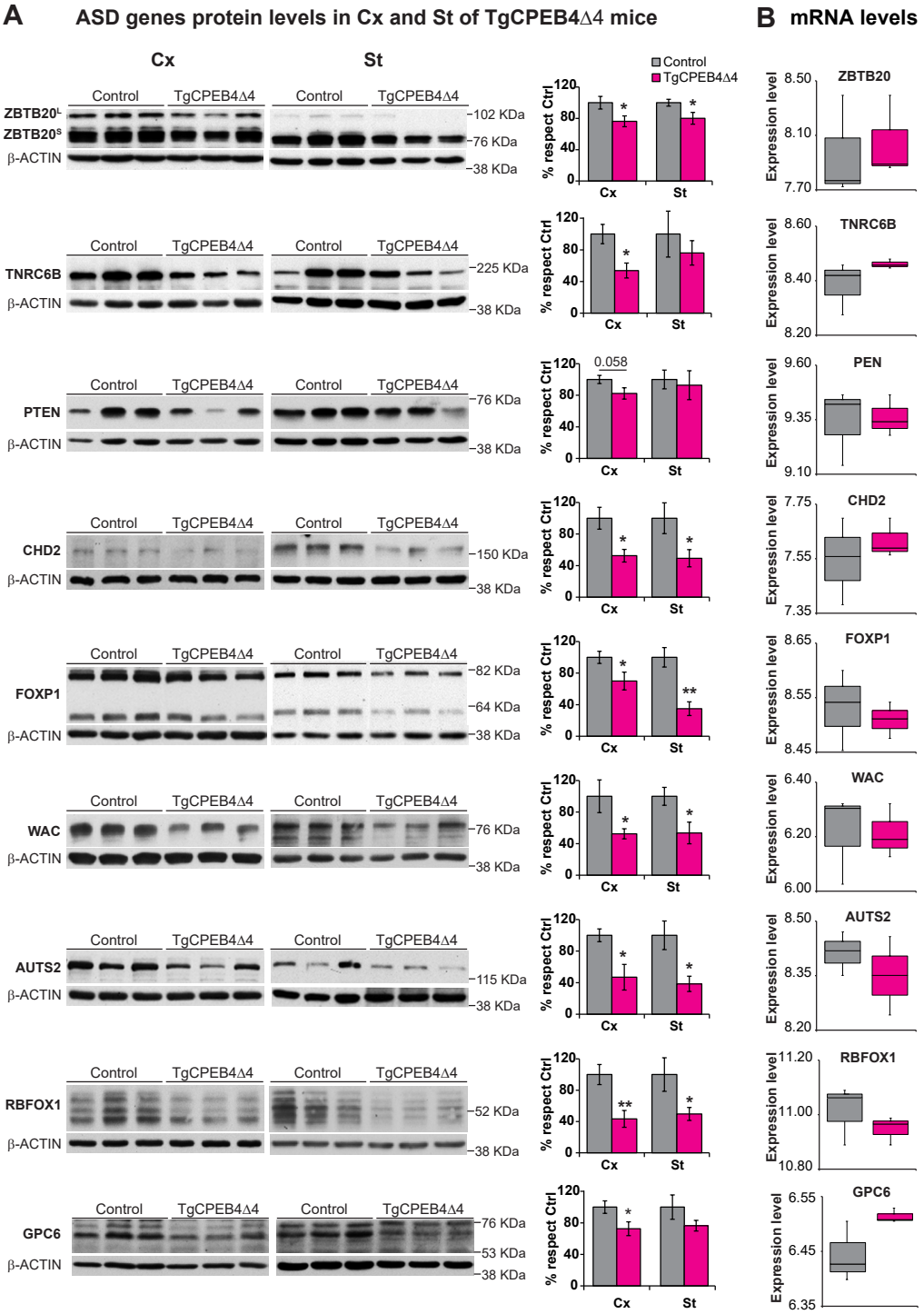

Figure 43: Protein and mRNA levels of ASD causing genes in ASD brains. (A) Western blot analysis in Cx and St of ASD genes whose poly(A) tail is shortened in 1.5-month-old TgCPEB4Δ4 mice (n=7). (B) mRNA expression levels in Cx-St samples of the same ASD genes in control and TgCPEB4Δ4 mice (n=3). Data are shown as mean ± SEM.* p<0.05, ** p<0.01.

Conclusion: Numerous deadenylated ASD genes show diminished protein levels in TgCPEB4Δ4 mice. These results demonstrate that *in vivo* selective alteration of the ratio of CPEB4 splicing isoforms in favor of CPEB4Δ4 is sufficient to alter the protein levels of numerous ASD risk genes.

6. CHARACTERIZATION OF ASD PHENOTYPE IN TGCPEB4Δ4 MICE

In view of the similar poly(A) tail- and protein level-alteration of multiple high confidence ASD genes in brains of idiopathic ASD patients and TgCPEB4Δ4 mice, we tested whether these mice developed ASD-related anatomical, electrophysiological and behavioral abnormalities.

TgCPEB4Δ4 mice show reduced brain weight and volumetric analysis of forebrain regions revealed 27.1% volume reduction in Cx, 24% in St and 15.7% in hippocampus (Figures 44A-B).

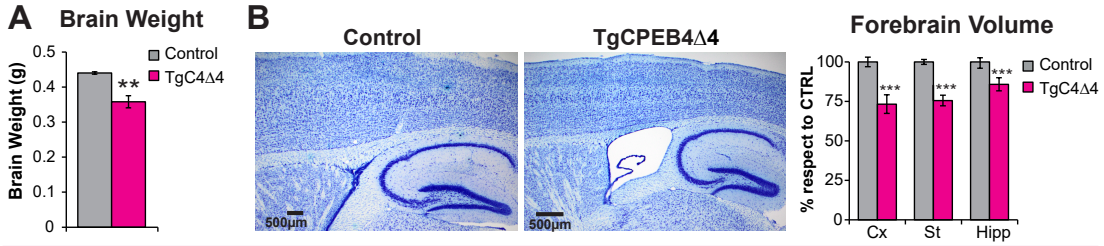

Figure 44: Brain weight and volume in TgCPEB4Δ4 mice. (A) Brain weight in control (n=24) vs. TgCPEB4Δ4 (n=7) mice. (B) Volumetric analysis of toluidine blue stained brain sections from control (n=10) and TgCPEB4Δ4 mice (n=5). Histogram shows percentage volume reduction of TgCPEB4Δ4 forebrain structures (cortex, striatum and hippocampus). Data are shown as mean ± SEM. ** p<0.01, ***p<0.001.

Because dendritic spine dysgenesis is frequent in ASD (Phillips and Pozzo-Miller, 2015) and mouse models (Chen et al., 2015), we analyzed this by rapid Golgi spine analysis. Similarly to other ASD models (Peca et al., 2011; Schmeisser et al., 2012), we found a 9.2% decrease in total spine density in TgCPEB4Δ4 mice (p=0.04) (Figure 45) without changes in their relative distribution among filopodia, thin, stubby or mushroom spines (data not shown).

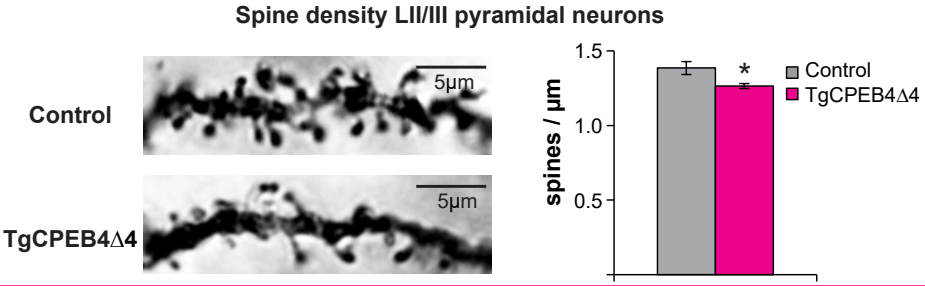

Figure 45: Spine morphology and density in TgCPEB4Δ4 mice. Confocal images of Golgi staining in Cortex. Histogram shows spine density (spines/µm) in layers II/III of pyramidal neurons (n=14 cells from 5 control and n=12 cells from 4 TgCPEB4Δ4 mice). Data are shown as mean ± SEM. * p<0.05.

Next we tested whether the decreased spine density in TgCPEB4Δ4 mice correlates with electrophysiological alterations, as observed in other ASD mouse models (Chen et al., 2015) like those with altered NLGN-neurexin function (Rabaneda et al., 2014). We thus performed whole-cell recordings of miniature excitatory

postsynaptic currents (mEPSCs) in layer V pyramidal neurons of somatosensory Cx. The analysis of the average mEPSCs in each cell reveals no difference in the mean amplitude, but the mean frequency was decreased in TgCPEB4Δ4 (7.41 ± 0.85 Hz) vs. control (10.95 ± 1.15 Hz) that is a 32% reduction (Figure 46). In line with the observed deficit in spine density, these observations are compatible with a presynaptic deficit in neurotransmitter release and/or a reduction in the number of excitatory synapses.

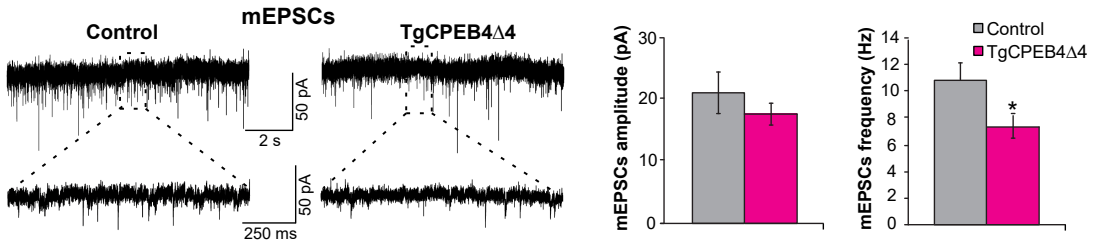

Figure 46: Electrophysiology characterization of TgCPEB4Δ4 mice. Representative traces and quantification of amplitude (pA) and frequency (Hz) of mEPSCs recorded from pyramidal neurons of the somatosensory Cx (n=11 cells from five control and n=9 cells from five TgCPEB4Δ4 mice). Data are shown as mean ± SEM.* p<0.05.

ASD diagnosis criteria in humans are based in behavioral symptoms rather than biochemical or neuroanatomical markers. To further validate TgCPEB4Δ4 mice as an ASD model, we performed a battery of ASD-related behavioral tests that included Open Field (OF), Ultrasonic Vocalization (UsV) and Social Approach (SAp) tests.

In the OF, a test to characterize the general activity pattern, TgCPEB4Δ4 mice showed stereotypical running at the periphery of the cage while they showed no difference in the distance walked in the center (Figure 47A). This higher activity in the periphery of the arena could suggest anxiety-related behavior and we thus decided to perform the Elevated Plus-Maze (EPM) test to explore this possibility. However, since TgCPEB4Δ4 mice spent about the same amount of time in open and closed arms, they rather show reduced anxiety (Figure 47B).

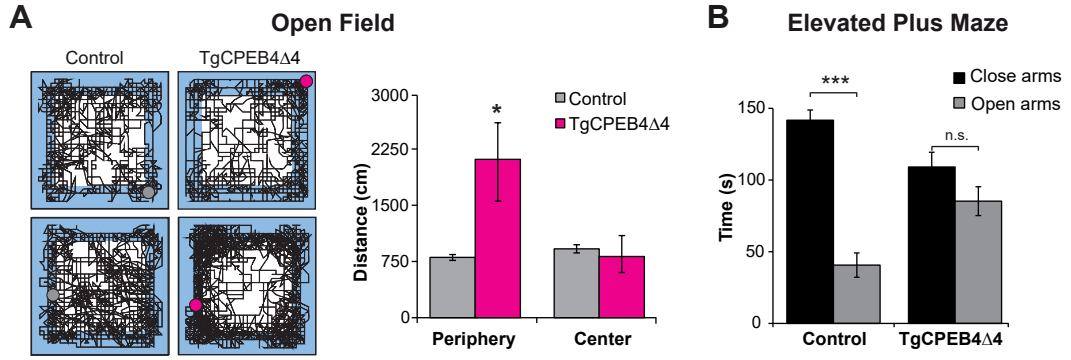

Figure 47: Evaluation of the open field and elevated plus maze tests in TgCPEB4Δ4 mice. (A) Representative traces of movement of control (n=51) and TgCPEB4Δ4 (n=13) mice in the open field test and quantification of distance travelled (cm) in the periphery and in the center. (B) Time spent in closed or open arms in the elevated plus maze of control (n=15) and TgCPEB4Δ4 (n=19) mice. Data are shown as mean ± SEM. n.s. non-significant, * p<0.05, *** p<0.001.

The UsV test analyzes ASD-relevant infant-mother communication by measuring isolation-induced calls emitted by pups in the absence of their mother (Silverman et al., 2010). We analyzed the pattern of UsV emission during postnatal development (P3-6-9-12) and found that, from P6 on, TgCPEB4Δ4 mice emitted significantly less UsVs (Figure 48).

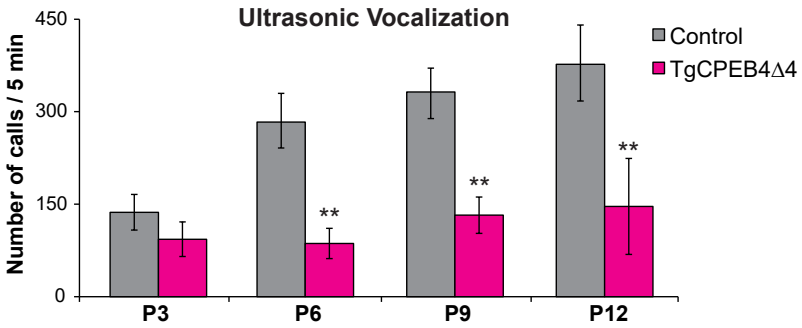

Figure 48: Analysis of ultrasonic vocalizations in TgCPEB4Δ4 pups. (A) Number of ultrasonic calls from pups during 5 min when separated from their mothers at postnatal day 3, 6, 9 and 12. Control (n=20) and TgCPEB4Δ4 (n=13) mice. Data are shown as mean ± SEM. ** p<0.01.

In order to analyze social behavior, we performed the SAp test, which measures sociability as a preference to interact with a cage containing a mouse rather than with an empty cage (Silverman et al., 2010). We found that while the controls spent significantly more time interacting with the mouse containing cage, indicative of normal sociability, TgCPEB4Δ4 mice did not show any significant preference to interact with either cage, indicating a dysfunction in sociability (Figure 49).

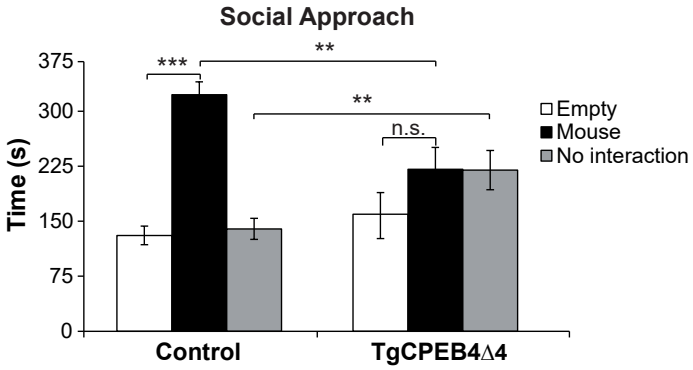

Figure 49: Assessment of social interaction behaviors in TgCPEB4Δ4 mice. Time interacting with either an inanimate object (empty cage), an unfamiliar mouse or without any interaction during 10 min. Control (n=20) and TgCPEB4Δ4 (n=7) mice. Data are shown as mean ± SEM. n.s non-significant, ** p < 0.01, *** p < 0.001.

Conclusion: TgCPEB4Δ4 mice show ASD-like neuroanatomical, electrophysiological and behavioral phenotypes. Together, the neuroanatomic alteration, the stereotypic behavior, the aberrant infant-mother communication and the deficit in social interaction demonstrate that ASD-like altered CPEB4 isoform ratio *in vivo* results in core ASD-related phenotype.

DISCUSSION

Huntington's disease (HD) is a high prevalence neurodegenerative disorder characterized by motor disturbance, cognitive decline, behavioral, psychological dysfunction and premature death. Thus, scientists are making huge efforts to understand how the HTT mutation causes the characteristic HD phenotype and to find new treatments.

In this thesis we focused on studying the potential role of CPEBs in HD. CPEBs are a family of proteins that regulate translational-repression or –activation through, respectively, cytoplasmic shortening or elongation of the mRNA poly(A) tail. We reasoned that altered CPEB function might contribute to HD based on different lines of evidence. Thus, the first aim of this thesis was to explore the status of CPEBs in HD and the potential genome-wide poly(A) tail changes of target mRNAs. Strikingly, we noticed that high confidence ASD-causing genes were unexpectedly overrepresented among CPEB4 targets. This serendipitous finding led us to hypothesize CPEB4 as a new hub in ASD gene expression. Thereby, the second aim was to study the status of CPEB4 in idiopathic ASD patients and finally to determinate its potential role in ASD risk gene regulation.

Altered mRNA polyadenylation and protein levels of neurodegeneration causing genes upon CPEB1/4 imbalance in Huntington's disease

As the first analysis of the status of CPEBs in HD, here we find strong imbalance of CPEBs in human HD St and also in others affected brain structure such Cx, Hipp or Cb (data not show), characterized by increased levels of CPEB1 and a decrease in CPEB4. Transgenic HD mouse models show similar CPEB imbalance with subsequent altered poly(A) tail length for hundreds of mRNAs. These transcripts are enriched in gene modules previously associated with neurodegeneration, not only in HD but also in AD and PD thus suggesting that CPEB alteration may represent a new common pathogenic mechanism across neurodegenerative diseases. Besides, this analysis has allowed detection of altered mRNA polyadenylation and protein levels of KTN1 that may explain the prominent striatal atrophy that occurs in HD.

Regarding the mechanism by which CPEB alteration takes place in HD, it would be expected to be an age-associated phenomenon triggered by the toxicity of the expanded CAG-mRNA and/or polyQ. For instance, global transcriptomic changes induced by expanded polyQ are well known mechanisms in HD pathogenesis (Valor, 2015) and the increase in CPEB1 protein could be explained by the observed increase in *CPEB1* mRNA level. However, the decrease in CPEB4 protein level is not mirrored by a change in its mRNA level. Interestingly, we have evidence that calpain activation,

which is known to happen along HD pathogenesis (Gafni and Ellerby, 2002), results in increased CPEB4 proteolysis and degradation (data not shown).

Regarding if both the excess of CPEB1 or defect of CPEB4 contribute to HD pathogenesis, we decided to correct these CPEB alterations in HD mice. Thus, on one hand we generated HD mice with decreased levels of CPEB1 by combining R6/1 and heterozygote CPEB1 KO (CPEB1 +/-) mice. On the other hand we generated HD mice with overexpression of CPEB4 by combining R6/1 and transgenic CPEB4Δ4 mice. The average half-life of CPEB1+/- R6/1 double transgenic mice was even lower that of the R6/1 mice and we founded no improvement of HD-like phenotype (data not show). However, TgCPEB4Δ4 R6/1 double transgenic mice showed slight attenuation of motor symptoms in rotarod and in open field tests without any change in life span (data not shown). These results suggest that decrease of CPEB4 protein levels in HD is more relevant for disease pathogenesis. We did not find strong attenuation of HD-like phenotype probably because we only restored the levels of CPEB4Δ4 isoform in R6/1. Now, our effort is to generate a transgenic mouse with overexpression of the neural specific CPEB4 isoform, the full length CPEB4. Finally, we will study the HD phenotypic progression by crossing with HD mice.

One of the most salient features in this thesis is the enrichment in genes of the HD-, AD- or PD-related modules among the genes with significant poly(A) tail length alteration in HD mice. This suggests that CPEB alteration in HD is pathogenic by aberrant polyadenylation of many neurodegeneration-associated genes. Two genes classically implicated in HD etiology, *HTT* itself and *BDNF* are among the genes displaying altered poly(A) tail length, increased for *HTT* and decreased for *BDNF* mRNA. mHTT toxicity is obviously mediated by its expanded polyQ tract and decreased BDNF protein levels can be explained by its well documented decreased transcription (Zuccato and Cattaneo, 2009). However, our data suggest that CPEB mediated dysregulation may exacerbate both toxic entities by further increasing *mHTT* translation and further decreasing *BDNF* translation. In fact, there was previous evidence of CPEB mediated regulation of *BDNF* in non-pathological conditions (Baj et al., 2016; Ma et al., 2010; Oe and Yoneda, 2010; Vicario et al., 2015). Recently, our lab and others have demonstrated that two genes associated to AD, *MAPT* and *GSK3*β, are also implicated in HD (Fernandez-Nogales et al., 2014; Fernandez-Nogales et al., 2015; Vuono et al., 2015). Intriguingly, excess Tau and decreased GSK3β protein levels without matching altered transcript levels have been shown to contribute to HD-like phenotype in R6/1 mice (Fernandez-Nogales et al., 2014; Fernandez-Nogales et al., 2015). The here reported increased poly(A) tail length in *MAPT* and decreased poly(A) tail length in *GSK3*β provide an explanation for such pathogenic altered protein levels.

The high incidence of neurodegeneration causing genes among transcripts with poly(A) tail alteration in the mice with CPEB alteration also suggests that similar or even complementary CPEB alterations might underlie other neurodegenerative diseases. Now, we are analyzing levels and patterns of all CPEBs in brain structures affected in patients of other neurodegenerative diseases as PD or AD (data not shown).

Kinectin 1 is an integral endoplasmic reticulum (ER) membrane protein that anchors kinesin-1 to extend the ER along microtubules and that also anchors elongation factor-1 complex to facilitate translation in the ER (Ng et al., 2016; Ong et al., 2006). As mentioned, striatal volume has recently been reported to be proportional to *KTN1* gene expression in Cx (Hibar et al., 2015a). At least in mice, *Ktn1* mRNA is much higher in Cx than in St (http://mouse.brain-map.org/). All this, together with the here showed decreased KTN1 protein levels both in cortical and striatal tissue and the predominant neuropil immunostaining of kinectin in St, suggest that striatal atrophy might be secondary to decreased microtubule dependent transport and protein synthesis in cortico-striatal afferences.

Thus, it would be crucial to study in depth the status of CPEBs and global polyadenylation not only in HD, but also in other neurodegenerative diseases such AD and PD. We could think of a common pathogenic mechanism in all neurodegenerative diseases as CPEBs are very well positioned to trigger aberrant gene expression of multiple neurodegeneration-associated genes in patient's brain.

In summary, by showing CPEB1/CPEB4 imbalance in HD leading to poly(A) tail changes in numerous transcripts previously associated to neurodegeneration, not only in HD but also in AD and PD, our results suggest a common new CPEB-related pathogenic mechanism across neurodegenerative diseases. Altered polyadenylation of multiple transcripts therefore becomes a new molecular signature in HD and possibly other neurodegenerative diseases that will allow identification of new pathogenic effectors. In this regard, we here identify diminished KTN1 as a likely etiology player responsible for the prominent striatal atrophy in HD.

CPEB4 mis-splicing reprograms mRNA polyadenylation and gene expression in autism

Our study of CPEBs in HD serendipitously took us to discover a new molecular mechanism in the highly prevalent neurodevelopmental disorder ASD.

We found an unexpected and very significant enrichment of ASD susceptibility genes among CPEB4 targets with shortened poly(A) tail in a mouse model of HD. Indeed, CPE sequences are present in 3' UTRs of most high confidence ASD gene transcripts which in turn are overrepresented among the CPEB4-binding transcripts. Moreover, by analyzing postmortem brains of idiopathic ASD cases we found that CPEB4 shows diminished protein levels and it is mis-spliced in favor of the isoform lacking a neuronal-specific microexon. This led us to discover a new molecular signature in idiopathic ASD brains consisting on poly(A) tail length shortening in 9% of the transcriptome that prominently affects high confidence ASD risk genes (as an example, half of the SFARI Cat. 1 genes show decreased poly(A) tail length in idiopathic ASD brains). This is accompanied by concomitant decreased protein levels without mRNA levels alteration of deadenylated CPEB4-target ASD genes in autistic brains. The causal role of the CPEB4 alteration on these ASD gene poly(A) tail length- and protein level-changes is evidenced by the fact that equivalent imbalance in CPEB4 splicing isoforms in transgenic mice results in similar poly(A) tail length-changes and in decreased protein levels of a plethora of ASD genes including *AUTS2, CHD2*, *FOXP1*, *GPC6*, *RBFOX1*, *TNRC6B*, *WAC* and *ZBTB20*. As expected, these mice show robust ASD-like anatomical, electrophysiological and behavioral phenotypes.

Unlike mutations responsible for monogenic syndromes with autistic features, such as Rett or Fragile X, most mutations associated with non-syndromic ASD have a limited impact *per se* (Gaugler et al., 2014). Therefore, the co-existence of multiple genetic factors together with perturbations of neurodevelopment able to impact expression of other ASD related genes are believed to contribute to non-syndromic and idiopathic ASD (Kim and Leventhal, 2015). A critical goal of in ASD research is to identify potentially convergent molecular pathways (Parikshak et al., 2013; Voineagu et al., 2011) as well as finding altered regulators able to simultaneously orchestrate expression of multiple ASD genes in concordance to neurodevelopment affecting cues. Interestingly, our study reveals that CPEB4 is excellently positioned to act as such a hub in ASD gene expression and to become a therapeutic target for a wide range of idiopathic and even syndromic ASD etiologies.

CPEB4 shows highest expression levels both in mouse embryo and in adult brain (Shin et al., 2016; Theis et al., 2003) and CPEBs modulate translation of specific

transcripts during gametogenesis and early development in response to extracellular stimuli such as progesterone and insulin (Sarkissian et al., 2004). Thus, it is conceivable that other development-modifying factors such as vitamins, nutrients, pollutants or mediators of inflammation that have been proposed as possible environmental factors accounting for the 50% of ASD causality that is not genetic (Hallmayer et al., 2011; Sandin et al., 2014) could also impact CPEB4 developmental functions. This way, CPEB4 might modulate, as a consequence of development perturbations, the expression of many of the genes that have individually been proven to contribute to ASD pathogenesis. Besides, we have demonstrated that the pathogenic effect of CPEB4 isoforms imbalance is exerted during mouse early development. More precisely, we observed that conditional TgCPEB4Δ4 mice did not show any ASD-like phenotype if we prevent the exogenous CPEB4Δ4 expression by treating dams during pregnancy with doxycycline (data not shown). However, they did not correct or attenuate ASD phenotype if the doxycycline treatment was given after weaning (data not shown). Thus, CPEB4 becomes a potential therapeutic target in pregnant mother that have been exposed to toxins or have suffered infection and/or immune activation.

With this hub position of CPEB4 in ASD gene expression, the question emerges of why the powerful genomic analyses of large ASD cohorts did not identify mutations in CPEB4. We could list different possible explanations: It is estimated that ~1000 genes are likely to be involved to ASD however only a few hundred are known, thus, probably CPEB4 had not been reported yet. CPEB4 deficient mice do not mimic the molecular signature observed in ASD patients nor show the ASD-like electrophysiological and behavioral alterations observed in TgCPEB4Δ4 mice (data not shown). Therefore, neither deletions harboring the CPEB4 gene, nor loss of function mutations or promoter polymorphisms leading to decreased expression of CPEB4 are expected to be ASD-causative. Other likely explanation is that the pathogenic CPEB4 alteration that leads to ASD is triggered by environmental factors that indirectly alter its splicing and function. In fact, we have preliminary evidence of altered CPEB4 splicing in the maternal immune activation model of ASD (data not shown). Furthermore, prenatal cytomegalovirus (CMV) infection has been related to ASD (Engman et al., 2015; Ornoy et al., 2015), and recent study has shown than CPEB1 was highly induced and also CPEB4, after CMV infection. This results in widespread alternative splicing (AS), shortening of 3' UTRs and lengthening of poly(A) tails in host gene transcripts (Batra et al., 2016).

Recently, we have generated mice with double CPEB4 modification (heterozygote KO of endogenous CPEB4 and CPEB4Δ4 overexpression). These double TgCPEB44:CPEB4 KO mice show imbalance of CPEB4Δ4 isoform but do not show excess of total CPEB4.

As we expected, they show ASD-like anatomical and behavioral phenotype (data not shown), confirming that only the alteration of the ratio of CPEB4 splicing isoforms in favor of CPEB4Δ4 induces ASD phenotype. Thus, the only genetic variants that would mimic the pathogenic splicing alteration would be intronic mutations flanking the 24-nt microexon or selective deletion of this single exon. Such mutations would most likely have gone unnoticed in most genetic screens as these normally detect exonic mutations (De Rubeis et al., 2014; Iossifov et al., 2014) and bigger CNV (Levy et al., 2011). It is worth noting though that the SFARI collection of large CNV associated with ASD includes a duplication within the CPEB4-containing 5q35.1-q35.3 region (Kaminsky et al., 2011) .

Splicing alteration and particularly of microexons has previously been implicated in ASD pathogenesis (Irimia et al., 2014; Xiong et al., 2015). Interestingly, RBFOX1 is one of the few splicing factors known to enable microexon processing (Li et al., 2015) and it has recently been shown to regulate alternative splicing of *CPEB4* in muscle (Pedrotti et al., 2015). Here we show that *RBFOX1* transcript is a target of CPEB4 and that RBFOX1 protein levels are decreased in idiopathic ASD brains and in TgCPEB4Δ4 mice. This leads us to speculate on a potential feed forward loop. CPEB4 alteration in ASD patients will lead to decreased RBFOX1 levels that would impact *CPEB4* splicing further favoring the pathogenic mis-spliced isoform encoding a *CPEB4* isoform refractive to regulation by various kinases thus further dysregulating CPEB4 activity, that in turn will further decrease *RBFOX1* translation.

We have demonstrated here that the ASD-CPEB4 splicing variant results in altered expression of multiple genes that had been previously linked to ASD with high confidence because they harbor mutations that co-segregate with disease. It is possible though that other poly(A)-altered genes in the less confidence categories or not in SFARI gene database at all may also significantly contribute to pathogenesis. Their protein levels may change selectively in neurons specifically at late embryonic or postnatal developmental stages, but that their mutations have not been found replicated in multiple studies or that they cannot harbor mutations themselves, for instance because these would be lethal when expressed in all cell types and/or during earlier developmental stages. Since our study unravels a new molecular signature, -poly(A) tail length shortening- associated to the change in gene expression, correlation analysis of the genes with altered poly(A) tail length with proteomics data and the genes in modules functionally involved in ASD may unravel new effectors in idiopathic ASD.

We still do not fully understand the pathogenic mechanism by which imbalance of CPEB4Δ4 caused ASD. Interestingly, CPEB4Δ4 lacks a microexon that may regulate

CPEB4 activity by phosphorylation (Theis et al., 2003; Wang and Cooper, 2010) and the decreased protein synthesis and polyadenylation of ASD-related genes in TgCPEB4Δ4 mice and ASD brains together with decreased CPEB4 total protein levels suggest a dominan negative (DN) effect of CPEB4Δ4 isoform over CPEB4 and most likely also over the other CPEBs. This may explain why molecular and behavioral phenotypes of CPEB4 KO(GT)/+ mice and CPEB4 KO mice are opposite to those of TgCPEB4Δ4 mice. The different CPEBs bind in a competitive manner the same *cis-acting* element (CPE) and therefore can bind the same mRNAs (Afroz et al., 2014; Stepien et al., 2016). As an example, here we describe that 7.9% of transcripts were bound only by CPEB4, 5.8% only by CPEB1 and 7.0% by both. Expression of a DN-CPEB4 will not change this distribution, but CPEB4-KO will free the CPEB4-enriched targets to become CPEB1 targets. Thus KO of a CPEB causes a rearrangement in the regulation of CPE-mRNAs distinct from a CPEB-DN (as reviewed in Fernandez-Miranda and Mendez, 2012) (Figure 50).

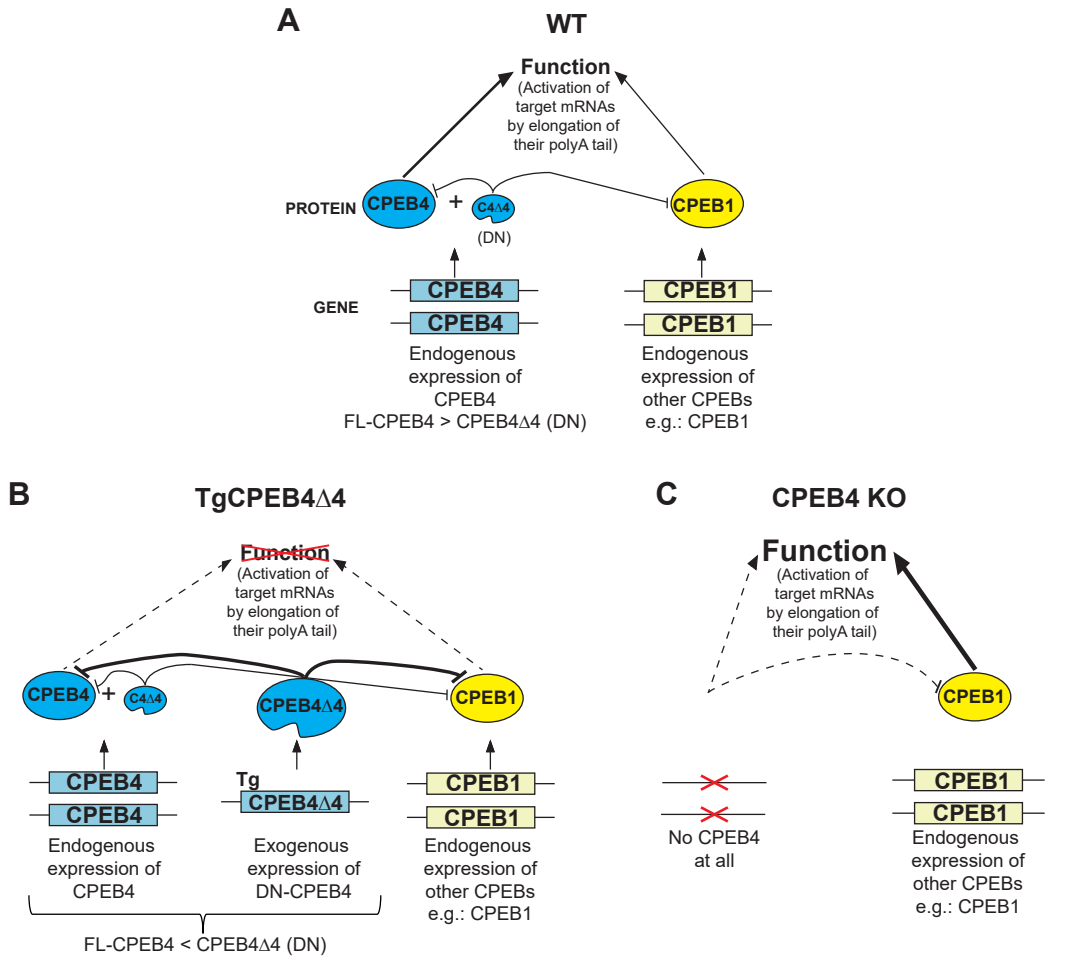

Figure 50: Mouse and human data fit a dominant negative effect of CPEB4Δ4 over CPEB4 and also over the other CPEBs. Schematic cartoon showing the dominant negative (DN) effect of CPEB4Δ4 over CPEB4 and over other CPEBs (e.g. CPEB1) in three different scenarios (A) WT (B) TgCPEB4Δ4 and (C) CPEB4 KO mice.

Recent advances in splicing modulating therapies and the use of antisense oligonucleotides (AONs) to treat neurological disorders (Evers et al., 2015) might open new possibilities for CPEB4 as a therapeutical target for ASD. In this case, induction of exon inclusion, could be attempted for instance with AONs targeting putative splicing silencers affecting this microexon or by adding an oligonucleotide tail that recruits exon inclusion factors. In this case, *RBFOX1* would be an excellent candidate for the above mentioned reasons. Another gene therapy strategy could be based on specific silencing of the transcripts lacking the microexon.

In summary, we demonstrate that CPEB4, which was known to participate in development and in brain plasticity, is altered in ASD with a concomitant new molecular signature of decreased polyadenylation and altered translation of numerous high confidence ASD causing genes, thus providing a potential link between genetic and environmental factors in ASD. Collectively, these data unravel a key role of CPEB4 in ASD and open new therapeutic opportunities for a wide range of idiopathic ASD etiologies.

Final remarks

By showing CPEB1/CPEB4 imbalance in Huntington's disease leading to poly(A) tail changes in hundreds of transcripts previously associated to neurodegeneration not only in HD but also in AD and PD, our results suggest a common new CPEB-related pathogenic mechanism across neurodegenerative diseases. We also demonstrate that CPEB4, which was known to participate in development and in brain plasticity, is altered in ASD and plays a crucial role in translationally controlling expression of the majority of high confidence ASD causing genes, thus providing a potential link between genetic and environmental factors in ASD. Collectively, this thesis unravels a key role of CPEB4 in neurodegeneration and autism spectrum disease.

MATERIALS AND METHODS

1. BRAIN TISSUE SAMPLES

1.1. Patients Samples

Brain specimens used in immunoblot and IHC from frontal Cx and St of HD patients and controls (CTRL) were provided by Institute of Neuropathology Brain Bank (HUB-ICO-IDIBELL, Hospitalet de Llobregat, Spain), the Neurological Tissue Bank of the IDIBAPS Biobank (Barcelona, Spain), the Banco de Tejidos Fundación Cien (BT-CIEN, Madrid, Spain) and the Netherlands Brain Bank (Amsterdam, The Netherlands). Brain specimens used in immunoblot, poly(U) chromatography and qRT-PCR from frontal cortex - BA8/9 of ASD patients and CTRL were provided by University of Maryland Brain and Tissue Bank, NIH NeuroBioBank (NBB) (Baltimore,MD) and the Autism Tissue Program (ATP) brain bank at The Harvard Brain and Tissue Bank (Blemont, MA). Written informed consent for brain removal after death for diagnostic and research purposes was obtained from brain donors and/or next of kin. Procedures, information and consent forms have been approved by the Bioethics Subcommittee of Consejo Superior de Investigaciones Científicas (CSIC, Madrid, Spain). RNA sequencing data from human brain tissue (ASD and CTRL individuals) were directly obtained from (Irimia et al., 2014) and (Parikshak et al., 2016).

1.2. Mouse Models

We used different previously reported mouse models: R6/1 transgenic mice for the human exon-1-Htt gene (Mangiarini et al., 1996) in B6CBAF1 background, HD94 mice that express N-terminal Htt with an interrupted 94 CAG repeat (Yamamoto et al., 2000) and heterozygous knock-in of an expanded CAG track in exon 1 of huntingtin gene, zQ175 mice (Menalled et al., 2012) both in C57BL/6J background, heterozygous CPEB4 gene trap (CPEB4 GT/+) and CPEB4 KO (Calderone et al., 2016). Conditional mice expressing human CPEB4 lacking exon 4 (TgCPEB4Δ4) in C57BL/6 background were generated for this study (for details, see “Generation of TgCPEB4Δ4 mice” below). All mice were housed at the Centro de Biología Molecular “Severo Ochoa” animal facility. Mice were housed four per cage with food and water available ad libitum and maintained in a temperature-controlled environment on a 12/12 h light-dark cycle with light onset at 08:00. Animal housing and maintenance protocols followed the guidelines of Council of Europe Convention ETS123, recently revised as indicated in the Directive 86/609/EEC. Animal experiments were performed under protocols (P15/P16/P18/P22) approved by the Centro de Biología Molecular Severo Ochoa Institutional Animal Care and Utilization Committee (Comité de Ética de Experimentación Animal del CBM, CEEA-CBM), Madrid, Spain.

2. EXPERIMENTAL TECHNIQUES

2.1. Genotype

Mouse genomic DNA was isolated from tail biopsies following digestion at 60°C in buffer containing 100 mM Tris-HCl (pH 7.8), 5 mM EDTA, 200 mM NaCl, 0.1% SDS and 1mg/ml proteinase K, followed by heat inactivation. After add NaCl 6M, samples were centrifuged at 13000 rpm for 10 min and supernatants were removed to new tube with 500 µl of isopropanol. Samples were centrifuged 13000 rpm for 10 min and pellets were washed with 300 µl of ethanol. Finally, DNA was resuspended in 100 µl of nuclease-free water.

PCR was performed according to the manufacturer's instructions (Promega, GotTaq® G2 Flexi DNA polymerase, M7805) and with specific primer pairs:

R6/1	Forward	5'-tgggacgcaaggcgccgtg-3'
	Reverse	5'-tggaaggacttgagggactc-3'
zQ175	Forward	5'-gatcggccattgaacaagatg-3'
	Reverse	5'-agagcagccgattgtctgttg-3'
tTA	Forward	5'-actaagtcatcgcgatggagc-3'
	Reverse	5'-cgaaatcgtctagcgcgtcgg-3'
BitetO	Forward	5'-catggtcaggtcatggatgacc-3'
	Reverse	5'-taatcagccactgatccacccag-3'
CPEB4 (+)	Forward	5'-ggacgtttgacatgcactcac-3'
	Reverse	5'-cactctggctacatggtagcat-3'
CPEB4 (-)	Forward	5'-tggcatccatgcttgtgtat-3'
	Reverse	5'-cgcgtcgagaagttcctatt-3'

2.2. Immunoblot

Samples from human brain were stored at -80°C and were ground with a mortar in a frozen environment with liquid nitrogen to prevent thawing of the samples, resulting in tissue powder. For mouse, brains were quickly dissected on an ice-cold plate and the different structures stored at -80°C. Human and mouse extracts were prepared by homogenizing the brain areas in ice-cold extraction buffer (20 mM HEPES pH 7.4, 100 mM NaCl, 20 mM NaF, 1% Triton X-100, 1 mM sodium orthovanadate, 1µM okadaic acid, 5 mM sodium pyrophosphate, 30 mM β-glycerophosphate, 5 mM EDTA, protease inhibitors (Complete, Roche, Cat. No 11697498001)). Homogenates were centrifuged at 15000g for 15 min at 4°C. The resulting supernatant was collected, and protein content determined by Quick Start Bradford kit assay (Bio-Rad, 500-0203). Between 10 and 20 µg of total protein were electrophoresed on 10% SDS-polyacrylamide gel, transferred to a nitrocellulose blotting membrane (Amersham

Protran 0.45 µm, GE Healthcare Life Sciences, 10600002) and blocked in TBS-T (150 mM NaCl, 20 mM Tris–HCl, pH 7.5, 0.1% Tween 20) supplemented with 5% non-fat dry milk. Membranes were incubated overnight at 4°C with the primary antibody in TBS-T supplemented with 5% non-fat dry milk, washed with TBS-T and next incubated with secondary HRP-conjugated anti-mouse IgG (1:2000, DAKO, P0447), anti-rabbit IgG (1:2000, DAKO, P0448), anti-goat IgG-Fc fragment (1:4000, Bethyl, A110-104P) or anti-rat IgG-Fc fragment (1:5000, Bethyl, A110-136P) and developed using the ECL detection kit (PerkinElmer, NEL105001EA).

Antibodies: Rabbit CPEB1 (1:350, Santacruz, sc-33193); rabbit CPEB2 (1:1000, Abcam, ab51069); rabbit CPEB3 (1:1000, Abcam, ab10883); rabbit CPEB4 (1:1000, Abcam, ab83009); rabbit AUTS2 (1:750, Sigma, HPA000390); mouse STX6 (1:1000, BD transduction laboratories, Cat. No. 610635), mouse TAU-5 (1:1000, Merck Milliporte, Cat. 577801), mouse GSK3α/β (1:1000, ThermoFisher scientific, Cat. 44–610), mouse α-SYN (1:1000, Abcam, [4D6] ab1903); rabbit KTN1 (1:1000, Proteintech, Cat. 19841-1-AP). rabbit PTEN (1:1000, Cell Signaling, 9559S); mouse DYRK1A (1:1000, Abnova, H00001859-M01); rabbit FOXP1 (1:2000 for mouse and 1:500 for human samples, Abcam, ab16645); rabbit WAC (1:500, Merk Millipore, ABE471); mouse RBFOX1 (1:2000 for mouse and 1:1000 for human samples, Merk Millipore, MABE985), rabbit PCDH9 (1:500, Abcam, ab171166); rabbit ZBTB20 (1:300, SantaCruz, sc-99728); rabbit TNRC6B (1:500, Merk Millipore, AB9913); rat CHD2 (1:750, Merk Millipore, MABE873); rabbit GPC6 (1:1000, Abcam, ab136295); mouse β-GAL (1:3000, Promega, Z378A); mouse β-ACTIN (1:25000, Sigma, A2228).

2.3. Real-time quantitative reverse transcriptase-PCR

Total tissue RNA was extracted from frontal Cx - BA8/9 of ASD and CTRL subjects, St and Cx of HD and CTRL subjects, St and Cx of WT and R6/1 mice WT and, Control, CPEB4 GT/+ and TgCPEB4Δ4 mice using the Maxwell® 16 LEV simplyRNA Tissue Kit (Promega, AS1280). The resulting total RNA was used for cDNA synthesis with a Super Script III First-Strand Synthesis SuperMix kit (Invitrogen, PN 11752250) with the amplification protocol 30” at 95°C + (5” at 95°C + 5” at 60°C) x 40 + (5” at 60°C + 5” at 95°C). Quantification was performed by real-time PCR using a CFX 384 System (Bio-Rad) in combination with SsoFast Eva Green (Bio-Rad, #1725204) and 0.25µM of primer pair was used. Data were analyzed by GenEx 5.3.7 software (Multid AnaLyses AB). The mRNA levels were normalized first relative to total RNA and then relative to the *18S* ribosome subunit, β-*ACTIN*, *GAPDH* and β-*TUBULIN* gene expression in each sample.

Absolute quantitative PCR was performed to determine the percentage of each CPEB4 splicing isoform in both human and mouse species using specific primers. For every primer couple, specificity was tested by PCR-mediated amplification of specific amplicons from each isoform. No product was detected in any non-specific combination. Amplicons of each CPEB4 isoform were serially diluted to generate a calibration curve. Next, total tissue RNA was extracted, and quantitative real-time RT-PCR was performed. Finally, the percentage of each CPEB4 isoform with respect to total CPEB4 copies was calculated.

Human primers

CPEB1	Forward	5'-ggcagccatcttgaacga-3'
	Reverse	5'-aagtcacacgaccagaacca-3'
CPEB2	Forward	5'-gcctcataaagcagaaagcaa-3'
	Reverse	5'-agcatcaatgagtgcctgaa-3'
CPEB3	Forward	5'-gaacgctactctagaaaggtgtttg-3'
	Reverse	5'-cgaaagctggcagtgatct-3'
Total CPEB4	Forward	5'-cactgtttccaatggaagatgg-3'
	Reverse	5'-ggtgaacccaggccactatg-3'
CPEB4Δ3	Forward	5'-agctgaaaatgataccattaaagcaa-3'
	Reverse	5'-ccattggaaacagtgaagactgac-3'
CPEB4Δ4	Forward	5'-atccgatagctctctgcttattaatggt-3'
	Reverse	5'-cacggccatcatccaagaat-3'
CPEB4Δ3Δ4	Forward	5'-agctgaaaatgataccattaaaggtca-3'
	Reverse	5'-aggctgatccccacggc-3'
Full Length CPEB4	Forward	5'-gtctaaactattcatatccaggatccg-3'
	Reverse	5'-cctctccttcgcccatatgtc-3'
AUTS2	Forward	5'-gaagcggagagagtccacct-3'
	Reverse	5'-tcctgaggcttaagtgctacatc-3'
18S	Forward	5'-atccattggagggcaagtc-3'
	Reverse	5'-gctcccaagatccaactacg-3'

Mouse primers

Cpeb1	Forward	5'-ttatctgcagctcacaacctg-3'
	Reverse	5'-gcaaaagtacttgaagcagacct-3'
Cpeb2	Forward	5'-ctgcagcagaggaactcgta-3'
	Reverse	5'-ggttgctccaaggagactgt-3'
Cpeb3	Forward	5'-aaaacccagccccagtct-3'
	Reverse	5'-gcttggggatctctgagga-3'

Total Cpeb4	Forward	5'-caaatcttattttccaccaaaagg-3'
	Reverse	5'-catcaatgagagcctgaacaga-3'
Cpeb4Δ3	Forward	5'-agctgaaaatgattccattaaagcaa-3'
	Reverse	5'-ccatcggaaacaatgaagactgac-3'
Cpeb4Δ4	Forward	5'-atccgatagttctctgcttattaatggt-3'
	Reverse	5'-acggccatcatccaggaat-3'
Cpeb4Δ3Δ4	Forward	5'-gctgaaaatgattccattaaaggtca-3'
	Reverse	5'-gaggttgatccccacggc-3'
Full Length Cpeb4	Forward	5'-ctaaactattcatacccaggatccg-3'
	Reverse	5'-cctctccttcgcccataagtc-3'
Auts2	Forward	5'-cctccaggccctagtctctt-3'
	Reverse	5'-aaggggtcccagtaggatgt-3'
Stx6	Forward	5'-cggggtgctgaagaacat-3'
	Reverse	5'-ctccaactcgtgagagaaatcat-3'
Mapt	Forward	5'-agggaacatccatcacaagc-3'
	Reverse	5'-tggactctgtccttgaagtcc-3'
Gsk3 β	Forward	5'-ggcagcaaggtaaccacagt-3'
	Reverse	5'-gatggcaaccagttctccag-3'
Snca	Forward	5'-tggcagtgaggcttatga-3'
	Reverse	5'-gcttcaggctcatagtct-3'
18s	Forward	5'-ctcaacacgggaaacctcac-3'
	Reverse	5'-cgctccaccaactaagaacg-3'
β-Actin	Forward	5'-ctaaggccaaccgtgaaaag-3'
	Reverse	5'-accagaggcatacagggaca-3'
Gapdh	Forward	5'-ctcccactcttccaccttcg-3'
	Reverse	5'-cataccaggaaatgagcttgacaa-3'
β-Tubulin	Forward	5'-gacctatcatggggacagtga-3'
	Reverse	5'-cggctctgggaacatagttt-3'

Human and mouse common primers

Total CPEB4	Forward	5'-ttgctccatttttctgtgctaa-3'
	Reverse	5'-agcagcccagcaatattcac-3'

2.4. Histopathology tissue analysis. Immunohistochemistry and immunofluorescence

For human samples, formalin-fixed (4%, 24 h), paraffin-embedded tissue from Cx and St were used. Sections (5 µm thick) were mounted on superfrost-plus tissue slides (Menzel-Gläser, 631-9483) and deparaffinized. Peroxidase activity was quenched with 0.3% H_2O_2 in methanol for 30 min, followed by antigen retrieval with 10 mM pH 6.0 citrate buffer heated by microwave for 15 min.

Mice euthanasia was performed using CO_2. Brains were immediately removed and dissected on an ice-cold plate and left hemispheres, processed for histology, were placed in 4% paraformaldehyde (PFA) in Sorensen's phosphate buffer overnight and then immersed in 30% sucrose in phosphate buffered saline (PBS) for 72 h. Once cryoprotected, the samples were included in optimum cutting temperature (OCT) compound (Tissue-Tek, Sakura Finetek Europe, ref. 4583), frozen and stored at -80°C until use. 30 µm sagittal sections were cut on a cryostat (Thermo Scientific), collected and stored free floating in glycol containing buffer (30% glycerol, 30% ethylene glycol in 0.02 M phosphate buffer) at -20°C. Before staining, sections were washed with PBS to eliminate the cryoprotective buffer and immersed in 0.3% H_2O_2 in PBS for 30 min to quench endogenous peroxidase activity.

For ***immunohistochemistry*** staining, sections were immersed for 1h in blocking solution (PBS containing 0.5% Fetal Bovine Serum, 0.3% Triton X-100 and 1% BSA and incubated overnight at 4°C with the corresponding primary antibody diluted in blocking solution. After washing, brain sections were incubated first with biotinylated anti-rabbit or anti-mouse secondary antibody and then with avidin-biotin complex using the Elite Vectastain kit (Vector Laboratories, PK-6101-2). Chromogen reactions were performed with diaminobenzidine (SIGMAFAST DAB, Sigma, D4293) for 10 min. Mouse sections were mounted on glass slides and coverslipped with Mowiol (Calbiochem, Cat. 475904) while human slides were dehydrated and coverslipped with DePex (Serva). Images were captured using an Olympus BX41 microscope with an Olympus camera DP-70 (Olympus Denmark A/S).

Antibodies: Rabbit CPEB4 (1:1000, AVIVA, ARP41024_P050); monoclonal mouse CPEB4 (1:100 and 1:1500 in human and mouse tissue respectively, generated by Mendez R. Lab); rabbit KTN1 (1:100, Proteintech, Cat. 19841-1-AP).

For ***immunofluorescence***, sections were pretreated with 0.1% Triton X-100 for 30 min, 1 M glycine for 15 min and blocking solution (1% BSA, 0.3% FBS and 0.1% Triton X-100) for 1 h. Sections were then incubated overnight at 4 °C with monoclonal mouse anti CPEB4 (1:1000, generated by Mendez R. Lab) and goat anti huntingtin (1:200, N-18 Santacruz, sc-8767) in blocking solution. The following day, sections were washed in PBS and incubated with secondary antibodies for 2 h: anti-goat-Alexa 555 (1:500, ThermoFisher, A-21432) and anti-mouse-biotin (from Elite Vectastain kit, Vector Laboratories, PK-6102), followed by signal amplification with Streptavidin-Alexa488 (1:500, ThermoFisher, S32354) for 1h. After washing, nuclei were counterstained with DAPI (1:5000, Calbiochem, 28718-90-3). Finally, sections were mounted on glass slides, coverslipped with Mowiol (Calbiochem, 475904) and maintained at 4°C.

Images were acquired with a laser confocal LSM710 system coupled to the invert Axioobserver microscope with a 63×, 1.4 numerical aperture oil-immersion objective using the Zen2010B sp1 software (Carl Zeiss). Sequential optic sections (1 µm) were acquired in z stacks. Images were processed using ImageJ 1.45s.

2.5. Poly(U) chromatography

Mouse samples: WT and R6/1 mice 7.5 month-old (n=4); WT, CPEB4 GT/+ and CPEB4 KO (n=2); control and TgCPEB4Δ4 mice (n=3) 1.5 month-old were sacrificed by cervical dislocation. St in the case of WT versus R6/1 mice and Cx and St together in all other cases were quickly dissected on an ice-cold plate.

Human samples: brain specimens from frontal cortex - BA8/9 of ASD patients (n=6) and controls (n=5) with age between 5-23 years old.

Human and mouse samples were homogenized and total RNA was extracted using the Maxwell® 16 LEV simplyRNA Tissue Kit (Promega, AS1280), and stored at -80°C until use. The poly(A) RNA fraction was purified by poly(U) chromatography. Poly(U)-agarose (Sigma, p8563) was suspended in swelling buffer (0.05 M Tris-HCl, pH 7.5, 1 M NaCl) 35 ml/g, incubated overnight at room temperature and loaded into the chromatography column. An aliquot of total RNA was stored at -80°C ("Input") and the rest was incubated with sample buffer (0.01 M Tris-HCl, pH 7.5, 1 mM EDTA, 1% SDS) for 5 min at 65°C and chilled on ice. Binding buffer was added (0.05 M Tris-HCl, pH 7.5, 0.7 M NaCl, 10 mM EDTA, 25% [v/v] formamide) and then the sample was loaded into the poly(U)-agarose chromatography column (Mobitec, M1002s) and incubated for 30 min at room temperature (25°C) with agitation. Next, the column containing the sample was washed three times at 25°C and six times at 55°C with washing buffer (0.05 M Tris-HCl, pH 7.5, 0.1 M NaCl, 10 mM EDTA, 25% [v/v] formamide). The 55°C washes were collected and stored at -80°C ("Short poly(A)-tail fraction"). The remaining poly(A) RNA ("Long poly(A)-tail fraction") was eluted with elution buffer (0.05 M HEPES, pH 7, 10 mM EDTA, 90% [v/v] formamide) at 55°C and stored at -80°C. The RNA of the two poly(A) fractions was precipitated by adding 1 volume of isopropanol, 1/10th volumes of sodium acetate 3 M pH 5.2 and 20 µg of glycogen (Sigma, G1767). The samples were incubated at -20°C for 20 min and centrifuged 15 min at 14000g at 4°C. The supernatant was removed and the pellet was washed with 750 µL of ethanol and centrifuged at 14000g and 4°C for 5 min. The supernatant was removed and the pellet was air-dried for 5 min. The RNAs were resuspended in 300 µL of nuclease-free water and then 300 µL of acid Phenol:Chloroform (5:1) were added to them. Samples were vortexed and centrifuged for 10 min at 14000g and 4°C.

The aqueous phase was recovered, mixed with 1 volume of chloroform, vortexed and centrifuged again. The aqueous phase was recovered and precipitated again using the isopropanol precipitation.

2.6. RNA immunoprecipitation

WT and R6/1 mice (n=4) were sacrificed by cervical dislocation at the age of 7-8 months. Total St was quickly dissected on an ice-cold plate and cut into pieces. The pool of the four WT or R6/1 striata was washed twice with PBS, crosslinked with 0.5% PFA in PBS for 7 min at room temperature and treated with glycine 1M for 5 min. After two washes with cold PBS, pool samples were homogenized in lysis buffer (50 mM Tris, pH 8.0, 150 mM NaCl, 1% NP-40, 0.5% deoxicolate, 0.1% SDS, 1 mM EDTA, protease inhibitor (Complete, Roche, 11697498001), RNAse inhibitor (Ribolock, Life Technologies, EO0381)) and centrifuged at 13000 g for 10 min at 4°C. Dynabeads protein A (Life Technologies, 10001D) were washed twice with PBS and incubated with anti-CPEB4 antibody (10 µg, Abcam, ab83009), anti-CPEB1 antibody (5 µg, Proteintech, 13274-1-AP) or rabbit IgG (5 µg, Sigma, I5006) for 2h. Next, dynabeads were washed once with PBS and twice with triethanolamine 0.2M pH 8.2, incubated with dimethyl pimelimidate 20 mM for 30 min, treated with Tris 50mM pH 8.0 and washed twice with lysis buffer. Lysates were precleared with unconjugated dynabeads for 20 min at 4°C in a wheel, an aliquot was stored at -80°C ("Input") and the rest of the extract was immunoprecipitated with the antibody-conjugated dynabeads overnight at 4°C in a wheel. Immunoprecipitates were washed six times in cold lysis buffer.

For protein extraction, samples were incubated with Laemmli buffer (10% SDS, 0.325 M Tris HCl pH7.5, Glycerol 25%) for 20 min at 60°C. Dynabeads were removed with the help of a magnet and samples were boiled after adding DTT 0.1 M and bromophenol blue 0.1%.

For RNA extraction, immunoprecipitates were resuspended in 100µl of proteinase K buffer (200 mM Tris pH 7.5, 100 mM NaCl, 10 mM EDTA, 1% SDS) containing 0.7 µg/µl of proteinase K (Roche, 03115852001) and incubated 1h at 42°C and 1h at 65°C. RNA was extracted using the TRIzol reagent (Invitrogen, 15596018). Briefly, samples were resuspended in 300 µl of TRIzol. Then, 20 µg of glycogen was added. Samples were vortexed, incubated for 5 min at room temperature and centrifuged at 14000g for 15 min at 4°C. The aqueous phase was recovered, mixed with 1 volume of isopropanol, incubated for 5 min at room temperature and precipitated at 14000g 30 min at 4°C. The pellet was washed with 300 µl of ice-cold 75% ethanol and centrifuged at 14000g

10 min at 4°C. The pellets were resuspended in 100 µl of nuclease-free water. To ensure the complete removal of the phenol, the RNA was precipitated again. To this aim, 10 µl of sodium acetate 3 M pH 5.6 and 250 µl of 75% ethanol were added. Samples were vortexed and stored at -20°C for 1h. Then, they were precipitated at 14000g for 30 min at 4°C. The pellet was washed with 75% ethanol and centrifuged again at 14000g for 10 min at 4°C. Pellets were air-dried for 5 min and resuspended in nuclease-free water.

2.7. Poly(A) test assay

Total mRNA from a pool of 2 St from control and TgCPEB4Δ4 was extracted using GenElute mRNA Miniprep Kit (Sigma, MRN70) and treated with DNaseI (TURBO DNA-free, Thermo Fisher Scientific, AM1907) following the manufacturer's recommendations. 6 µg of this mRNA was incubated for 30 min at 37°C with 20 µM of an oligo dT primer and 0.2U of RNase H (New England Biolabs, M0297S) or H_2O, and purified using Phenol/Chloroform extraction. 4 µg of RNA were ligated to 0.4 µg of SP2 anchor primer using T4 RNA ligase (New England Biolabs, M0204S) in a final volume of 10 µl. The whole ligation was retrotranscribed into cDNA using the RevertAid First Strand cDNA Synthesis kit (ThermoFisher Scientific, K1621) and 0.4 µg of ASP2T antisense primer in a final volume of 50 µl. 1 µl of cDNA was amplified by PCR using BioTaq DNA polymerase (Bioline, Bio-21040) in a final volume of 50 µl, using the forward primers and the reverse primer ASP2T.

Half of the PCR products were run in a 2% agarose/GelRed gel and run at 120V for 1.5h. A picture of the gel was taken together with a ruler so as to know the position of the ladder bands after the hybridization. Gels were washed upside-down in lysing buffer (1.5M NaCl, 0.5M NaOH) for 30 min, briefly washed 3 times with ddH_2O and incubated in neutralization buffer (1.5M NaCl, 1M Tris-HCl pH 7.4) for 45 min. DNA was transferred overnight to a Biodyne® nylon bidine membrane (0.45µm, Pall Corporation, 60102) and cross-linked (254 nm; 0.12 J). The membrane was pre-hybridized in church buffer (342mM Na_2HPO_4, 158mM NaH_2PO_4, 6% [w/v] SDS, 1mM EDTA, pH 7.2) for 3h at 55ºC and hybridized overnight with 32P-labeled probes diluted in church buffer at 55ºC. The following day, membranes were washed with washing buffer (0.1% SDS in SSC 1X) until background signal was removed. Membranes were exposed to an autoradiography film and developed.

For the labelling of the probes, 20 pmol of each DNA oligo were labelled with 3 µl of 32Pγ-ATP 3000 Ci/mmol in a final volume of 10 µl for 30 min at 37ºC using T4 polynucleotide kinase (New England Biolabs, M0201S). Labelled probes were purified

with illustra MicroSpin G-25 columns (GE Healthcare, 27-5325-01) and diluted in 25 ml of pre-warmed church buffer.

Primers sequence:

SP2	5'-P-ggtcacctctgatctggaagcgac-NH_2-3'
ASP2T	5'-gtcgcttccagatcagaggtgacctttt-3'
AUTS2	5'-ggacattaaccctcttgtctacatatttgg-3'

2.8. High-Resolution poly(A) tail (Hire-PAT) assay

To confirm the poly(A) tail length measured by polyU chromatography and by PAT assay, the USB® Poly(A) Tail-Length Assay Kit (Affimetrix, catalog 76455) based on Hire-PAT method, was used. Total striatal RNA from 1.5 month-old control and TgCPEB4Δ4 mice (n=3) was extracted using the Maxwell® 16 LEV simplyRNA Tissue Kit (Promega, AS1280) and stored at -80ºC until use. G/I tailing (1 µg of total RNA) and reverse transcription were performed according to the manufacturer's instructions. Poly(A) size was determined by subtracting the PCR amplicon size obtained with the Universal primer and *Auts2* forward specific primers. To verify that the measured poly(A) tail corresponds to *Auts2*, three different forward specific primers were tested. PCR products were resolved on 2.5% agarose/gelgreen (Biotium, 41004) gels run at 120V for 1.5h.

Primer sequences:

***Auts2* -F1**	5'-tttggagagaatatgactttactagccgag-3'
***Auts2* -F2**	5'-aaatacactatatcttgtctactggcctg-3'
***Auts2* -F3**	5'-ccatttggtcctctagtatattaaagtgc-3'
***Auts2* -R**	5'-gaaaataaaacaaaacaaaaaacaggataacaatg-3'

2.9. Generation of TgCPEB4Δ4 mice

Human CPEB4 lacking exon 4 (CPEB4Δ4, without 8 aminoacids) cDNA was cloned into a plasmid containing a bidirectional TetO sequence flanked by CMV minimal promotors with lacZ reporter sequences coupled to a nuclear localization signal (pBI-G, Clontech, 631004) and microinjected into single-cell CBAxC57BL/6 embryos. Founder mice were then backcrossed with WT C57BL/6J mice (TetO βGal/CPEB4Δ4). TetO βGal/CPEB4Δ4 was crossed with CamkII-tTa (Tta) mouse line (Mayford et al., 1996) to obtain the conditional transgenic mice with forebrain neural specific CPEB4Δ4 overexpression mice (TgCPEB4Δ4 mice).

2.10. Golgi Staining

Three month-old mice were completely anesthetized with an intraperitoneal pentobarbital injection (60 mg/kg Dolethal®, Vetoquinol). The whole brain was extracted and immersed in Golgi-Cox staining solution (FD Rapid GolgiStainTM kit, FD Neurotechnologies, cat. PK401). 150 µm sagittal sections were obtained in a Leica VT1200S vibratome and mounted on gelatin-coated slides. Golgi staining was performed as manufacturer's instructions. Afterwards, all sections were counterstained with toluidine blue pH 4.0 (1 g/l Toluidine Blue (Sigma, 198161), 0.8 M glacial acetic acid) and coverslipped with DePeX (Amsbio, 18243.02).

Pyramidal neurons from layer II/III of the cortex were identified by their distance from pia mater and their distinct morphologies. Secondary, tertiary and quaternary dendrites of these neurons were selected for analysis. Z-stacks of the entire apical dendritic tree of Golgi stained pyramidal neurons (up to 80 µm total on Z-axis, optical section thickness = 0.5 µm) were taken at 40x magnification with 2x optical zoom on a vertical Zeiss Axio Imager.Z1 M. Spine density, length and classification were performed according to (Risher et al., 2014), unbiased blinded to genotype.

2.11. Brain weight and volumetric analysis

1.5 month-old mice were completely anesthetized with an intraperitoneal pentobarbital injection (60 mg/kg Dolethal®, Vetoquinol). The whole brain was extracted and weight in a precision scale (Metter Toledo, AB265-S). Left hemispheres were fixed in 4% paraformaldehyde, immersed in 30% sucrose, included in OCT compound (Tissue-Tek, Sakura Finetek Europe, 4583), frozen and stored at -80°C. Sagittal sections (30 µm thick) were cut on a cryostat and every sixth section was counterstained with toluidine blue pH 4.0 (1g/l Toluidine Blue (Sigma, 198161), 0.8 M glacial acetic acid). Digital images were captured at a 2.5x magnification (Canon EOS 450D digital camera) and the hippocampal, striatal and motor and somatosensory cortical area from 20-22 sections for each animal was calculated by means of the ImageJ software (Schneider et al., 2012). Considering a separation of 180 µm between each section, total structure volume in each mouse was calculated.

2.12. Electrophysiology

For preparation of brain slices, we based on the N-methyl-D-glucamine (NMDG) protective recovery method described by the lab of Guoping Feng (Ting et al., 2014).

Briefly, 5-6 weeks old control (n=5) and TgCPEB4Δ4 (n=5) mice of both sexes were anesthetized with 2% tribromoethanol (0.15 ml/10 mg) and rapidly decapitated. The brains were dissected out and transferred to NMDG ice-cold artificial cerebrospinal fluid (ACSF) composed of: 93mM NMDG, 2.5mM KCl, 1.2mM NaH_2PO_4, 30nM $NaHCO_3$, 25mM D-glucose, 20mM HEPES, 5mM Na-ascorbate, 2mM thiourea, 3mM Na-pyruvate, 10mM $MgSO_4$, and 0.5mM $CaCl_2$. The pH of the solution was titrated to pH 7.3-7.4 with concentrated HCl (osmolality 310-315 mOsmol·kg^{-1}) and bubbled with carbogen (5% CO_2 - 95% O_2). 350 µm coronal slices were cut on a Vibratome VT1200S (Leica) and transferred for initial recovery to NMDG ACSF at 33 ± 1°C. Finally, slices were placed in a holding chamber at room temperature with normal ACSF composed of: 126mM NaCl, 2.5mM KCl, 2mM $CaCl_2$, 2mM $MgCl_2$, 1.25mM NaH_2PO_4, 26mM $NaHCO_3$, and 10mM D-glucose (osmolality 305–315 mOsmol·kg^{-1}), pH 7.4, when bubbled with carbogen (5% CO_2–95% O_2).

For whole-cell patch-clamp recordings, slices were transferred into a recording chamber that was perfused with 33 ± 1°C bubbled ACSF at 2–3 ml/min. Pyramidal neurons of the somatosensory cortex were visualized by a Nikon Eclipse FN1 microscope, a 40x water immersion objective (Nikon), and a USB 2.0 monochrome camera (DMK 31BU03.H, TheImagingSource). Whole-cell recordings were performed using a double patch clamp EPC10 plus amplifier (HEKA). Under voltage-clamp conditions, the patch-pipettes for excitatory postsynaptic currents recording (EPSCs) contained: 120mM K-gluconate, 10mM KCl, 10mM phosphocreatine disodium salt, 2mM MgATP, 0.3mM NaGTP, 0.1mM EGTA, 10mM HEPES, pH 7.2 adjusted with KOH, osmolality 280-290 mOsmol·kg^{-1}. Recording of miniature EPSCs (mEPSCs) were done in the presence of tetrodotoxin (1 µM) and picrotoxin (50 µM) to block sodium channels and $GABA_A$ receptors, respectively. Cells were held in voltage-clamp mode at a holding potential (Vhold) of -70 mV, while resistance was compensated by 70% (lag 10 µs). Recordings were discontinued if series resistances increased by > 50% or exceeded 15 MΩ.

Currents were low-pass filtered at 3 kHz, digitized at 20 kHz, and acquired using PatchMaster software (HEKA). All miniature postsynaptic currents were analyzed with the program Stimfit (Guzman et al., 2014). Recordings were first digitally filtered at 1 kHz. For each cell, all events were inspected to avoid false-positive events, and then an average of all events detected was made.

3. MOUSE BEHAVIORAL TEST

3.1. Body Weight (BW)

Starting at 2 weeks of age, mice were weighed every weeks in in a precision scale (AND, EK-3000i).

3.2. Open Field (OF)

Locomotor activity was measured at the age of 5 weeks in TgCPEB4Δ4 mice in clear Plexiglas® boxes measuring 27.5 cm x 27.5 cm, outfitted with photo-beam detectors for monitoring horizontal and vertical activity. Activity levels were recorded with a MED Associates' Activity Monitor (MED Associates, St. Albans, VT) and were analyzed with the MED Associates' Activity Monitor Data Analysis software. Mice were placed in the center of the open-field apparatus and left to move freely. Data were individually recorded for each animal during 15 min. Distance walked in the periphery of the box (3.5 cm from the edges) was measured.

3.3. Ultrasonic Vocalization (UsV)

UsV was measured at the age of 3, 6, 9 and 12 postnatal days in TgCPEB4Δ4 mice. Dam was removed from a temperature-controlled home cage where the pups remained. Then, pups were removed individually and placed in a plate equipped to record UsV for 5 min (Avisoft Recorder). To avoid potential confounding effects due to temperature, the room was maintained at 21°C and body temperature was measured with an axillary probe after the 5 min test. UsV was analyzed with Avisoft SASLab Pro software.

3.4. Social Approach (SAp)

SAp was examined at the age of 5 weeks in TgCPEB4Δ4 mice. The first day (training), mice were allowed to explore an empty Plexiglas® box measuring 45 cm x 45 cm during 10 min. The next day (test), mice were placed in the same box containing two wire cages placed in opposite corners, one empty and the other with an unknown (gender paired) mouse on it. Mice were recorded during 10 min and the time expended interacting with each cage was measured.

3.5. Elevated plus maze (EPM)

Anxiety-like behavior was examined at the age of 5 weeks TgCPEB4Δ4 mice. Animals were tested in a 5-min single trial EPM in which the mouse was allowed to move freely along the apparatus under a constant intense white light. Animal movement was recorded and the total time spent standing or walking on the open and closed arms was measured. The criterion was the head, forelimbs and hindlimbs being placed on open or closed arms. Our maze consists of four arms (two open without walls and two enclosed by 15 cm high walls) 26 cm long and 5 cm wide. It is elevated 40 cm off the floor it is on.

4. BIOINFORMATICS AND DATA ANALYSIS

4.1. Microarrays analysis of poly(U) chromatography

cDNA Library preparation and amplification were performed according to the manufacturer's (Sigma-Aldrich) instructions for the WTA2 kit from 25 ng starting material. The cDNA was amplified for 17 cycles and purified using PureLink Quick PCR Purification Kit (Invitrogen, K310001). Quantification of amplified cDNA was done on a Nanodrop ND-1000 spectrophotometer (Thermo-Fisher Scientific, Waltham). 8.5 ug of the cDNA from each sample were fragmented and labeling with GeneChip Mapping 250 K Nsp assay kit (Affymetrix, 900753) following the instructions of manufacturer.

Human: samples ready to hybridize were denatured at 99°C for 2 min prior to incubation into the GeneChip Human PrimeView arrays (Affymetrix, 901838). Hybridization was performed for 16 h at 45 °C / 60 rpm in the GeneChip Hybridization Oven 645 (Affymetrix, 00-0331). Washing and stain steps after hybridization were performed in the GeneChip Fluidics Station 450 (Affymetrix, 00-0079), following the specific script for PrimeView arrays. Finally, the arrays were scanned with GeneChip Scanner GCS3000 (Affymetrix) using default parameters, and the generation of CEL files for bioinformatics analysis was done with Command Console software (Affymetrix). ***Mouse:*** hybridization was performed using the GeneAtlas Hyb, Wash and Stain Kit for 3' IVT arrays.

Samples ready to hybridize were denatured at 96°C for 10 min prior to incubation into Mouse MG-430 PM Array Strip (Affymetrix, 901570), the hybridization was performed for 16 h at 45°C in the GeneAtlas Hybridization Oven (Affymetrix, 00-0331). Washing and Stain steps after hybridization were performed in the GeneAtlas Fluidics Station (Affymetrix, 00-0079), following the specific script for Mouse MG-430 PM Arrays. Finally, the arrays were scanned with GeneAtlas Scanner (Affymetrix)

using default parameters, and the generation of CEL files for bioinformatics analysis was done with GeneAtlas software (Affymetrix).

Processing of microarray samples was performed using R (R Development Core Team, 2014) and Bioconductor (Gentleman et al., 2004). Raw CEL files were normalized using RMA background correction and summarization (Irizarry et al., 2003). Standard quality controls were performed in order to identify abnormal samples regarding: a) spatial artifacts in the hybridization process (scan images and pseudo-images from probe level models); b) intensity dependences of differences between chips (MvA plots); c) RNA quality (RNA digest plot); and d) global intensity levels (boxplot of perfect match log-intensity distributions before and after normalization and RLE plots). No samples were discarded due to poor quality. Probeset annotation was performed using the information available in Affymetrix web page (https://www.affymetrix.com/analysis/index.affx) using version na35.

Expression values were adjusted for technical biases as described in (Eklund and Szallasi, 2008) using a linear model and implemented with the R package "limma" (Ritchie et al., 2015). For each biological replicate the log2 fold change was computed between "WASH" and "ELUTED" samples and used to find significant differences between WT vs CPEB4 GT/+ and CPEB4 KO mice (n=2), Control vs. TgCPEB4Δ4 (n=3) and control (n=5) vs ASD patients (n=6). Differential expression was performed using a linear model with fluidics and amplification batch as covariates. P-values were adjusted with the Benjamini and Hochberg correction.

In the case if WT vs R6/1 mice value ≤ -1.5 in at least one probe means that the transcript is shortened in R6/1 mice, ≥ 1.5 means that is lengthened and the values in between mean no change. In all other cases, we considered one transcript is shortened when p-value < 0.05 and f.c. is negative and lengthened when p-value < 0.05 and f.c. is positive, in at least one probe. If the same transcript showed opposite results for different probes, it was considered as not changed.

4.2. Microarrays analysis of RNA immunoprecipitation

Input and immunoprecipitated RNA were purified using Agencourt RNAClean XP bead suspension (Beckman Coulter, A66514). Library preparation and amplification were performed following the distributor's (Sigma-Aldrich) recommendations for WTA2 from purified immunoprecipitated or diluted input RNA. SYBR Green (Sigma-Aldrich, 163795-75-3) was added to the amplification reaction, which was performed in a CFX Real-time instrument (Bio-Rad) to monitor amplification yield. When the SYBR

Green signal reached a plateau after 27 cycles, the reaction was stopped. Amplified cDNA was purified and quantified on a Nanodrop ND-1000 spectrophotometer (Thermo-Fischer). 8 µg of cDNA were subsequently fragmented by DNAseI and biotinylated by terminal transferase obtained from GeneChip Mapping 250K Nsp Assay Kit (Affymetrix, 900753). After hybridization for 16h at 45°C, washing and staining was performed in the Affymetrix GeneAtlas Fluidics Station. The arrays were scanned in the GeneAtlas Imaging Station. All processing was performed according to manufacturer's recommendations. CEL files were generated from DAT files using Affymetrix Command Console software. To generate the log2 expression estimates, overall array intensity was normalized between arrays and the probe intensity of all probes in a probe set summarized to a single value using Robust Multiarray Average (RMA) algorithm (Irizarry et al., 2003).

In order to compare samples from different conditions, fold changes were computed after MA mean and variance normalization using a Generalized Additive Model (GAM). An empirical Bayes partial density model was then used to compute the posterior probability of differential expression. Differentially expressed genes were defined as those with a maximum False Discovery Rate (FDR) of 5% and a $\log_2$ fold change threshold of 1.75. We calculated the Input vs. Eluted f.c. for CPEB1 and CPEB4 binders considering a transcript positive when at least one probe showed a f.c. above 1.75 in WT or R6/1 mice.

4.3. Gene Ontology analysis

CPEB4 coimmunoprecipitated mRNAs from RWP-1 cells (Ortiz-Zapater et al., 2011) and transcripts with changes in their poly(A) tail length in St of symptomatic R6/1 mice (f.c. ≤ -2 or ≥ 2) were analyzed with DAVID Bioinformatics Resources 6.7, KEGG pathway annotation (Huang da et al., 2009).

4.4. Analysis of CPE sequences

The longest 3'UTR sequences from selected gene sets were extracted from Ensembl (http://www.ensembl.org/) (Yates et al., 2016) and *ncbi* gene (https://www.ncbi.nlm.nih.gov/gene). Incidence of functional CPE sequences, Hex and PBE (pumilio binding element) sequences in the 3'UTR was detected using the algorithm described in (Pique et al., 2008) (http://genome.crg.es/CPE/). The list of 1223 genes in the group "increased in brain" was obtained from *The human protein atlas* (http://

proteinatlas.org/humanproteome/brain). SFARI Cat. 1, 2 and 3 was obtained from SFARI database (https://gene.sfari.org/autdb/GS_Home.do) in September 2016. ASD39 gene list consists of the 39 genes harboring rare *de novo* protein disrupting mutations identified in two whole exome sequencing studies in simplex ASD (De Rubeis et al., 2014; Iossifov et al., 2014).

4.5. Enrichment and co-expression network analysis of CPEB binders

Enrichment analysis studies use Fisher's exact test (the hypergeometric test is equivalent to a one-sided Fisher's exact test) to evaluate whether a gene set, in this case CPEB4 or CPEB1 binders determined by RIP, is enriched over background, providing a p-value and enrichment value. We used curated ASD candidate gene list from SFARI AutDB database, referred as ASD SFARI list and a more restrictive, smaller ASD only gene list, where genes linked to intellectual disability were removed. The gene set (CPEB4 and CPEB1 binders) was also used to study enrichment in functional co-expression modules that represent shared pathology in ASD brain. These gene modules derived from previous unbiased Weighted Gene Co-expression Network Analysis (WGCNA) obtained by gene array (Voineagu et al., 2011) and by RNA-seq (Parikshak et al., 2016) studies from ASD postmortem samples.

4.6. Differential expression analysis

RNA-seq data

CPEBs expression levels in idiopathic ASD (n=43) and control (n=63) postmortem prefrontal cortex samples were evaluated from RNA-seq data from (Parikshak et al., 2016). Briefly, the paired-end raw reads were mapped to the human reference genome assembly GRCh37.73 using Tophat2 (Kim et al., 2013) and the counts were quantified using HTSeq (Anders et al., 2015). Gene length, G+C content and library size were normalized (referred to as "Normalized FPKM") using the cqn package in R (Hansen et al., 2012). Linear mixed effects (LME) were used, modeling to account for effects from biological covariates (condition, age, sex, brain region), technical variables related to sample processing (RIN, brain bank, sequencing batch), technical variables related to sequencing quality metrics and individual ID was set as a random effect accounting for the fact that multiple samples came from the same individual.

Microarray data

Individual probeset expression values for each selected gene were annotated with Annmap webservice (http://annmap.cruk.manchester.ac.uk), using *Homo Sapiens* v84 Primeview Human Gene Array and *Mus musculus* v84 Mouse Genome 430A 2.0 databases. Those probesets annotated as 'reliable', in which all probes hit the genome only once and localize to exons, were preferentially selected for analysis. For those genes lacking a 'reliable' probeset, the whole group of probesets was taken for comparisons. Graph bars were plotted using the mean of RMA normalized expression values from the Primeview human gene array in case of human samples and Mouse genome 430 PM array in case of mice. The expression values were calculated using R and BioConductor packages. Graph bars were plotted using the mean of RMA normalized expression values from the Primeview human gene array in case of human samples and Mouse genome 430 PM array in case of mice. The expression values were calculated using R and BioConductor packages.

4.7. Differential alternative splicing

We computed percent spliced in (PSI) values using Multivariate Analysis of Transcript Splicing (MATS, v3.08), which utilizes TopHat2 (Shen et al., 2012) aligned reads and a custom splice-junction library. In total, we used 81 control samples and 82 ASD cortical samples as reported (Parikshak et al., 2016). In order to account for the effects of covariates, we utilized PSI values in the linear mixed effects model described below for differential splicing analysis:

```
lme(PSI ~ diagnosis + age + sex + brain_region + sequencing.batch +
brain.bank.batch + RIN + seqSV1 + seqSV2, rand = ~1|individualID)
```

Where two sequencing surrogate variables (seqSV1 and seqSV2) were used as covariates.

4.8. Human-mouse altered poly(A) tail length geneset comparison

In order to compare transcripts with altered poly(A) tail in ASD patients and CPEB4 modified mice, we first converted the gene set from mouse into their human orthologs (18649 total orthologos genes) using Ensembl Genes 85 Mus musculus GRCm38p4 Biomart (http://www.ensembl.org/biomart/) (Yates et al., 2016). Then we calculated the statistical significance of the overlap between genes with poly(A) changes in human ASD and CPEB4 modified mice (http://nemates.org/MA/progs/overlap_stats.html). We considered overlapping when the representation factor is > 1 and $p < 0.05$, and dissimilar when the representation factor is < 1 and $p < 0.05$.

4.9. Statistics

Statistical analysis was performed with SPSS 21.0 (SPSS® Statistic IBM®). Data are represented as Mean ± SEM (Standard Error of the Mean). The normality of the data was analyzed by Shapiro-Wilk test. For 2 group comparison, two tail t-Student's test (data with normal distribution) or Mann-Whitney U-test (data with non-normal distribution) was performed. For multiple comparisons, data with a normal distribution were analyzed by one way-ANOVA test followed by a LSD or a Games Howell post-hoc test. Statistical significance of non-parametric data for multiple comparisons was determined by Kruskal-Wallis test followed by a Mann-Whitney U-test for analysis of paired genotypes. A critical value for significance of $p < 0.05$ was used throughout the study.

CONCLUSIONS

1. Brain of HD patients and mouse models show a CPEB1/CPEB4 imbalance, being CPEB1 levels increased and CPEB4 decreased.

2. 19% of transcripts in R6/1 HD mouse model exhibit altered poly(A) tail length which fits concomitant alteration of their encoded proteins.

3. Polyadenylation changes in R6/1 mice prominently affects Huntington's-, Alzheimer's- and Parkinson's disease related genes.

3. The striatal atrophy associated gene *KTN1* with multiple CPE sequences in its 3'UTR shows poly(A) shorting in R6/1 mice and decreased protein in HD mouse and human brain.

4. CPEB4 binding transcripts are enriched in both risk-genes and gene-modules involved in ASD. Accordingly, the majority of high confidence ASD genes harbor functional CPEs in their 3' UTR.

5. In idiopathic ASD brains, CPEB4 presents diminished protein levels and its mRNA is mis-spliced in favor of the isoform lacking a neuronal-specific microexon.

6. Most high-confidence ASD genes are deadenylated and their encoded protein levels are decreased in idiopathic ASD brain.

7. CPEB4 microexon splicing isoform-imbalance in TgCPEB4Δ4 mice is sufficient to mimic the deadenylation and diminished protein level of ASD risk genes observed in human ASD cases.

8. TgCPEB4Δ4 mice show ASD-like neuroanatomical, electrophysiological and behavioral phenotype.

9. Collectively, these results suggest a role of CPEB-mediated altered polyadenylation in HD and other neurodegenerative diseases and unravel CPEB4 as a new node in ASD gene expression.

REFERENCES

Abrahams, B.S., and Geschwind, D.H. (2008). Advances in autism genetics: on the threshold of a new neurobiology. Nat Rev Genet 9, 341-355.

Alarcon, J.M., Hodgman, R., Theis, M., Huang, Y.S., Kandel, E.R., and Richter, J.D. (2004). Selective modulation of some forms of schaffer collateral-CA1 synaptic plasticity in mice with a disruption of the CPEB-1 gene. Learn Mem 11, 318-327.

Alexandrov, I.M., Ivshina, M., Jung, D.Y., Friedline, R., Ko, H.J., Xu, M., O'Sullivan-Murphy, B., Bortell, R., Huang, Y.T., Urano, F., et al. (2012). Cytoplasmic polyadenylation element binding protein deficiency stimulates PTEN and Stat3 mRNA translation and induces hepatic insulin resistance. PLoS Genet 8, e1002457.

Alpert, T., Herzel, L., and Neugebauer, K.M. (2016). Perfect timing: splicing and transcription rates in living cells. Wiley Interdiscip Rev RNA.

Amir, R.E., Van den Veyver, I.B., Wan, M., Tran, C.Q., Francke, U., and Zoghbi, H.Y. (1999). Rett syndrome is caused by mutations in X-linked MECP2, encoding methyl-CpG-binding protein 2. Nat Genet 23, 185-188.

Anders, S., Pyl, P.T., and Huber, W. (2015). HTSeq--a Python framework to work with high-throughput sequencing data. Bioinformatics 31, 166-169.

Andrew, S.E., Goldberg, Y.P., Kremer, B., Telenius, H., Theilmann, J., Adam, S., Starr, E., Squitieri, F., Lin, B., Kalchman, M.A., et al. (1993). The relationship between trinucleotide (CAG) repeat length and clinical features of Huntington's disease. Nat Genet 4, 398-403.

Arrasate, M., and Finkbeiner, S. (2012). Protein aggregates in Huntington's disease. Exp Neurol 238, 1-11.

Atkins, C.M., Davare, M.A., Oh, M.C., Derkach, V., and Soderling, T.R. (2005). Bidirectional regulation of cytoplasmic polyadenylation element-binding protein phosphorylation by Ca2+/calmodulin-dependent protein kinase II and protein phosphatase 1 during hippocampal long-term potentiation. J Neurosci 25, 5604-5610.

Atkins, C.M., Nozaki, N., Shigeri, Y., and Soderling, T.R. (2004). Cytoplasmic polyadenylation element binding protein-dependent protein synthesis is regulated by calcium/calmodulin-dependent protein kinase II. J Neurosci 24, 5193-5201.

Baj, G., Pinhero, V., Vaghi, V., and Tongiorgi, E. (2016). Signaling pathways controlling activity-dependent local translation of BDNF and their localization in dendritic arbors. J Cell Sci 129, 2852-2864.

Banez-Coronel, M., Ayhan, F., Tarabochia, A.D., Zu, T., Perez, B.A., Tusi, S.K., Pletnikova, O., Borchelt, D.R., Ross, C.A., Margolis, R.L., et al. (2015). RAN Translation in Huntington Disease. Neuron 88, 667-677.

Bates, G.P., Dorsey, R., Gusella, J.F., Hayden, M.R., Kay, C., Leavitt, B.R., Nance, M., Ross, C.A., Scahill, R.I., Wetzel, R., et al. (2015). Huntington disease. Nat Rev Dis Primers 1, 15005.

Batra, R., Stark, T.J., Clark, E., Belzile, J.P., Wheeler, E.C., Yee, B.A., Huang, H., Gelboin-Burkhart, C., Huelga, S.C., Aigner, S., et al. (2016). RNA-binding protein CPEB1 remodels host and viral RNA landscapes. Nat Struct Mol Biol 23, 1101-1110.

Baudouin, S.J., Gaudias, J., Gerharz, S., Hatstatt, L., Zhou, K., Punnakkal, P., Tanaka, K.F., Spooren, W., Hen, R., De Zeeuw, C.I., et al. (2012). Shared synaptic pathophysiology in syndromic and nonsyndromic rodent models of autism. Science 338, 128-132.

Bava, F.A., Eliscovich, C., Ferreira, P.G., Minana, B., Ben-Dov, C., Guigo, R., Valcarcel, J., and Mendez, R. (2013). CPEB1 coordinates alternative 3'-UTR formation with translational regulation. Nature 495, 121-125.

Bentley, D.L. (2014). Coupling mRNA processing with transcription in time and space. Nat Rev Genet 15, 163-175.

Berger-Sweeney, J., Zearfoss, N.R., and Richter, J.D. (2006). Reduced extinction of hippocampal-dependent memories in CPEB knockout mice. Learn Mem 13, 4-7.

Betancur, C. (2011). Etiological heterogeneity in autism spectrum disorders: more than 100 genetic and genomic disorders and still counting. Brain Res 1380, 42-77.

Bilen, J., and Bonini, N.M. (2007). Genome-wide screen for modifiers of ataxin-3 neurodegeneration in Drosophila. PLoS Genet 3, 1950-1964.

Buffington, S.A., Huang, W., and Costa-Mattioli, M. (2014). Translational control in synaptic plasticity and cognitive dysfunction. Annu Rev Neurosci 37, 17-38.

Burns, D.M., D'Ambrogio, A., Nottrott, S., and Richter, J.D. (2011). CPEB and two poly(A) polymerases control miR-122 stability and p53 mRNA translation. Nature 473, 105-108.

Burns, D.M., and Richter, J.D. (2008). CPEB regulation of human cellular senescence, energy metabolism, and p53 mRNA translation. Genes Dev 22, 3449-3460.

Cabrera, J.R., and Lucas, J.J. (2016). MAP2 Splicing is Altered in Huntington's Disease. Brain Pathol.

Calderone, V., Gallego, J., Fernandez-Miranda, G., Garcia-Pras, E., Maillo, C., Berzigotti, A., Mejias, M., Bava, F.A., Angulo-Urarte, A., Graupera, M., et al. (2016). Sequential Functions of CPEB1 and CPEB4 Regulate Pathologic Expression of Vascular Endothelial Growth Factor and Angiogenesis in Chronic Liver Disease. Gastroenterology 150, 982-997 e930.

Corrochano, S., Renna, M., Carter, S., Chrobot, N., Kent, R., Stewart, M., Cooper, J., Brown, S.D., Rubinsztein, D.C., and Acevedo-Arozena, A. (2012). alpha-Synuclein levels modulate Huntington's disease in mice. Hum Mol Genet 21, 485-494.

Curinha, A., Oliveira Braz, S., Pereira-Castro, I., Cruz, A., and Moreira, A. (2014). Implications of polyadenylation in health and disease. Nucleus 5, 508-519.

Chao, H.W., Tsai, L.Y., Lu, Y.L., Lin, P.Y., Huang, W.H., Chou, H.J., Lu, W.H., Lin, H.C., Lee, P.T., and Huang, Y.S. (2013). Deletion of CPEB3 enhances hippocampus-dependent memory via increasing expressions of PSD95 and NMDA receptors. J Neurosci 33, 17008-17022.

Charlesworth, A., Meijer, H.A., and de Moor, C.H. (2013). Specificity factors in cytoplasmic polyadenylation. Wiley Interdiscip Rev RNA 4, 437-461.

Chen, J.A., Penagarikano, O., Belgard, T.G., Swarup, V., and Geschwind, D.H. (2015). The emerging picture of autism spectrum disorder: genetics and pathology. Annu Rev Pathol 10, 111-144.

Chen, Y., Tsai, Y.H., and Tseng, S.H. (2016). Regulation of the Expression of Cytoplasmic Polyadenylation Element Binding Proteins for the Treatment of Cancer. Anticancer Res 36, 5673-5680.

Darnell, J.C., and Klann, E. (2013). The translation of translational control by FMRP: therapeutic targets for FXS. Nat Neurosci 16, 1530-1536.

Darnell, J.E., Jr. (2013). Reflections on the history of pre-mRNA processing and highlights of current knowledge: a unified picture. RNA 19, 443-460.

Davies, S.W., Turmaine, M., Cozens, B.A., DiFiglia, M., Sharp, A.H., Ross, C.A., Scherzinger, E., Wanker, E.E., Mangiarini, L., and Bates, G.P. (1997). Formation of neuronal intranuclear inclusions underlies the neurological dysfunction in mice transgenic for the HD mutation. Cell 90, 537-548.

De Rubeis, S., and Buxbaum, J.D. (2015). Recent advances in the genetics of autism spectrum disorder. Curr Neurol Neurosci Rep 15, 36.

De Rubeis, S., He, X., Goldberg, A.P., Poultney, C.S., Samocha, K., Cicek, A.E., Kou, Y., Liu, L., Fromer, M., Walker, S., et al. (2014). Synaptic, transcriptional and chromatin genes disrupted in autism. Nature 515, 209-215.

Delorme, R., Ey, E., Toro, R., Leboyer, M., Gillberg, C., and Bourgeron, T. (2013). Progress toward treatments for synaptic defects in autism. Nat Med 19, 685-694.

Di Giammartino, D.C., Nishida, K., and Manley, J.L. (2011). Mechanisms and consequences of alternative polyadenylation. Mol Cell 43, 853-866.

Diaz-Hernandez, M., Torres-Peraza, J., Salvatori-Abarca, A., Moran, M.A., Gomez-Ramos, P., Alberch, J., and Lucas, J.J. (2005). Full motor recovery despite striatal neuron loss and formation of irreversible amyloid-like inclusions in a conditional mouse model of Huntington's disease. J Neurosci 25, 9773-9781.

Donlon, T.A. (1988). Similar molecular deletions on chromosome 15q11.2 are encountered in both the Prader-Willi and Angelman syndromes. Hum Genet 80, 322-328.

Drisaldi, B., Colnaghi, L., Fioriti, L., Rao, N., Myers, C., Snyder, A.M., Metzger, D.J., Tarasoff, J., Konstantinov, E., Fraser, P.E., et al. (2015). SUMOylation Is an Inhibitory Constraint that Regulates the Prion-like Aggregation and Activity of CPEB3. Cell Rep 11, 1694-1702.

DSM-V (2013). Diagnostic and Statistical Manual of Mental Disorders, Fifth Edition.

Ehrnhoefer, D.E., Butland, S.L., Pouladi, M.A., and Hayden, M.R. (2009). Mouse models of Huntington disease: variations on a theme. Dis Model Mech 2, 123-129.

Eklund, A.C., and Szallasi, Z. (2008). Correction of technical bias in clinical microarray data improves concordance with known biological information. Genome Biol 9, R26.

El-Daher, M.T., Hangen, E., Bruyere, J., Poizat, G., Al-Ramahi, I., Pardo, R., Bourg, N., Souquere, S., Mayet, C., Pierron, G., et al. (2015). Huntingtin proteolysis releases non-polyQ fragments that cause toxicity through dynamin 1 dysregulation. EMBO J 34, 2255-2271.

Elsabbagh, M., Divan, G., Koh, Y.J., Kim, Y.S., Kauchali, S., Marcin, C., Montiel-Nava, C., Patel, V., Paula, C.S., Wang, C., et al. (2012). Global prevalence of autism and other pervasive developmental disorders. Autism Res 5, 160-179.

Engman, M.L., Sundin, M., Miniscalco, C., Westerlund, J., Lewensohn-Fuchs, I., Gillberg, C., and Fernell, E. (2015). Prenatal acquired cytomegalovirus infection should be considered in children with autism. Acta Paediatr 104, 792-795.

Estes, M.L., and McAllister, A.K. (2015). Immune mediators in the brain and peripheral tissues in autism spectrum disorder. Nat Rev Neurosci 16, 469-486.

Estes, M.L., and McAllister, A.K. (2016). Maternal immune activation: Implications for neuropsychiatric disorders. Science 353, 772-777.

Estrada-Sanchez, A.M., and Rebec, G.V. (2013). Role of cerebral cortex in the neuropathology of Huntington's disease. Front Neural Circuits 7, 19.

Evers, M.M., Toonen, L.J., and van Roon-Mom, W.M. (2015). Antisense oligonucleotides in therapy for neurodegenerative disorders. Adv Drug Deliv Rev 87, 90-103.

Fernandez-Miranda, G., and Mendez, R. (2012). The CPEB-family of proteins, translational control in senescence and cancer. Ageing Res Rev 11, 460-472.

Fernandez-Nogales, M., Cabrera, J.R., Santos-Galindo, M., Hoozemans, J.J., Ferrer, I., Rozemuller, A.J., Hernandez, F., Avila, J., and Lucas, J.J. (2014). Huntington's disease is a four-repeat tauopathy with tau nuclear rods. Nat Med 20, 881-885.

Fernandez-Nogales, M., Hernandez, F., Miguez, A., Alberch, J., Gines, S., Perez-Navarro, E., and Lucas, J.J. (2015). Decreased glycogen synthase kinase-3 levels and activity contribute to Huntington's disease. Hum Mol Genet 24, 5040-5052.

Furtado, S., Suchowersky, O., Rewcastle, B., Graham, L., Klimek, M.L., and Garber, A. (1996). Relationship between trinucleotide repeats and neuropathological changes in Huntington's disease. Ann Neurol 39, 132-136.

Gafni, J., and Ellerby, L.M. (2002). Calpain activation in Huntington's disease. J Neurosci 22, 4842-4849.

Gandal, M.J., Leppa, V., Won, H., Parikshak, N.N., and Geschwind, D.H. (2016). The road to precision psychiatry: translating genetics into disease mechanisms. Nat Neurosci 19, 1397-1407.

Gaugler, T., Klei, L., Sanders, S.J., Bodea, C.A., Goldberg, A.P., Lee, A.B., Mahajan, M., Manaa, D., Pawitan, Y., Reichert, J., et al. (2014). Most genetic risk for autism resides with common variation. Nat Genet 46, 881-885.

Gentleman, R.C., Carey, V.J., Bates, D.M., Bolstad, B., Dettling, M., Dudoit, S., Ellis, B., Gautier, L., Ge, Y., Gentry, J., et al. (2004). Bioconductor: open software development for computational biology and bioinformatics. Genome Biol 5, R80.

Geschwind, D.H., and State, M.W. (2015). Gene hunting in autism spectrum disorder: on the path to precision medicine. Lancet Neurol 14, 1109-1120.

Godin, J.D., Colombo, K., Molina-Calavita, M., Keryer, G., Zala, D., Charrin, B.C., Dietrich, P., Volvert, M.L., Guillemot, F., Dragatsis, I., et al. (2010). Huntingtin is required for mitotic spindle orientation and mammalian neurogenesis. Neuron 67, 392-406.

Gomez-Esteban, J.C., Lezcano, E., Zarranz, J.J., Velasco, F., Garamendi, I., Perez, T., and Tijero, B. (2007). Monozygotic twins suffering from Huntington's disease show different cognitive and behavioural symptoms. Eur Neurol 57, 26-30.

Grabrucker, A.M. (2012). Environmental factors in autism. Front Psychiatry 3, 118.

Gray, M., Shirasaki, D.I., Cepeda, C., Andre, V.M., Wilburn, B., Lu, X.H., Tao, J., Yamazaki, I., Li, S.H., Sun, Y.E., et al. (2008). Full-length human mutant huntingtin with a stable polyglutamine repeat can elicit progressive and selective neuropathogenesis in BACHD mice. J Neurosci 28, 6182-6195.

Guillen-Boixet, J., Buzon, V., Salvatella, X., and Mendez, R. (2016). CPEB4 is regulated during cell cycle by ERK2/Cdk1-mediated phosphorylation and its assembly into liquid-like droplets. Elife 5.

Gusella, J.F., and MacDonald, M.E. (2009). Huntington's disease: the case for genetic modifiers. Genome Med 1, 80.

Gusella, J.F., Wexler, N.S., Conneally, P.M., Naylor, S.L., Anderson, M.A., Tanzi, R.E., Watkins, P.C., Ottina, K., Wallace, M.R., Sakaguchi, A.Y., et al. (1983). A polymorphic DNA marker genetically linked to Huntington's disease. Nature 306, 234-238.

Gutekunst, C.A., Li, S.H., Yi, H., Mulroy, J.S., Kuemmerle, S., Jones, R., Rye, D., Ferrante, R.J., Hersch, S.M., and Li, X.J. (1999). Nuclear and neuropil aggregates in Huntington's disease: relationship to neuropathology. J Neurosci 19, 2522-2534.

Guzman, S.J., Schlogl, A., and Schmidt-Hieber, C. (2014). Stimfit: quantifying electrophysiological data with Python. Front Neuroinform 8, 16.

Hafer, N., Xu, S., Bhat, K.M., and Schedl, P. (2011). The Drosophila CPEB protein Orb2 has a novel expression pattern and is important for asymmetric cell division and nervous system function. Genetics 189, 907-921.

Hallmayer, J., Cleveland, S., Torres, A., Phillips, J., Cohen, B., Torigoe, T., Miller, J., Fedele, A., Collins, J., Smith, K., et al. (2011). Genetic heritability and shared environmental factors among twin pairs with autism. Arch Gen Psychiatry 68, 1095-1102.

Hamdan, F.F., Daoud, H., Rochefort, D., Piton, A., Gauthier, J., Langlois, M., Foomani, G., Dobrzeniecka, S., Krebs, M.O., Joober, R., et al. (2010). De novo mutations in FOXP1 in cases with intellectual disability, autism, and language impairment. Am J Hum Genet 87, 671-678.

Hansen, K.D., Irizarry, R.A., and Wu, Z. (2012). Removing technical variability in RNA-seq data using conditional quantile normalization. Biostatistics 13, 204-216.

Hardy, J., and Gwinn-Hardy, K. (1998). Genetic classification of primary neurodegenerative disease. Science 282, 1075-1079.

Harjes, P., and Wanker, E.E. (2003). The hunt for huntingtin function: interaction partners tell many different stories. Trends Biochem Sci 28, 425-433.

HDCRG (1993). A novel gene containing a trinucleotide repeat that is expanded and unstable on Huntington's disease chromosomes. The Huntington's Disease Collaborative Research Group. Cell 72, 971-983.

Heemskerk, A.W., and Roos, R.A. (2012). Aspiration pneumonia and death in Huntington's disease. PLoS Curr 4, RRN1293.

Hernandez, F., Lucas, J.J., and Avila, J. (2013). GSK3 and tau: two convergence points in Alzheimer's disease. J Alzheimers Dis 33 Suppl 1, S141-144.

Hibar, D.P., Stein, J.L., Renteria, M.E., Arias-Vasquez, A., Desrivieres, S., Jahanshad, N., Toro, R., Wittfeld, K., Abramovic, L., Andersson, M., et al. (2015a). Common genetic variants influence human subcortical brain structures. Nature 520, 224-229.

Hibar, D.P., Stein, J.L., Renteria, M.E., Arias-Vasquez, A., Desrivieres, S., Jahanshad, N., Toro, R., Wittfeld, K., Abramovic, L., Andersson, M., et al. (2015b). Common genetic variants influence human subcortical brain structures. Nature 520, 224-229.

Ho, A.K., Sahakian, B.J., Brown, R.G., Barker, R.A., Hodges, J.R., Ane, M.N., Snowden, J., Thompson, J., Esmonde, T., Gentry, R., et al. (2003). Profile of cognitive progression in early Huntington's disease. Neurology 61, 1702-1706.

Homberg, J.R., Kyzar, E.J., Scattoni, M.L., Norton, W.H., Pittman, J., Gaikwad, S., Nguyen, M., Poudel, M.K., Ullmann, J.F., Diamond, D.M., et al. (2016). Genetic and environmental modulation of neurodevelopmental disorders: Translational insights from labs to beds. Brain Res Bull 125, 79-91.

Hu, W., Yuan, B., and Lodish, H.F. (2014). Cpeb4-mediated translational regulatory circuitry controls terminal erythroid differentiation. Dev Cell 30, 660-672.

Huang da, W., Sherman, B.T., and Lempicki, R.A. (2009). Systematic and integrative analysis of large gene lists using DAVID bioinformatics resources. Nat Protoc 4, 44-57.

Huang, Y., Yao, X., and Wang, G. (2015). 'Mediator-ing' messenger RNA processing. Wiley Interdiscip Rev RNA 6, 257-269.

Huang, Y.S., Carson, J.H., Barbarese, E., and Richter, J.D. (2003). Facilitation of dendritic mRNA transport by CPEB. Genes Dev 17, 638-653.

Huang, Y.S., Kan, M.C., Lin, C.L., and Richter, J.D. (2006). CPEB3 and CPEB4 in neurons: analysis of RNA-binding specificity and translational control of AMPA receptor GluR2 mRNA. EMBO J 25, 4865-4876.

Huntington, G. (1872). On chorea. Med. Sur. Rep. 26, 317–321. Reedited: Huntington, G. (2003). On chorea. J. Neuropsychiatry Clin. Neurosci. 15, 109–112.

Igea, A., and Mendez, R. (2010). Meiosis requires a translational positive loop where CPEB1 ensues its replacement by CPEB4. EMBO J 29, 2182-2193.

Ikeda, H., Yamaguchi, M., Sugai, S., Aze, Y., Narumiya, S., and Kakizuka, A. (1996). Expanded polyglutamine in the Machado-Joseph disease protein induces cell death in vitro and in vivo. Nat Genet 13, 196-202.

Iossifov, I., O'Roak, B.J., Sanders, S.J., Ronemus, M., Krumm, N., Levy, D., Stessman, H.A., Witherspoon, K.T., Vives, L., Patterson, K.E., et al. (2014). The contribution of de novo coding mutations to autism spectrum disorder. Nature 515, 216-221.

Irimia, M., Weatheritt, R.J., Ellis, J.D., Parikshak, N.N., Gonatopoulos-Pournatzis, T., Babor, M., Quesnel-Vallieres, M., Tapial, J., Raj, B., O'Hanlon, D., et al. (2014). A highly conserved program of neuronal microexons is misregulated in autistic brains. Cell 159, 1511-1523.

Irizarry, R.A., Hobbs, B., Collin, F., Beazer-Barclay, Y.D., Antonellis, K.J., Scherf, U., and Speed, T.P. (2003). Exploration, normalization, and summaries of high density oligonucleotide array probe level data. Biostatistics 4, 249-264.

Ivshina, M., Lasko, P., and Richter, J.D. (2014). Cytoplasmic polyadenylation element binding proteins in development, health, and disease. Annu Rev Cell Dev Biol 30, 393-415.

Jackson, R.J., Hellen, C.U., and Pestova, T.V. (2012). Termination and post-termination events in eukaryotic translation. Adv Protein Chem Struct Biol 86, 45-93.

Jamain, S., Quach, H., Betancur, C., Rastam, M., Colineaux, C., Gillberg, I.C., Soderstrom, H., Giros, B., Leboyer, M., Gillberg, C., et al. (2003). Mutations of the X-linked genes encoding neuroligins NLGN3 and NLGN4 are associated with autism. Nat Genet 34, 27-29.

Jarvelin, A.I., Noerenberg, M., Davis, I., and Castello, A. (2016). The new (dis)order in RNA regulation. Cell Commun Signal 14, 9.

Johnson, R.M., Vu, N.T., Griffin, B.P., Gentry, A.E., Archer, K.J., Chalfant, C.E., and Park, M.A. (2015). The Alternative Splicing of Cytoplasmic Polyadenylation Element Binding Protein 2 Drives Anoikis Resistance and the Metastasis of Triple Negative Breast Cancer. J Biol Chem 290, 25717-25727.

Jones, E.J., Gliga, T., Bedford, R., Charman, T., and Johnson, M.H. (2014). Developmental pathways to autism: a review of prospective studies of infants at risk. Neurosci Biobehav Rev 39, 1-33.

Kaczmarczyk, L., Labrie-Dion, E., Sehgal, K., Sylvester, M., Skubal, M., Josten, M., Steinhauser, C., De Koninck, P., and Theis, M. (2016). New Phosphospecific Antibody Reveals Isoform-Specific Phosphorylation of CPEB3 Protein. PLoS One 11, e0150000.

Kaminsky, E.B., Kaul, V., Paschall, J., Church, D.M., Bunke, B., Kunig, D., Moreno-De-Luca, D., Moreno-De-Luca, A., Mulle, J.G., Warren, S.T., et al. (2011). An evidence-based approach to establish the functional and clinical significance of copy number variants in intellectual and developmental disabilities. Genet Med 13, 777-784.

Kan, M.C., Oruganty-Das, A., Cooper-Morgan, A., Jin, G., Swanger, S.A., Bassell, G.J., Florman, H., van Leyen, K., and Richter, J.D. (2010). CPEB4 is a cell survival protein retained in the nucleus upon ischemia or endoplasmic reticulum calcium depletion. Mol Cell Biol 30, 5658-5671.

Katahira, J. (2015). Nuclear export of messenger RNA. Genes (Basel) 6, 163-184.

Kelleher, R.J., 3rd, and Bear, M.F. (2008). The autistic neuron: troubled translation? Cell 135, 401-406.

Khabar, K.S. (2016). Hallmarks of cancer and AU-rich elements. Wiley Interdiscip Rev RNA.

Khan, M.R., Li, L., Perez-Sanchez, C., Saraf, A., Florens, L., Slaughter, B.D., Unruh, J.R., and Si, K. (2015). Amyloidogenic Oligomerization Transforms Drosophila Orb2 from a Translation Repressor to an Activator. Cell 163, 1468-1483.

Kim, D., Pertea, G., Trapnell, C., Pimentel, H., Kelley, R., and Salzberg, S.L. (2013). TopHat2: accurate alignment of transcriptomes in the presence of insertions, deletions and gene fusions. Genome Biol 14, R36.

Kim, K.C., Oh, W.J., Ko, K.H., Shin, C.Y., and Wells, D.G. (2011). Cyclin B1 expression regulated by cytoplasmic polyadenylation element binding protein in astrocytes. J Neurosci 31, 12118-12128.

Kim, Y.S., and Leventhal, B.L. (2015). Genetic epidemiology and insights into interactive genetic and environmental effects in autism spectrum disorders. Biol Psychiatry 77, 66-74.

Kimble, J., and Crittenden, S.L. (2007). Controls of germline stem cells, entry into meiosis, and the sperm/oocyte decision in Caenorhabditis elegans. Annu Rev Cell Dev Biol 23, 405-433.

Kinney, D.K., Munir, K.M., Crowley, D.J., and Miller, A.M. (2008). Prenatal stress and risk for autism. Neurosci Biobehav Rev 32, 1519-1532.

Kiriyama, Y., and Nochi, H. (2015). The Function of Autophagy in Neurodegenerative Diseases. Int J Mol Sci 16, 26797-26812.

Klein, C., and Westenberger, A. (2012). Genetics of Parkinson's disease. Cold Spring Harb Perspect Med 2, a008888.

Kremer, B., Goldberg, P., Andrew, S.E., Theilmann, J., Telenius, H., Zeisler, J., Squitieri, F., Lin, B., Bassett, A., Almqvist, E., et al. (1994). A worldwide study of the Huntington's disease mutation. The sensitivity and specificity of measuring CAG repeats. N Engl J Med 330, 1401-1406.

Kumar, A., Vaish, M., and Ratan, R.R. (2014). Transcriptional dysregulation in Huntington's disease: a failure of adaptive transcriptional homeostasis. Drug Discov Today 19, 956-962.

La Spada, A.R., and Taylor, J.P. (2010). Repeat expansion disease: progress and puzzles in disease pathogenesis. Nat Rev Genet 11, 247-258.

Lai, Y.T., Su, C.K., Jiang, S.T., Chang, Y.J., Lai, A.C., and Huang, Y.S. (2016). Deficiency of CPEB2-Confined ChAT Expression in the Dorsal Motor Nucleus of Vagus Causes Hyperactivated Parasympathetic Signaling-Associated Bronchoconstriction. J Neurosci.

Lamont, L.B., and Kimble, J. (2007). Developmental expression of FOG-1/CPEB protein and its control in the Caenorhabditis elegans hermaphrodite germ line. Dev Dyn 236, 871-879.

Lee, J.M., Ramos, E.M., Lee, J.H., Gillis, T., Mysore, J.S., Hayden, M.R., Warby, S.C., Morrison, P., Nance, M., Ross, C.A., et al. (2012). CAG repeat expansion in Huntington disease determines age at onset in a fully dominant fashion. Neurology 78, 690-695.

Lein, E.S., Hawrylycz, M.J., Ao, N., Ayres, M., Bensinger, A., Bernard, A., Boe, A.F., Boguski, M.S., Brockway, K.S., Byrnes, E.J., et al. (2007). Genome-wide atlas of gene expression in the adult mouse brain. Nature 445, 168-176.

Levy, D., Ronemus, M., Yamrom, B., Lee, Y.H., Leotta, A., Kendall, J., Marks, S., Lakshmi, B., Pai, D., Ye, K., et al. (2011). Rare de novo and transmitted copy-number variation in autistic spectrum disorders. Neuron 70, 886-897.

Li, Y.I., Sanchez-Pulido, L., Haerty, W., and Ponting, C.P. (2015). RBFOX and PTBP1 proteins regulate the alternative splicing of micro-exons in human brain transcripts. Genome Res 25, 1-13.

Lin, C.L., Evans, V., Shen, S., Xing, Y., and Richter, J.D. (2010). The nuclear experience of CPEB: implications for RNA processing and translational control. RNA 16, 338-348.

Liot, G., Valette, J., Pepin, J., Flament, J., and Brouillet, E. (2016). Energy defects in Huntington's disease: Why "in vivo" evidence matters. Biochem Biophys Res Commun.

Liu, Y., Zhao, D., Dong, R., Yang, X., Zhang, Y., Tammimies, K., Uddin, M., Scherer, S.W., and Gai, Z. (2015). De novo exon 1 deletion of AUTS2 gene in a patient with autism spectrum disorder and developmental delay: a case report and a brief literature review. Am J Med Genet A 167, 1381-1385.

Ma, B., Culver, B.P., Baj, G., Tongiorgi, E., Chao, M.V., and Tanese, N. (2010). Localization of BDNF mRNA with the Huntington's disease protein in rat brain. Mol Neurodegener 5, 22.

Maillo, C., Martin, J., Sebastian, D., Hernandez-Alvarez, M., Garcia-Rocha, M., Reina, O., Zorzano, A., Fernandez, M., and Mendez, R. (2017). Circadian- and UPR-dependent control of CPEB4 mediates a translational response to counteract hepatic steatosis under ER stress. Nat Cell Biol.

Majumdar, A., Cesario, W.C., White-Grindley, E., Jiang, H., Ren, F., Khan, M.R., Li, L., Choi, E.M., Kannan, K., Guo, F., et al. (2012). Critical role of amyloid-like oligomers of Drosophila Orb2 in the persistence of memory. Cell 148, 515-529.

Mangiarini, L., Sathasivam, K., Seller, M., Cozens, B., Harper, A., Hetherington, C., Lawton, M., Trottier, Y., Lehrach, H., Davies, S.W., et al. (1996). Exon 1 of the HD gene with an expanded CAG repeat is sufficient to cause a progressive neurological phenotype in transgenic mice. Cell 87, 493-506.

Marder, K., Zhao, H., Eberly, S., Tanner, C.M., Oakes, D., Shoulson, I., and Huntington Study, G. (2009). Dietary intake in adults at risk for Huntington disease: analysis of PHAROS research participants. Neurology 73, 385-392.

Marques Sousa, C., and Humbert, S. (2013). Huntingtin: here, there, everywhere! J Huntingtons Dis 2, 395-403.

Mayford, M., Bach, M.E., Huang, Y.Y., Wang, L., Hawkins, R.D., and Kandel, E.R. (1996). Control of memory formation through regulated expression of a CaMKII transgene. Science 274, 1678-1683.

Mehrabi, N.F., Waldvogel, H.J., Tippett, L.J., Hogg, V.M., Synek, B.J., and Faull, R.L. (2016). Symptom heterogeneity in Huntington's disease correlates with neuronal degeneration in the cerebral cortex. Neurobiol Dis 96, 67-74.

Menalled, L., and Brunner, D. (2014). Animal models of Huntington's disease for translation to the clinic: best practices. Mov Disord 29, 1375-1390.

Menalled, L.B., Kudwa, A.E., Miller, S., Fitzpatrick, J., Watson-Johnson, J., Keating, N., Ruiz, M., Mushlin, R., Alosio, W., McConnell, K., et al. (2012). Comprehensive behavioral and molecular characterization of a new knock-in mouse model of Huntington's disease: zQ175. PLoS One 7, e49838.

Mendez, R., Barnard, D., and Richter, J.D. (2002). Differential mRNA translation and meiotic progression require Cdc2-mediated CPEB destruction. EMBO J 21, 1833-1844.

Mendez, R., Hake, L.E., Andresson, T., Littlepage, L.E., Ruderman, J.V., and Richter, J.D. (2000). Phosphorylation of CPE binding factor by Eg2 regulates translation of c-mos mRNA. Nature 404, 302-307.

Nagaoka, K., Fujii, K., Zhang, H., Usuda, K., Watanabe, G., Ivshina, M., and Richter, J.D. (2016). CPEB1 mediates epithelial-to-mesenchyme transition and breast cancer metastasis. Oncogene 35, 2893-2901.

Nalavade, R., Griesche, N., Ryan, D.P., Hildebrand, S., and Krauss, S. (2013). Mechanisms of RNA-induced toxicity in CAG repeat disorders. Cell Death Dis 4, e752.

Nalivaeva, N.N., Belyaev, N.D., Kerridge, C., and Turner, A.J. (2014). Amyloid-clearing proteins and their epigenetic regulation as a therapeutic target in Alzheimer's disease. Front Aging Neurosci 6, 235.

Nardone, S., and Elliott, E. (2016). The Interaction between the Immune System and Epigenetics in the Etiology of Autism Spectrum Disorders. Front Neurosci 10, 329.

Nasir, J., Floresco, S.B., O'Kusky, J.R., Diewert, V.M., Richman, J.M., Zeisler, J., Borowski, A., Marth, J.D., Phillips, A.G., and Hayden, M.R. (1995). Targeted disruption of the Huntington's disease gene results in embryonic lethality and behavioral and morphological changes in heterozygotes. Cell 81, 811-823.

Negi, J.S., Singh, P., Geeta, and Rawat, M.S. (2010). Trace elements contents in Asparagus curillus (Buch.-Ham.) ex Roxb. Biol Trace Elem Res 136, 364-371.

Ng, I.C., Pawijit, P., Teo, L.Y., Li, H., Lee, S.Y., and Yu, H. (2016). Kinectin-dependent ER transport supports the focal complex maturation required for chemotaxis in shallow gradients. J Cell Sci 129, 2660-2672.

Novoa, I., Gallego, J., Ferreira, P.G., and Mendez, R. (2010). Mitotic cell-cycle progression is regulated by CPEB1 and CPEB4-dependent translational control. Nat Cell Biol 12, 447-456.

Oe, S., and Yoneda, Y. (2010). Cytoplasmic polyadenylation element-like sequences are involved in dendritic targeting of BDNF mRNA in hippocampal neurons. FEBS Lett 584, 3424-3430.

Omer, S., Harlow, T.J., and Gogarten, J.P. (2016). Does Sequence Conservation Provide Evidence for Biological Function? Trends Microbiol.

Ong, L.L., Lin, P.C., Zhang, X., Chia, S.M., and Yu, H. (2006). Kinectin-dependent assembly of translation elongation factor-1 complex on endoplasmic reticulum regulates protein synthesis. J Biol Chem 281, 33621-33634.

Ornoy, A., Weinstein-Fudim, L., and Ergaz, Z. (2015). Prenatal factors associated with autism spectrum disorder (ASD). Reprod Toxicol 56, 155-169.

Ortega, Z., and Lucas, J.J. (2014). Ubiquitin-proteasome system involvement in Huntington's disease. Front Mol Neurosci 7, 77.

Ortiz-Zapater, E., Pineda, D., Martinez-Bosch, N., Fernandez-Miranda, G., Iglesias, M., Alameda, F., Moreno, M., Eliscovich, C., Eyras, E., Real, F.X., et al. (2011). Key contribution of CPEB4-mediated translational control to cancer progression. Nat Med 18, 83-90.

Oruganty-Das, A., Ng, T., Udagawa, T., Goh, E.L., and Richter, J.D. (2012). Translational control of mitochondrial energy production mediates neuron morphogenesis. Cell Metab 16, 789-800.

Parikshak, N.N., Luo, R., Zhang, A., Won, H., Lowe, J.K., Chandran, V., Horvath, S., and Geschwind, D.H. (2013). Integrative functional genomic analyses implicate specific molecular pathways and circuits in autism. Cell 155, 1008-1021.

Parikshak, N.N., Swarup, V., Belgard, T.G., Irimia, M., Ramaswami, G., Gandal, M.J., Hartl, C., Leppa, V., Ubieta, L.T., Huang, J., et al. (2016). Genome-wide changes in lncRNA, splicing, and regional gene expression patterns in autism. Nature.

Parker, R., and Song, H. (2004). The enzymes and control of eukaryotic mRNA turnover. Nat Struct Mol Biol 11, 121-127.

Pavlopoulos, E., Trifilieff, P., Chevaleyre, V., Fioriti, L., Zairis, S., Pagano, A., Malleret, G., and Kandel, E.R. (2011). Neuralized1 activates CPEB3: a function for nonproteolytic ubiquitin in synaptic plasticity and memory storage. Cell 147, 1369-1383.

Peca, J., Feliciano, C., Ting, J.T., Wang, W., Wells, M.F., Venkatraman, T.N., Lascola, C.D., Fu, Z., and Feng, G. (2011). Shank3 mutant mice display autistic-like behaviours and striatal dysfunction. Nature 472, 437-442.

Pedrotti, S., Giudice, J., Dagnino-Acosta, A., Knoblauch, M., Singh, R.K., Hanna, A., Mo, Q., Hicks, J., Hamilton, S., and Cooper, T.A. (2015). The RNA-binding protein Rbfox1 regulates splicing required for skeletal muscle structure and function. Hum Mol Genet 24, 2360-2374.

Phillips, M., and Pozzo-Miller, L. (2015). Dendritic spine dysgenesis in autism related disorders. Neurosci Lett 601, 30-40.

Pique, M., Lopez, J.M., Foissac, S., Guigo, R., and Mendez, R. (2008). A combinatorial code for CPE-mediated translational control. Cell 132, 434-448.

Pringsheim, T., Wiltshire, K., Day, L., Dykeman, J., Steeves, T., and Jette, N. (2012). The incidence and prevalence of Huntington's disease: a systematic review and meta-analysis. Mov Disord 27, 1083-1091.

Rabaneda, L.G., Robles-Lanuza, E., Nieto-Gonzalez, J.L., and Scholl, F.G. (2014). Neurexin dysfunction in adult neurons results in autistic-like behavior in mice. Cell Rep 8, 338-346.

Ramanathan, A., Robb, G.B., and Chan, S.H. (2016). mRNA capping: biological functions and applications. Nucleic Acids Res 44, 7511-7526.

Ranen, N.G., Stine, O.C., Abbott, M.H., Sherr, M., Codori, A.M., Franz, M.L., Chao, N.I., Chung, A.S., Pleasant, N., Callahan, C., et al. (1995). Anticipation and instability of IT-15 (CAG)n repeats in parent-offspring pairs with Huntington disease. Am J Hum Genet 57, 593-602.

Raveendra, B.L., Siemer, A.B., Puthanveettil, S.V., Hendrickson, W.A., Kandel, E.R., and McDermott, A.E. (2013). Characterization of prion-like conformational changes of the neuronal isoform of Aplysia CPEB. Nat Struct Mol Biol 20, 495-501.

Reyes, J.M., and Ross, P.J. (2016). Cytoplasmic polyadenylation in mammalian oocyte maturation. Wiley Interdiscip Rev RNA 7, 71-89.

Richter, J.D. (2007). CPEB: a life in translation. Trends Biochem Sci 32, 279-285.

Richter, J.D., and Coller, J. (2015). Pausing on Polyribosomes: Make Way for Elongation in Translational Control. Cell 163, 292-300.

Risher, W.C., Ustunkaya, T., Singh Alvarado, J., and Eroglu, C. (2014). Rapid Golgi analysis method for efficient and unbiased classification of dendritic spines. PLoS One 9, e107591.

Ritchie, M.E., Phipson, B., Wu, D., Hu, Y., Law, C.W., Shi, W., and Smyth, G.K. (2015). limma powers differential expression analyses for RNA-sequencing and microarray studies. Nucleic Acids Res 43, e47.

Robinson, E.B., St Pourcain, B., Anttila, V., Kosmicki, J.A., Bulik-Sullivan, B., Grove, J., Maller, J., Samocha, K.E., Sanders, S.J., Ripke, S., et al. (2016). Genetic risk for autism spectrum disorders and neuropsychiatric variation in the general population. Nat Genet 48, 552-555.

Rub, U., Vonsattel, J.P., Heinsen, H., and Korf, H.W. (2015). The Neuropathology of Huntington s disease: classical findings, recent developments and correlation to functional neuroanatomy. Adv Anat Embryol Cell Biol 217, 1-146.

Sandin, S., Lichtenstein, P., Kuja-Halkola, R., Larsson, H., Hultman, C.M., and Reichenberg, A. (2014). The familial risk of autism. JAMA 311, 1770-1777.

Santini, E., and Klann, E. (2014). Reciprocal signaling between translational control pathways and synaptic proteins in autism spectrum disorders. Sci Signal 7, re10.

Sarkissian, M., Mendez, R., and Richter, J.D. (2004). Progesterone and insulin stimulation of CPEB-dependent polyadenylation is regulated by Aurora A and glycogen synthase kinase-3. Genes Dev 18, 48-61.

Saudou, F., and Humbert, S. (2016). The Biology of Huntingtin. Neuron 89, 910-926.

Schmeisser, M.J., Ey, E., Wegener, S., Bockmann, J., Stempel, A.V., Kuebler, A., Janssen, A.L., Udvardi, P.T., Shiban, E., Spilker, C., et al. (2012). Autistic-like behaviours and hyperactivity in mice lacking ProSAP1/Shank2. Nature 486, 256-260.

Schneider, C.A., Rasband, W.S., and Eliceiri, K.W. (2012). NIH Image to ImageJ: 25 years of image analysis. Nat Methods 9, 671-675.

Sebat, J., Lakshmi, B., Malhotra, D., Troge, J., Lese-Martin, C., Walsh, T., Yamrom, B., Yoon, S., Krasnitz, A., Kendall, J., et al. (2007). Strong association of de novo copy number mutations with autism. Science 316, 445-449.

Setoh, P., Marschik, P.B., Einspieler, C., and Esposito, G. (2016). Autism spectrum disorder and early motor abnormalities: Connected or coincidental companions? Res Dev Disabil 60, 13-15.

Sharon, G., Sampson, T.R., Geschwind, D.H., and Mazmanian, S.K. (2016). The Central Nervous System and the Gut Microbiome. Cell 167, 915-932.

Shen, S., Park, J.W., Huang, J., Dittmar, K.A., Lu, Z.X., Zhou, Q., Carstens, R.P., and Xing, Y. (2012). MATS: a Bayesian framework for flexible detection of differential alternative splicing from RNA-Seq data. Nucleic Acids Res 40, e61.

Shi, Y., and Manley, J.L. (2015). The end of the message: multiple protein-RNA interactions define the mRNA polyadenylation site. Genes Dev 29, 889-897.

Shieh, S.Y., and Bonini, N.M. (2011). Genes and pathways affected by CAG-repeat RNA-based toxicity in Drosophila. Hum Mol Genet 20, 4810-4821.

Shin, J., Salameh, J.S., and Richter, J.D. (2016). Impaired neurodevelopment by the low complexity domain of CPEB4 reveals a convergent pathway with neurodegeneration. Sci Rep 6, 29395.

Si, K., Choi, Y.B., White-Grindley, E., Majumdar, A., and Kandel, E.R. (2010). Aplysia CPEB can form prion-like multimers in sensory neurons that contribute to long-term facilitation. Cell 140, 421-435.

Si, K., Giustetto, M., Etkin, A., Hsu, R., Janisiewicz, A.M., Miniaci, M.C., Kim, J.H., Zhu, H., and Kandel, E.R. (2003a). A neuronal isoform of CPEB regulates local protein synthesis and stabilizes synapse-specific long-term facilitation in aplysia. Cell 115, 893-904.

Si, K., Lindquist, S., and Kandel, E.R. (2003b). A neuronal isoform of the aplysia CPEB has prion-like properties. Cell 115, 879-891.

Silverman, J.L., Yang, M., Lord, C., and Crawley, J.N. (2010). Behavioural phenotyping assays for mouse models of autism. Nat Rev Neurosci 11, 490-502.

Skubal, M., Gielen, G.H., Waha, A., Gessi, M., Kaczmarczyk, L., Seifert, G., Freihoff, D., Freihoff, J., Pietsch, T., Simon, M., et al. (2016). Altered splicing leads to reduced activation of CPEB3 in high-grade gliomas. Oncotarget 7, 41898-41912.

Slow, E.J., van Raamsdonk, J., Rogers, D., Coleman, S.H., Graham, R.K., Deng, Y., Oh, R., Bissada, N., Hossain, S.M., Yang, Y.Z., et al. (2003). Selective striatal neuronal loss in a YAC128 mouse model of Huntington disease. Hum Mol Genet 12, 1555-1567.

Sonenberg, N., and Hinnebusch, A.G. (2009). Regulation of translation initiation in eukaryotes: mechanisms and biological targets. Cell 136, 731-745.

Sorensen, S.A., and Fenger, K. (1992). Causes of death in patients with Huntington's disease and in unaffected first degree relatives. J Med Genet 29, 911-914.

Sousa Martins, J.P., Liu, X., Oke, A., Arora, R., Franciosi, F., Viville, S., Laird, D.J., Fung, J.C., and Conti, M. (2016). DAZL and CPEB1 regulate mRNA translation synergistically during oocyte maturation. J Cell Sci 129, 1271-1282.

Stephan, J.S., Fioriti, L., Lamba, N., Colnaghi, L., Karl, K., Derkatch, I.L., and Kandel, E.R. (2015). The CPEB3 Protein Is a Functional Prion that Interacts with the Actin Cytoskeleton. Cell Rep 11, 1772-1785.

Stepien, B.K., Oppitz, C., Gerlach, D., Dag, U., Novatchkova, M., Kruttner, S., Stark, A., and Keleman, K. (2016). RNA-binding profiles of Drosophila CPEB proteins Orb and Orb2. Proc Natl Acad Sci U S A.

Stessman, H.A., Willemsen, M.H., Fenckova, M., Penn, O., Hoischen, A., Xiong, B., Wang, T., Hoekzema, K., Vives, L., Vogel, I., et al. (2016). Disruption of POGZ Is Associated with Intellectual Disability and Autism Spectrum Disorders. Am J Hum Genet 98, 541-552.

Sultana, R., Yu, C.E., Yu, J., Munson, J., Chen, D., Hua, W., Estes, A., Cortes, F., de la Barra, F., Yu, D., et al. (2002). Identification of a novel gene on chromosome 7q11.2 interrupted by a translocation breakpoint in a pair of autistic twins. Genomics 80, 129-134.

Sutton, M.A., and Schuman, E.M. (2006). Dendritic protein synthesis, synaptic plasticity, and memory. Cell 127, 49-58.

Sztainberg, Y., and Zoghbi, H.Y. (2016). Lessons learned from studying syndromic autism spectrum disorders. Nat Neurosci 19, 1408-1417.

Theis, M., Si, K., and Kandel, E.R. (2003). Two previously undescribed members of the mouse CPEB family of genes and their inducible expression in the principal cell layers of the hippocampus. Proc Natl Acad Sci U S A 100, 9602-9607.

Thompson, J.C., Harris, J., Sollom, A.C., Stopford, C.L., Howard, E., Snowden, J.S., and Craufurd, D. (2012). Longitudinal evaluation of neuropsychiatric symptoms in Huntington's disease. J Neuropsychiatry Clin Neurosci 24, 53-60.

Thompson, P.D., Berardelli, A., Rothwell, J.C., Day, B.L., Dick, J.P., Benecke, R., and Marsden, C.D. (1988). The coexistence of bradykinesia and chorea in Huntington's disease and its implications for theories of basal ganglia control of movement. Brain 111 (Pt 2), 223-244.

Thu, D.C., Oorschot, D.E., Tippett, L.J., Nana, A.L., Hogg, V.M., Synek, B.J., Luthi-Carter, R., Waldvogel, H.J., and Faull, R.L. (2010). Cell loss in the motor and cingulate cortex correlates with symptomatology in Huntington's disease. Brain 133, 1094-1110.

Ting, J.T., Daigle, T.L., Chen, Q., and Feng, G. (2014). Acute brain slice methods for adult and aging animals: application of targeted patch clamp analysis and optogenetics. Methods Mol Biol 1183, 221-242.

Tomas-Zapico, C., Diez-Zaera, M., Ferrer, I., Gomez-Ramos, P., Moran, M.A., Miras-Portugal, M.T., Diaz-Hernandez, M., and Lucas, J.J. (2012). alpha-Synuclein accumulates in huntingtin inclusions but forms independent filaments and its deficiency attenuates early phenotype in a mouse model of Huntington's disease. Hum Mol Genet 21, 495-510.

Trottier, Y., Devys, D., Imbert, G., Saudou, F., An, I., Lutz, Y., Weber, C., Agid, Y., Hirsch, E.C., and Mandel, J.L. (1995). Cellular localization of the Huntington's disease protein and discrimination of the normal and mutated form. Nat Genet 10, 104-110.

Tsai, L.Y., Chang, Y.W., Lin, P.Y., Chou, H.J., Liu, T.J., Lee, P.T., Huang, W.H., Tsou, Y.L., and Huang, Y.S. (2013). CPEB4 knockout mice exhibit normal hippocampus-related synaptic plasticity and memory. PLoS One 8, e84978.

Tsuda, K., Kuwasako, K., Nagata, T., Takahashi, M., Kigawa, T., Kobayashi, N., Guntert, P., Shirouzu, M., Yokoyama, S., and Muto, Y. (2014). Novel RNA recognition motif domain in the cytoplasmic polyadenylation element binding protein 3. Proteins 82, 2879-2886.

Tuchman, R., and Rapin, I. (2002). Epilepsy in autism. Lancet Neurol 1, 352-358.

Udagawa, T., Farny, N.G., Jakovcevski, M., Kaphzan, H., Alarcon, J.M., Anilkumar, S., Ivshina, M., Hurt, J.A., Nagaoka, K., Nalavadi, V.C., et al. (2013). Genetic and acute CPEB1 depletion ameliorate fragile X pathophysiology. Nat Med 19, 1473-1477.

Udagawa, T., Swanger, S.A., Takeuchi, K., Kim, J.H., Nalavadi, V., Shin, J., Lorenz, L.J., Zukin, R.S., Bassell, G.J., and Richter, J.D. (2012). Bidirectional control of mRNA translation and synaptic plasticity by the cytoplasmic polyadenylation complex. Mol Cell 47, 253-266.

UniProt, C. (2015). UniProt: a hub for protein information. Nucleic Acids Res 43, D204-212.

Vale, T.C., and Cardoso, F. (2015). Chorea: A Journey through History. Tremor Other Hyperkinet Mov (N Y) 5.

Valor, L.M. (2015). Transcription, epigenetics and ameliorative strategies in Huntington's Disease: a genome-wide perspective. Mol Neurobiol 51, 406-423.

Van Wijngaarden-Cremers, P.J., van Eeten, E., Groen, W.B., Van Deurzen, P.A., Oosterling, I.J., and Van der Gaag, R.J. (2014). Gender and age differences in the core triad of impairments in autism spectrum disorders: a systematic review and meta-analysis. J Autism Dev Disord 44, 627-635.

Verkerk, A.J., Pieretti, M., Sutcliffe, J.S., Fu, Y.H., Kuhl, D.P., Pizzuti, A., Reiner, O., Richards, S., Victoria, M.F., Zhang, F.P., et al. (1991). Identification of a gene (FMR-1) containing a CGG repeat coincident with a breakpoint cluster region exhibiting length variation in fragile X syndrome. Cell 65, 905-914.

Vicario, A., Colliva, A., Ratti, A., Davidovic, L., Baj, G., Gricman, L., Colombrita, C., Pallavicini, A., Jones, K.R., Bardoni, B., et al. (2015). Dendritic targeting of short and long 3' UTR BDNF mRNA is regulated by BDNF or NT-3 and distinct sets of RNA-binding proteins. Front Mol Neurosci 8, 62.

Villalba, A., Coll, O., and Gebauer, F. (2011). Cytoplasmic polyadenylation and translational control. Curr Opin Genet Dev 21, 452-457.

Voineagu, I., Wang, X., Johnston, P., Lowe, J.K., Tian, Y., Horvath, S., Mill, J., Cantor, R.M., Blencowe, B.J., and Geschwind, D.H. (2011). Transcriptomic analysis of autistic brain reveals convergent molecular pathology. Nature 474, 380-384.

Vonsattel, J.P. (2008). Huntington disease models and human neuropathology: similarities and differences. Acta Neuropathol 115, 55-69.

Vonsattel, J.P., and DiFiglia, M. (1998). Huntington disease. J Neuropathol Exp Neurol 57, 369-384.

Vonsattel, J.P., Myers, R.H., Stevens, T.J., Ferrante, R.J., Bird, E.D., and Richardson, E.P., Jr. (1985). Neuropathological classification of Huntington's disease. J Neuropathol Exp Neurol 44, 559-577.

Vuono, R., Winder-Rhodes, S., de Silva, R., Cisbani, G., Drouin-Ouellet, J., Spillantini, M.G., Cicchetti, F., and Barker, R.A. (2015). The role of tau in the pathological process and clinical expression of Huntington's disease. Brain 138, 1907-1918.

Waldvogel, H.J., Kim, E.H., Thu, D.C., Tippett, L.J., and Faull, R.L. (2012). New Perspectives on the Neuropathology in Huntington's Disease in the Human Brain and its Relation to Symptom Variation. J Huntingtons Dis 1, 143-153.

Wang, C.F., and Huang, Y.S. (2012). Calpain 2 activated through N-methyl-D-aspartic acid receptor signaling cleaves CPEB3 and abrogates CPEB3-repressed translation in neurons. Mol Cell Biol 32, 3321-3332.

Wang, N., Gray, M., Lu, X.H., Cantle, J.P., Holley, S.M., Greiner, E., Gu, X., Shirasaki, D., Cepeda, C., Li, Y., et al. (2014). Neuronal targets for reducing mutant huntingtin expression to ameliorate disease in a mouse model of Huntington's disease. Nat Med 20, 536-541.

Wang, X.P., and Cooper, N.G. (2010). Comparative in silico analyses of cpeb1-4 with functional predictions. Bioinform Biol Insights 4, 61-83.

Wang, Y., Wang, Z., and Tanaka Hall, T.M. (2013). Engineered proteins with Pumilio/fem-3 mRNA binding factor scaffold to manipulate RNA metabolism. FEBS J 280, 3755-3767.

Weill, L., Belloc, E., Bava, F.A., and Mendez, R. (2012). Translational control by changes in poly(A) tail length: recycling mRNAs. Nat Struct Mol Biol 19, 577-585.

Wexler, N.S., Lorimer, J., Porter, J., Gomez, F., Moskowitz, C., Shackell, E., Marder, K., Penchaszadeh, G., Roberts, S.A., Gayan, J., et al. (2004). Venezuelan kindreds reveal that genetic and environmental factors modulate Huntington's disease age of onset. Proc Natl Acad Sci U S A 101, 3498-3503.

White, S.W., Oswald, D., Ollendick, T., and Scahill, L. (2009). Anxiety in children and adolescents with autism spectrum disorders. Clin Psychol Rev 29, 216-229.

Willsey, A.J., and State, M.W. (2015). Autism spectrum disorders: from genes to neurobiology. Curr Opin Neurobiol 30, 92-99.

Wu, L., Wells, D., Tay, J., Mendis, D., Abbott, M.A., Barnitt, A., Quinlan, E., Heynen, A., Fallon, J.R., and Richter, J.D. (1998). CPEB-mediated cytoplasmic polyadenylation and the regulation of experience-dependent translation of alpha-CaMKII mRNA at synapses. Neuron 21, 1129-1139.

Xiaoping, L., Zhibin, Y., Wenjuan, L., Zeyou, W., Gang, X., Zhaohui, L., Ying, Z., Minghua, W., and Guiyuan, L. (2013). CPEB1, a histone-modified hypomethylated gene, is regulated by miR-101 and involved in cell senescence in glioma. Cell Death Dis 4, e675.

Xiong, H.Y., Alipanahi, B., Lee, L.J., Bretschneider, H., Merico, D., Yuen, R.K., Hua, Y., Gueroussov, S., Najafabadi, H.S., Hughes, T.R., et al. (2015). RNA splicing. The human splicing code reveals new insights into the genetic determinants of disease. Science 347, 1254806.

Yamamoto, A., Lucas, J.J., and Hen, R. (2000). Reversal of neuropathology and motor dysfunction in a conditional model of Huntington's disease. Cell 101, 57-66.

Yasuda, H., Yoshida, K., Yasuda, Y., and Tsutsui, T. (2011). Infantile zinc deficiency: association with autism spectrum disorders. Sci Rep 1, 129.

Yates, A., Akanni, W., Amode, M.R., Barrell, D., Billis, K., Carvalho-Silva, D., Cummins, C., Clapham, P., Fitzgerald, S., Gil, L., et al. (2016). Ensembl 2016. Nucleic Acids Res 44, D710-716.

Zhang, X., Virtanen, A., and Kleiman, F.E. (2010). To polyadenylate or to deadenylate: that is the question. Cell Cycle 9, 4437-4449.

Zuccato, C., and Cattaneo, E. (2009). Brain-derived neurotrophic factor in neurodegenerative diseases. Nat Rev Neurol 5, 311-322.

Zuccato, C., and Cattaneo, E. (2014). Huntington's disease. Handb Exp Pharmacol 220, 357-409.

Zuccato, C., Valenza, M., and Cattaneo, E. (2010). Molecular mechanisms and potential therapeutical targets in Huntington's disease. Physiol Rev 90, 905-981.